Developing Global Dataset of Salt Pans and Salt Playas Using Landsat-8 imagery: A Case Study of Western North America

by

Samira Safaee

B.S., Islamic Azad University, 2006

A THESIS

submitted in partial fulfillment of the requirements for the degree

MASTER OF ARTS

Department of Geography

College of Arts and Sciences

KANSASSTATEUNIVERSITY
Manhattan, Kansas

2018

Approved by:

Major Professor
Dr. Jida Wang

Copyright

Abstract

Monitoring salt pans is important especially for agricultural management in arid or semi-arid regions because salt pans can negatively affect human life, wildlife, and ecology. Some of the harmful impacts of salt pans are accelerated desertification, cropland loss, economic downturn, wildlife loss, and forced migration of humans and animals due to salt storms. Spectral salt pan indices based upon remotely sensed data (using spectral properties of Landsat-8 imagery) suggested in previous studies vary by location. In other words, the spectral configuration of a salt index for a given location may not be readily applicable to another location due to spatial heterogeneity of salt components across the continental surface. Using Landsat-8 OLI imagery and climate data sets, this study aims to develop a mapping framework which can effectively extract salt pans and salt playas under various spectral conditions in different geographic locations. Based on training samples selected in eight major salt pans/playas in North America, Central Asia, Africa, and Australia, the mapping framework was designed to include the following steps: i) a conservative salt index to highlight potential salt-covered regions, ii) a calibrated support vector machine (SVM) to extract high-salinity areas in the mask regions, and iii) a posterior quality assurance/ quality control (QA/QC) with assistance of auxiliary datasets (e.g., surface slope and land covers) to eliminate commission errors and refine the extracted saltpan areas.

The developed mapping framework was validated in the arid endorheic regions across the western United States, with a total area of 699 thousand square kilometers. Both qualitative and quantitative assessments of the results show reliability of the developed framework. The overall accuracy of the extracted salt pans prior to QA/QC is 97%. The final product after QA/QC achieves an overall accuracy of 99.95% and a Kappa statistic of 0.99.According to the results of

salt pans areas and endorheic basins areas, it can be concluded that two aforementioned variables of this study are positively correlated to each other, and 1.10 percent of the entire case study area is covered by salt pans. The accuracy of the results suggests a potential that the mapping framework, together with the collected training sample and algorithms, may be applicable to identify salt pan and salt playa regions across the Earth's land surface.

Table of Contents

List of Figures

List of Tables

Acknowledgements

First, I would like to express my appreciation to my major advisor Dr. Jida Wang, whose guidance, support, and motivation helped me carry out this research.

I would also like to thank my committee members Dr. Douglas Goodin, Dr. Shawn Hutchinson, and Dr. Bimal Paul, for their valuable insights and comments regarding my work.

I would like to appreciate Dr. Bradley Shaw for his supports and guidance.

Dedication

I would like to dedicate this work enthusiastically to my amazing husband and friend Mohammadreza and to my family, and my in-laws, whose love and constant support have been the foundation of my accomplishments.

Chapter 1 - Introduction

The Oxford Dictionary of English defines salt pans and salt playas as flat expanses of ground surface covered by salt evaporites. Salt pans are formed in lake basins or depressions as a consequence of excessive evaporation compared to surface inflow and precipitation. Layered evaporites can be accumulated in three main depositional forms; i) deep perennial basins (e.g., Dead Sea) ii) shallow perennial lakes or ponds (e.g., Great Salt Lake and the Gulf of Karabogaz); iii) ephemeral saline pans (e.g., Death Valley located in California) (Lowenstein and Hardie 1985). Salt pans can be identified based on their dominant mineral such as halite, potash, or gypsum (Lowenstein and Hardie, 1985). They are extensively distributed in arid or semi-arid regions such as Central Australia, the Western United States (U.S.), and the Middle East, and are dynamic landforms as a response to all local meteorological, hydrologic conditions, and man-made changes (Carpenter, 1969). According to Milewski et al. (2017), approximately 50,000 salt pans exist on the contemporary Earth surface. Salinization is the accumulation of salt soluble in the soil, a natural characteristic of soil, but secondary salinization occurs as a result of specific man-made activity (Dehni and Lounis 2012). In arid, semi-arid and some sub-humid regions the existence of salt-affected soils is a common result of secondary salinization (Dehni and Lounis 2012). In irrigated agricultural lands soil salinity and water logging are two leading restraints (Dehni and Lounis 2012).Salinity is an active phenomenon and may vary over different seasons (Shrestha and Farshad, 2009).More than 50% of the earth's continental areas are affected by degradation (Shrestha and Farshad, 2009). Secondary salinization as a result of the mismanagement of lands covers a 0.8 million km^2 area of irrigated lands (Shrestha and Farshad, 2009). The intensity of salinization can occur in the low-lying topography and less vegetated areas of farms (Asfaw et al. 2016). The main salt source in soil can be the result of rocks and minerals weathering, either made in-situ or conveyed by water or wind (Shrestha and Farshad, 2009). Furthermore, salt lakes usually can be converted to salt pans when the salt crust accumulates silt and clay, forming a sediment store for top layers by time (Scheffers and Kelletat 2016).

The main reasons for the development of salinization\alkalization include:

i) The use of saline water for irrigation (Shrestha and Farshad, 2009);ii) The balance of water disrupted between precipitation, on one hand, and surface flow, groundwater level, and evapotranspiration on the other (Shrestha and Farshad, 2009);iii) The original composition of the soils (containing plagioclase feldspars, i.e. sodium-rich minerals)(Dwivedi et al. 1999);iv) Groundwater rises as a result of forest clearance, overgrazing, and cutting bushes (Shrestha and Farshad, 2009); v) Passing water through saline surfaces (Shrestha and Farshad 2009); vi) Interference of sea water into the surface (Shrestha and Farshad, 2009). Consequently, groundwater comes into contact with rocks containing salt and therefore affects covering salt formations (Shrestha and Farshad, 2009). Alkalinization is a factor which can enhance salinization and form sodic soil causing the desalinization of salt-affected soil (Shrestha and Farshad, 2009). "Prevention is better than a cure" and "mapping salinity hazards might be better than mapping salinity itself" (Shrestha and Farshad, 2009).

Understanding the accurate distribution of salt pans will lead to evident geographic benchmarks for ephemeral or intermittent water storage in these arid regions where water resources are scarce by nature or due to human activities. Although salt pans concur with hyper-saline environments, their locations imply intermittent freshwater runoff in the upstream, and their size depicts a long-term availability of surface runoff under the local catchment climate (e.g., temperature and evaporation).

In addition, soil salinization is a significant environmental threat which can be caused by both natural processes and human activities (Al-Khaier, 2003). Natural processes include cyclic drought and low surface flow. Example of human-related factors such as excessive use of groundwater and dam construction. Saline soil negatively affects vegetation and crop growth (Al-Khaier, 2003). Salinization can greatly affect land productivity and it eventually causes cropland abandonment in semi-arid and arid areas. Extremely high soil salinity can result in land abandonment and thus accelerate desertification, which can cause the migration of affected people and animals because salt storms are harmful to human and crops. Soil salinization also negatively affects the economies of the nearby cities, which is followed by losing croplands or tourist attraction such as the situation that occurred at Lake Urmia of Iran. Coastal zones are the favorite places for industrial and agricultural activities and contribute greatly to to the affected countries' economic growth (Sridhar et al. 2008).

Given the aforementioned points, identifying salt-affected areas is important to improve agricultural management, particularly in arid and semi-arid regions (Farifteh et al., 2008). Despite its importance, we currently lack a broad-scale, finely-detailed salt pan inventory. The goal of this study is to provide a highly-accurate dataset of salt pans and salt playas across the world using Landsat-8 imagery. Mapping broad sizes of salt pans in the field does not provide high accuracy and frequency, but remote sensing can map significantly accurate maps across broad areas of interest.

Monitoring land cover and land use changes is an important process in order to protect the environment, animals, and humans. Remote sensing is a useful technology in monitoring large-scale environmental changes such as disaster occurrences, deforestation, phonologic dynamics, urbanization, and hydrologic cycles (Rokni et al., 2014). In addition increasing salinity and pollution of water resources have negative environmental impacts that put vegetation and wildlife into risk due to salt intrusion into the groundwater (DOE, 2014; Ghalibaf and Moussavi, 2014).

Soil salinization can be detected from multi-spectral imagery (Farifteh et al., 2007), using the unique signature of salt spectral reflectance, or indirectly, based on the spectral characteristics of vegetation of the saline soil (Al-Khaier, 2003).

Mapping salt-affected soil is easier at the advanced stage (when salt-related symptoms are located on the top of the surface and are detectable in the visible region of the spectrum), but it is harder to identify when the salinization process occurs in the subsoil (Shrestha and Farshad, 2009). Even with topsoil, it is hard to distinguish between salt and soil if the content of salt is lower than 10-15 percent (Mougenot et al., 1993). However, due to the performance (high accuracy and quality) of the developed framework in the current thesis, even lower than 10 percent salt existing on top soil can be easily distinguished from soil.

Different salt chemicals with different spectral signatures, temporal changes of salinity levels, interference of vegetation and crop growth, spectral confusion of features, and spatial distribution of salts on the surface all limit the use of remote sensing to map salt-affected areas (Metternicht and Zinck, 2003). Ground validation is still important in order to find a relationship between spectral reflectance and salt chemicals (Metternicht and Zinck, 2003). Metternicht and Zinck (2003) found that estimating salt quantities using remotely sensed data can be difficult due to: i) no specific absorption bands of some types of salt; ii) different chemical or physical properties of salt, and iii) similarities of some features' spectral signatures(such as alkaline surface) with those of salt.

In this research I utilized Landsat-8 operational land imager (OLI)multi-spectral imagery owing to their acceptable 30-m spatial resolution (Appendix A)with a temporal resolution of 16 days. I started with algorithmic development from samples distributed in various regions which encompass the Earth and aim to apply the algorithm to the entire continental surface. Here in the thesis, the method was trained on samples selected in different continents, but applied in southwestern region of the United States. For the purpose of this experiment, eight regions in different continents have been selected and examined. The main rationale for using multiple regions is to take into account various salt pan reflectance conditions. From these “training areas” , a thematic mapping framework was developed. In brief, this framework first flagged potential salt regions using simple band thresholding. Then, within these potential regions, supervised classification (e.g., SVM) was performed using collected salt/non-salt pixels (“spectral library”) as training samples. Then, the developed mapping algorithm was applied to the ideal time for salt pan mapping, here defined as the acquisition date that concurred with the driest surface conditions, i.e., when salt pans were maximally exposed, during Landsat-8’s operational period. Salinization is a dynamic process and the size of salt pans vary during the year, according to the availability of water. Based on the effects of wet periods during a year on the salt pans, distinguishing between fresh water and saline water can be hard if the size of the salt-affected area is small enough to be overwhelmed with rainfall or surface flow. Therefore based on the salt-pan maps created in this study, the potential seasonal saline water spots can be identified. For example, in dry seasons salt pans are more likely to appear, however, they can be filled by water in wet seasons. In this case, to check whether a water body is saline or not, referring to the salt pan maps of the location can be helpful. Different climate datasets have been collected and processed to determine the driest periods for the study area. I expected developing an accurate algorithm using one index applicable to highlight all different salt chemicals and using Landsat-8 bands 2-7 to delineate salt-affected areas all around the world.

The major objectives addressed in this work are:

i) to study and analyze the spectral behavior of salt compared to those of other land features ii) to define a conservative salt index to flag potential salt-covered regions iii) to define a comprehensive training sample, based upon different locations, applicable to the Earth's continental surface; iv) to qualitatively and quantitatively validate the proposed framework; v) to discover the limitations with the proposed framework; and vi) to interpret the statistics obtained from the results and investigate the relationship between variables of the study (e.g., salt pan distribution and endorheic basins).

Chapter 2 - Literature Review

Spectral sensors measure the electromagnetic reflection over space in the form of a wave which is determined by wavelength. The commonly used wavelengths in remote sensing are between 0.4 and 1.2 micrometers (Al-Khaier, 2003). Reviewing existing studies related to salt-affected surfaces assisted this study to trace and lead a worthwhile pathway of research to detect salt-affected areas.

2.1Satellite data and bands useful to detect salt

Menenti et al. (1986) showed that bands 1 to 5 and 7 (Appendix B) of TM imagery are useful for extracting salt minerals. They figured out that the thermal behavior of the soil surface can be affected by soil minerals, too.

Al-Khayer (2003) used ASTER bands based on the temporal relationship between existing salt in the soil before planting crops (in the bare soil), and examined a new biophysical approach (finding a relationship between the reflectance of bare soil and cotton-producing soil) to predict soil salinity. Al-Khayer (2003) mapped salt-affected surfaces and water-logged lands in India classifying TM data using bands 3 to 5 and band7.

Albed and Kumar (2013) predicted soil salinity based on the statistically significant correlation coefficient between surface color and the sodium absorption ratio. They suggest that color, salt content, surface roughness and moisture are good indicators to estimate soil salinity. They also believe that salt-concentrated areas can be detected based on the existence of vegetation species. They concluded that salt indices vary for each location and a single index may not be useful for all regions. They found that TM visible and infrared bands provide valuable information about salt surfaces. They also found TM thermal bands useful to detect salt in urban areas.

According to Alavi Panah (2000), an indicator of soil degradation would be the existence of surface crust. Alavi Panah (2000) found Landsat-5 Thematic Mapper (TM) imagery valuable to obtain distinct information about salt crust using visible and infrared bands as auxiliary informative bands to each other. He also found that the TM thermal band can contain useful information for separating urban from salt crust. Furthermore, he believes that having a high level of knowledge about characteristics of the crusted surface in desert regions increases image interpretation and the accuracy of results.

2.2 Spectral characteristics of salt-affected soils

Farifteh et al. (2007) found that soil salinization can be detected from remotely-sensed spectral imagery using the unique signature of salt spectral reflectance, or it may be indirectly based on the spectral characteristics of vegetation on the saline soil. It should be pointed out, however, they did not apply their algorithm on different locations since spectral reflectance of salt is not unique in different regions. According to their study, spectral reflectance of salt can be distinguished from those of other land features in infrared spectrums.

In another study Farifteh et al. (2008) found that the more salt existed in the soil the more spectral reflectance occurred for wavelengths longer than 1300nm, and especially for the water absorption wavelengths.

In another study, Sing and Sirohi (1994) found that in general saline soil is smoother than a non-saline surface, so it has high reflectance in visible and NIR regions. However, Metternicht et al. (2003) found that surface roughness increases when trampling causes alternation of the saline surface, and consequently the overall reflectance of salt decreases.

From this study it can be inferred that even the same salt chemical might have different spectral reflectance due to the amount of salt accumulation on the surface. This study makes clear that mapping salt-affected areas with a variety of salt accumulation levels would not be easily feasible.

2.3 Spectral characteristics of different salt chemicals

Howari et al. (2002) discovered that different salt chemicals located in different types of soil lead to different reflectance behaviors (Figure 1, each panel represents different spectral reflectance correlated with the sub-surface soil). In other words, spectral reflectance of soil will disappear in high salinity conditions and salt spectral reflectance is dominant. They mentioned that salt particles are finer than soil particles and consequently have higher spectral reflectance which confirms the conclusion made by Sing and Sing and Sirohi (1994). Moreover, when the surface is totally covered by salt, the spectral reflectance of the soil fades away. Howari et al. (2002) suggested that in multiple salt crusts the general spectral signature of salt can be obtained using hyperspectral imageries, but identifying crusts consisting of specific chemicals would not be easy. According to Howari et al. (2002), salt can have several compositions and different spectral signatures accordingly which with some solutions limits detecting salt. This study led me to consider different types of salt chemicals found in various regions of the world.

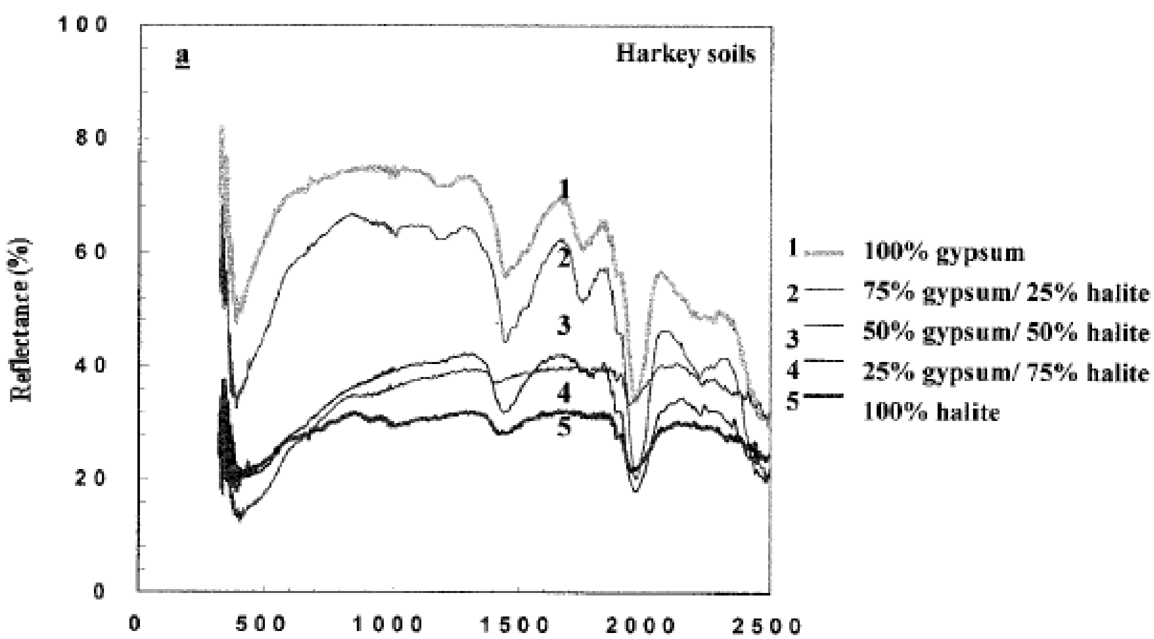

Figure 1. The spectral reflectance of soil treated with existence of different salt chemicals (Figure 2, panels 1-6); Reprinted from Howari et al. (2002)

2.4 Spectral salt indices and approaches used to detect salt

Iqbal and Mastorakis (2015) suggested using Salinity Indices (SI) and the Soil Adjacent Vegetation Index (SAVI) defined as:

$SI = ((B)(R))/2$ (1)

$SAVI = ((R - NIR)(R + NIR) + 0.5)(1 + 0.5)$ (2)

Where B is blue band, R is red band, and NIR is near infrared band in Landsat-5 TM imagery (wavelength details are provided in Appendix B).

They found that SI accurately identifies the overall salinity in bare agricultural lands Also, the thermal infrared band was found to be a useful band in this study because it indicates more reflectance compared to the other bands for the salt-affected areas.

Dwivedi (1969) delineated salt-affected soils using principal component analysis of MSS data (bands 1 to 4).

Asfaw et al. (2013) used site visit, remote sensing and GIS techniques to generate a model for delineating soil salinity. They believe that a combination of spectral bands and image enhancement improves the result of salt detection compared to using original imagery associated with a single band. They used different indices for soil salinity detection and concluded that their proposed salinity index (salinity index: the ratio of red band to NIR) performs with high accuracy. Their study shows the important role that the field visit plays in evaluating remote sensing studies. The salinity index was examined in my research, but the performance was not acceptable. Due to the weakness of existing spectral indices to extract salt pixels, developing an index applicable to different locations was necessary.

Ambast (1997) developed a new approach for classifying salt-affected regions and water logging zones based on biophysical parameters of salt affected crops. This approach was designed based on the dividing energy method named Surface Energy Balance Algorithm for Land.

In other research, Vidal et al. (1996) used the classification-tree algorithm. The first step in this approach was masking vegetation using NDVI. The next step was to apply a brightness index to distinguish the moisture and salinity condition of fallow and deserted lands. This study is significant because it showed the value of masking out features other than salt (which is the desired feature to be mapped).

Sridhar et al. (2008) also used Salt Pan Index that creates a model in ERDAS model maker and they compared supervised and unsupervised algorithms. The salt index equation is:

$$SPI = VISG - SWIR \tag{3}$$

Where SPI is Salt Pan Index, $VISG$ is visible green band reflectance including wavelengths from 0.52 µm to 0.60 µm, and $SWIR$ is shortwave infrared reflectance including wavelengths from 1.55 µm to1.75 µm.

In their study, to distinguish between sandy areas and salt pans the unsupervised classification approach has been used with 95% accuracy in mapping salt pans in coastal areas. Furthermore, it can be inferred that SWIR regions would be highly useful in characterizing salt. Simin et al. (2010) used the support vector machine (SVM) classifier for texture classification (using grey level co-occurrence matrix) based on the spectral signature of the features to extract salt-affected areas. In this study they found that the accuracy of mapped classes was enhanced using texture features in the classification. In other words, when the objects' spectral signatures are similar, using texture features can increase the objects' detection. This study suggests a back-up plan if one cannot use objects' spectral signatures to distinguish between land features.

Metternicht and Zinck (1997) found that the reflectance of the surface via visible and NIR regions highly depends on both the crust color and surface roughness. Decision Tree (DT) and Neural Networks using TM satellite data were found as unreliable approaches due to their inability in applying prior knowledge about the relationship between inputs and outputs. For this reason, DT and NN data were not tested in this study.

2.5 Summary

To sum up, and according to the existing literature, i) allocating a specific spectral signature to salt is not feasible based on the variety of spectral behavior of various salt chemicals in various soil types; ii) There are several similar land features to salt in terms of spectral behavior. Therefore, distinguishing salt from other features would not be easily feasible; iii) Furthermore, there is no spectral index applicable on different locations to extract salt pixels. All existing spectral indices are applicable to a specific location which in other locations may not perform as accurately as for the original location; iv) Masking out undesired land features was a practical way to flag desired pixels and narrow down the size of study areas according to the reviewed literature. This would not be easy based on issues cited in “i” and “ii”; v) SVM accompanied with spectral signature of desired land feature seems to be a useful approach to map salt pans. However, in some cases objects’ spectral signatures may not be capable of distinguishing between land features.

Chapter 3 - Study Area

3.1 Training areas

In the current research eight different locations across the Earth were selected as training areas in order to obtain comprehensive training samples and to map various salt chemicals across the Earth's continental surface. The following information describes the training areas in more detail and figure 4 shows the location of each TA.

1- Great Salt Lake (Figure 2, panel 1), located in the northern part of the U.S., in the state of Utah, is the largest saline water reservoir in the Western Hemisphere.

2- Rosamond Dry Lake bed (RDLB) (Figure 2, panel 2), containing fine-grained sediments filled with alkali salts, is a large, extensive area located in California's Mojave Desert on the southwestern edge of Edwards Air Force Base and the northeastern edge of Piute Ponds.

3- Salar de Uyuni salt flat (Figure 2, panel 3), located in the Daniel Campos Province in Potosí in southwest Bolivia, South America. Salar de Uyuni is the largest salt flat on the earth encompassing more than 4,000 square miles.

4- Baskunchak Lake (Figure 2, panel 4), located in Astrakhan Oblast, Russia. It is a protected area since 1997.

5- Lake Urmia, (Figure 2, panel 5), is an endorheic Salt Lake located in Iranian Azerbaijan, Iran and near Iran's border with Turkey. The lake has been shrinking since 2008.

6- Lake Assal (Figure 2, panel 6), located in Djibouti, Africa, is a protected area since the year 2000.

7- Etosha pan (Figure 2, panel 7) is a large endorheic salt pan located in northern Namibia as a part of the African Kalahari Basin**,** which is a protected wildlife park. After heavy rainfalls, the Etosha pan contains a thin layer of highly saline water due to the existence of mineral deposits on its surface. The Etosha pan area is about 2485.5 square miles (4000 km2) and is what remains from a larger lake during a former period of cooler climates (Scheffers and Kelletat 2016).

8- Lake Disappointment (Figure 2, panel 8) is a saline lake located in Western Australia.

Appendix C gives more information of Landsat-8 OLI images used in this part.

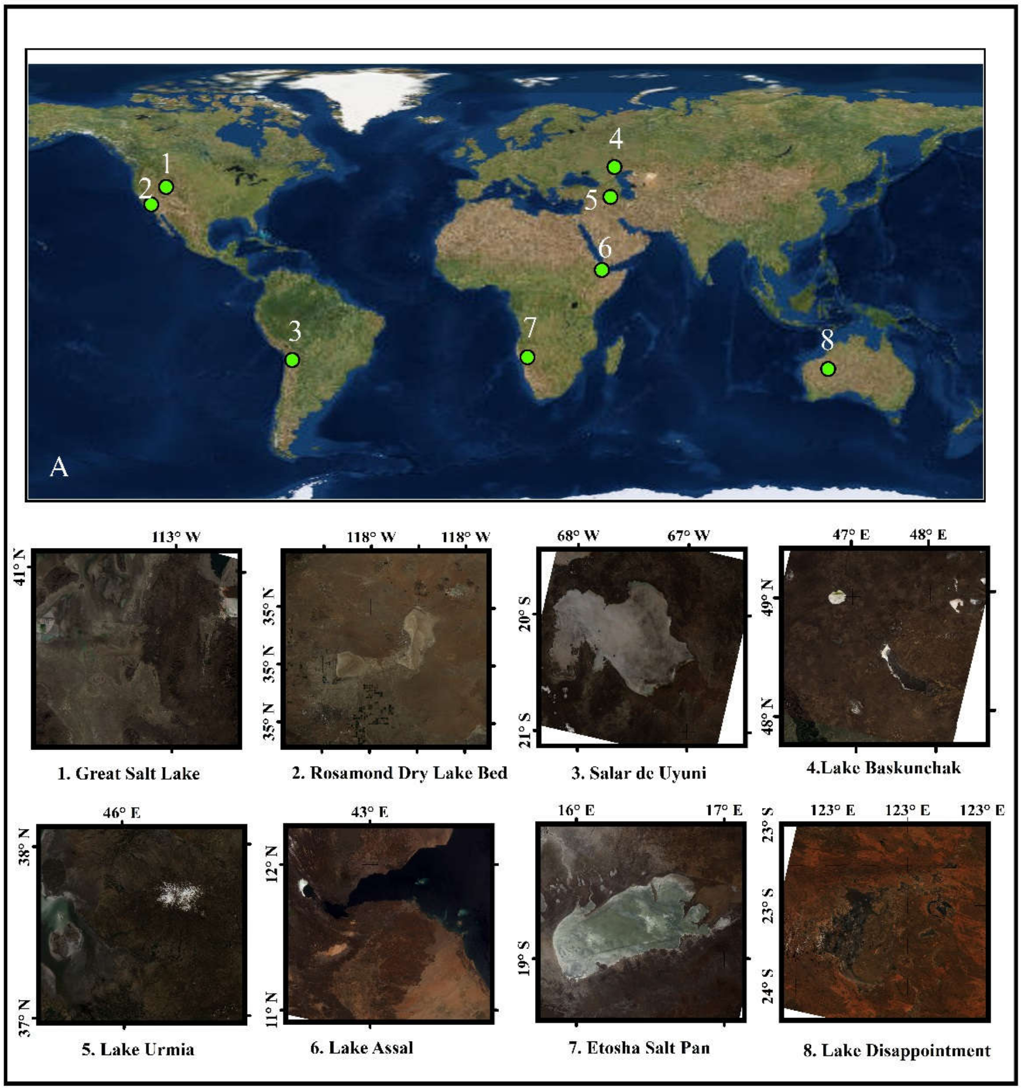

Figure 2. Locations and Landsat-8 OLI imageries of training areas. The world map (panel A) shows all training areas in a single view. Great Salt Lake (panel 1), Rosamond Dry Lake Bed (panel 2), Salar de Uyuni salt flat (panel 3), Baskunchak Lake (panel 4), Lake Urmia (panel 5), Lake Assal (panel 6), Etosha pan (panel 7), Lake Disappointment (panel 8). World map source: Environmental Systems Research Institute (Esri) digital globe, GeoEye, Earthstar Geographic, The Centre national d'études spatiales (CNES) (English: National Centre for Space Studies) \Airbus DS, United States Department of Agriculture (USDA), United States Geological Survey (USGS), AeroGRID, Institute Geographique National (IGN), and the GIS User Community. Training areas background source: Landsat-8 OLI TOAR image (Appendix C).

3.2 Case study and validation area

A total area of 698,999.8 km^2 covers the case study (Figure 3) including part of deserts of the western United States and Mexico including Mojave, a small part of Chihuahua, and the Great Basin Desert, including 455 endorheic basins.

The Mojave Desert is the hottest desert in North America. It is located in southeastern California, encompassing 56,980 km^2. The Chihuahuan Desert is the largest desert in North America and is located in southwestern United States and northern Mexico, covering 362,598 km^2. The Great Basin Desert covers a large part of the northern Basin and Range Province (north of the Mojave Desert), encompassing about 492,097 km^2.

An endorheic basin (land-locked drainage basin) allows no surface outflow. Therefore, evaporation may exceed inflow and consequently the formation of salt pans can occur in such areas. A sink point is the drainage terminus of endorheic basins can be a good indicator of salt pan locations in this study. Because sink points in endorheic basins are the ultimate place for all chemical residues carried in by streams (Carpenter, 1969). Sink points can indicate a permanent lake, a dry/intermittent lake (i.e., playa), or a point where surface water infiltrates underground. In an endorheic basin all streams and rivers flow toward the sink point.

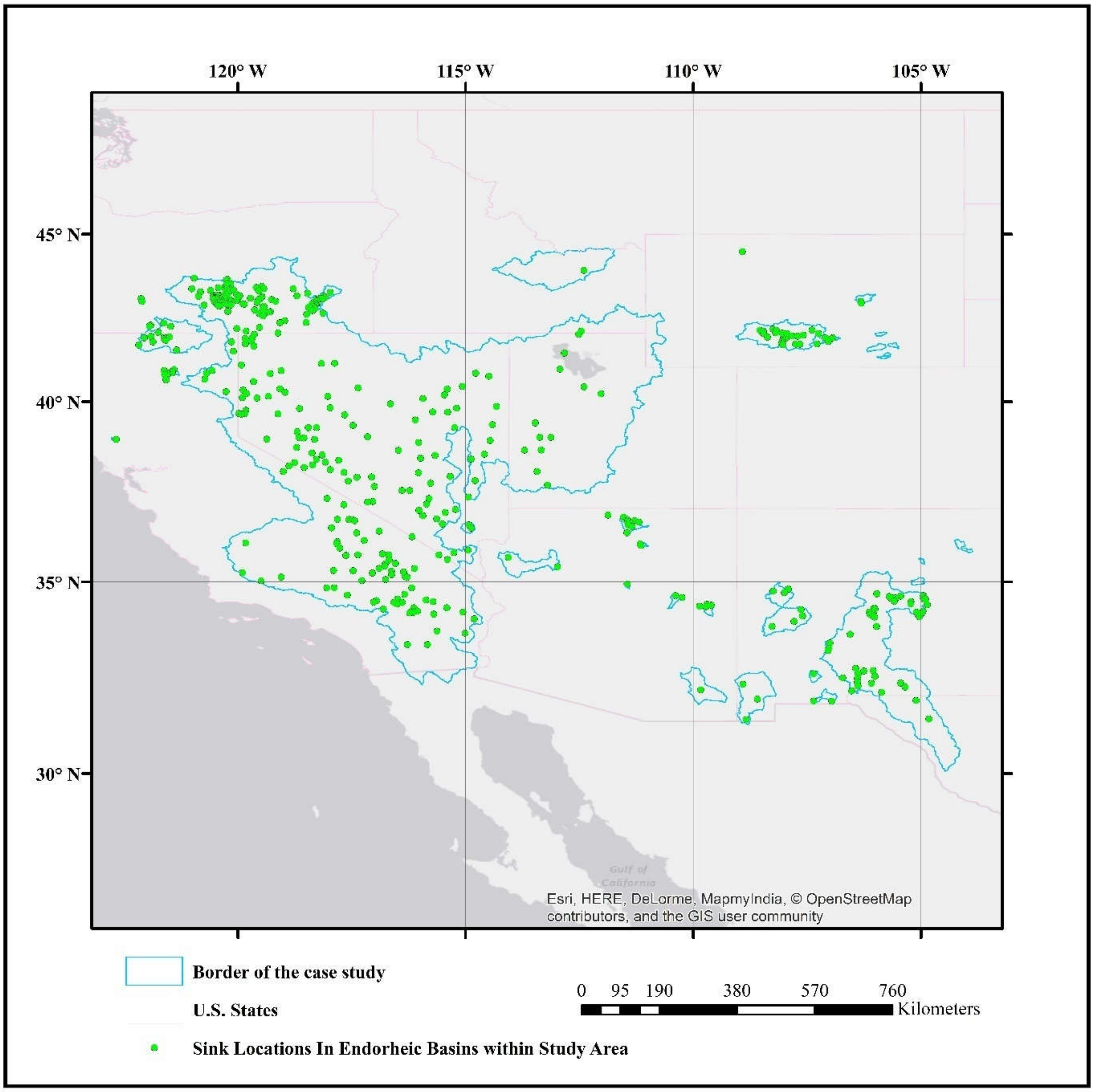

Figure 3. Case study and validation area in the endorheic western United States. This area includes a total number of 450 endorheic basins, where drainage sinks are illustrated by each green dot. Background image source: World Light Gray Canvas Basemap: Esri.

Chapter 4 - Software, Datasets, and Preprocessing

4.1 Software

ArcGIS and ENVI+IDL were the primary software programs used in this research. The parameters' values (Kernel Gamma and Kernel type) used in IDL coding were obtained from LIBSVM (Chang and Lin, 2011). Excel was used to interpret statistics of the results.

4.2 Dataset used

4.2.1 Landsat-8 imagery

In the first stage eight Landsat-8 OLI images (refer to Appendix A for more details), to cover all training areas, were used for framework development. Next, more than 300 Landsat-8 OLI images (refer to Appendix A for more details, with acceptable quality, were obtained during the driest month of years 2013 to 2015 for the entire case study in order to validate the framework by delineating salt pan extents at their maximal size and to mark the potential saline waters of the wet months. One challenge was obtaining cloud-free data in the defined time period (June 2013-2015) for the entire study area. A desired criteria that Landsat-8 images obtained were based upon was the selection of Landsat-8 images which had "cloud cover" (CC) value equal to zero and "cloud cover full" (CCF) less than 2.0.

4.2.1.1 Pre-process data for Landsat-8 imagery

The raw (digital number) Landsat-8 OLI data needs to be converted to surface reflectance in order to be able to obtain useful information related to the spectral information of features, and to compare the spectral signature of different features to those of salt. A signature is an object's expression on the image which allows the object to be detected (Floyd, 2007). Signature will be determined based on the characteristics of an object that controls its interaction with electromagnetic energy (Floyd, 2007). The spectral signature of a surface material is represented by a pattern of spectral brightness of the object at a specific wavelength of energy (Floyd, 2007).

Conversion of the raw data to reflectance data was done according to the metadata (gain factor, scale factor, and sun elevation angle) of each imagery using Equation 4 (http://landsat.usgs.gov/Landsat8_Using_Product.php): The top of atmosphere (TOA) reflectance with a correction for the sun angle is:

$$\rho\lambda = (\rho\lambda')/cos(\theta\_SZ\ ) \ = (\rho\lambda')/sin(\theta\_SE\ ) \tag{4}$$

Where $\rho\lambda$ is TOA planetary reflectance, $\rho\lambda'$ is TOA planetary reflectance, without correction for solar angle. Note that $\rho\lambda'$ does not contain a correction for the sun angle. θSE is Local sun elevation angle. The scene center sun elevation angle in degrees is provided in the metadata (SUN_ELEVATION), and θSZ is Local solar zenith angle; $\theta SZ = 90° - \theta SE$.

4.2.2 Climate datasets

In this study, precipitation and evaporation datasets were used to determine the driest month of the year for downloading Landsat-8 data. Monthly precipitation and evaporation data were explored from years 2013 to 2015. In order to account for uncertainty, five different evaporation datasets (Figure 4) and seven different precipitation datasets (Figure 5) through the years 2013 to 2015 were inspected.

Evaporation datasets obtained for this study are Global Land Data Assimilation System (GLDAS) products which generate a series of land surface state (e.g., soil moisture and surface temperature) and flux (e.g., evaporation and sensible heat flux) products simulated by different land surface models (https://ldas.gsfc.nasa.gov) as follows;

i) ERA-Interim reanalysis climate data archive (Dee et al., 2011) (European Center for Medium-Range Weather Forecasts; apps.ecmwf.int/datasets); ii) GLDAS VIC (Variable

Infiltration Capacity)(Rodell et al., 2004); iii) GLDAS CLM (Common Land Model)(Rodell et al., 2004); iv) GLDAS MLS (Mosaic Land Surface Model) (Rodell et al., 2004), v) GLDAS Noah (Rodell et al., 2004).

Precipitation datasets used in this study are;

i) GLDAS CLM; ii) GLDAS MLSM; iii) GLDAS Noah; iv) GLDAS VIC; v) CMAP (CMAP)(Xie and Arkin, 1997) (standard monthly mean;www.esrl.noaa.gov/psd/data/gridded/data.cmap.html); vi) GPCC (Global Precipitation Climatology Centre) (Schneider et al., 2011) (www.esrl.noaa.gov/psd/data/gridded/data.gpcc.html); vii) PREC/L (Precipitation Reconstruction over Land (Chen et al., 2002) (monthly mean; www.esrl.noaa.gov/psd/data/gridded/data.precl.html).

In order to derive the driest condition during the studied three years, net water budget (precipitation minus evaporation) (Figure 6) was obtained for three years. To summarize the results and discover the driest month in all three years of the study, average monthly evaporation and precipitation datasets (Figures 7 and 8) was calculated to achieve the averaged net water budget of all three years (Figure 9). The standard deviations associated with each month set June as the driest month of the studied three years.

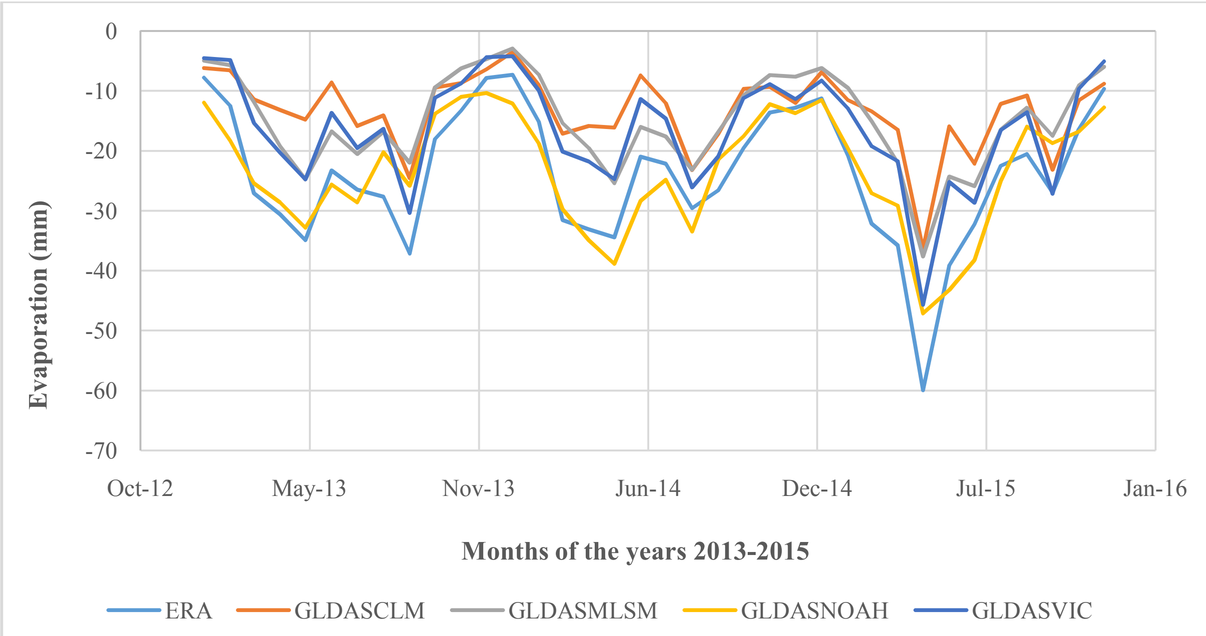

Figure 4. Monthly evaporations during 2013 to 2015.Evaporation datasets (mm) include; Global Land Data Assimilation System (GLDAS VIC ERA, GLDAS CLM,- GLDAS MLSM, GLDAS Noah, GLDAS VIC).

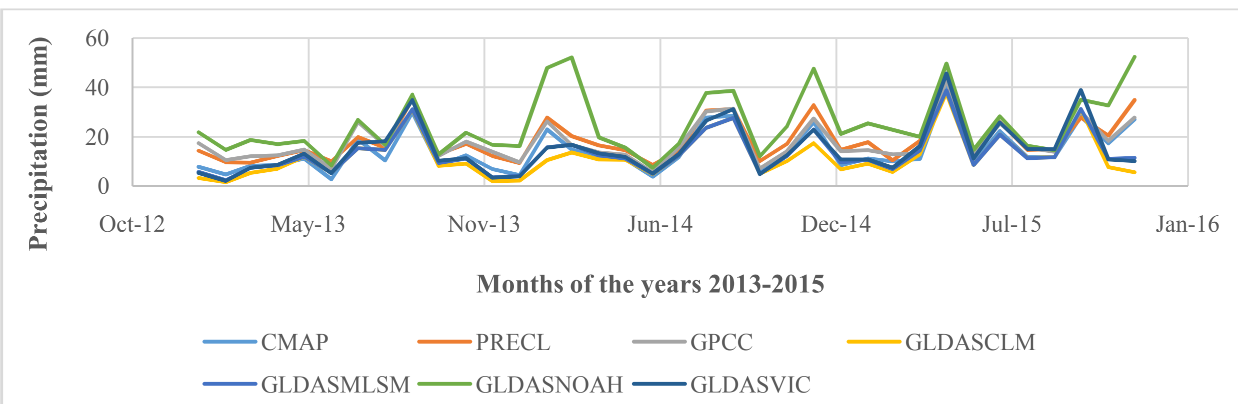

Figure 5. Monthly precipitations during 2013 to 2015.Precipitation datasets (mm) include; Global Land Data Assimilation System (GLDAS), The CPC Merged Analysis of Precipitation (CMAP), Precipitation Reconstruction Land. High quality station gauge measurements are used to provide land grid points. These data also have near real-time updates (PRECL), Global Precipitation Climatology Centre (GPCC).

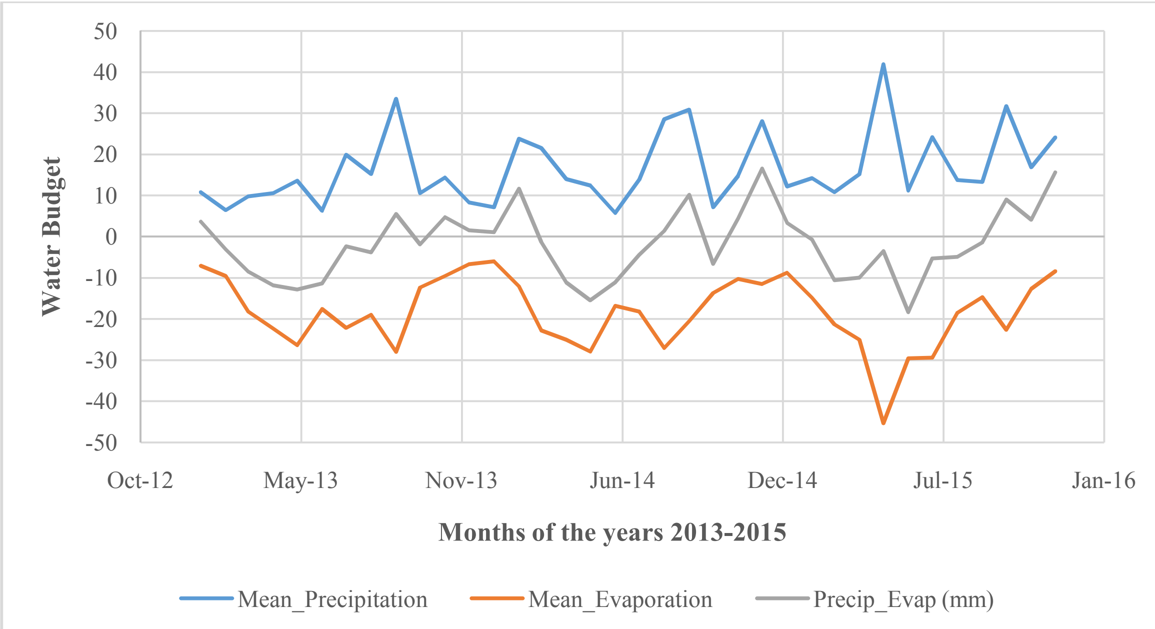

Figure 6. Monthly water budgets during 2013 to 2015.

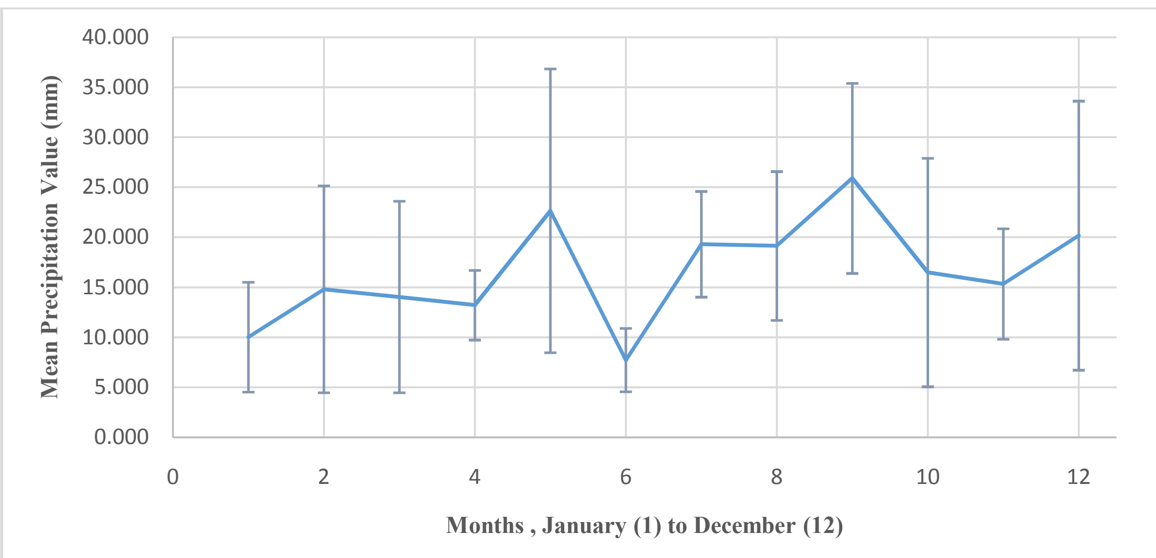

Figure 7.Mean monthly precipitations during 2013 to 2015.Error bars represent standard deviations. In this average annual cycle, the highest precipitation occurs in September and the lowest precipitation occurs in June.

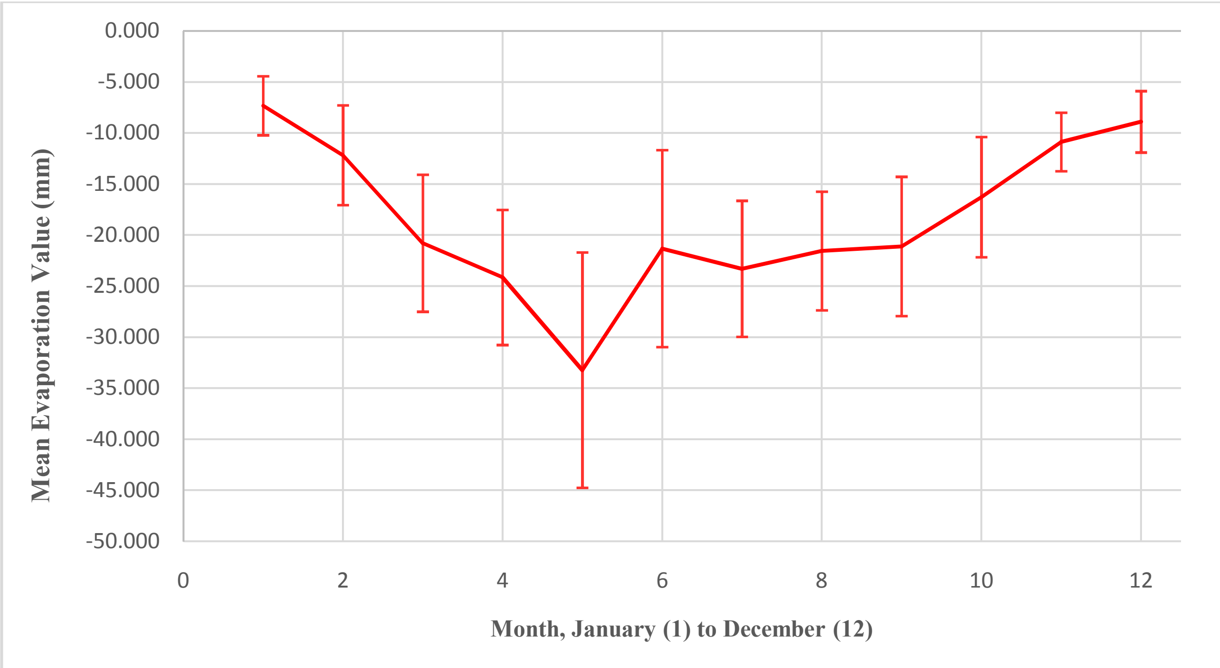

Figure 8. Mean monthly evaporations during 2013 to 2015. Error bars represent standard deviations. In this average annual cycle, high evaporation tends to occur in May and June.

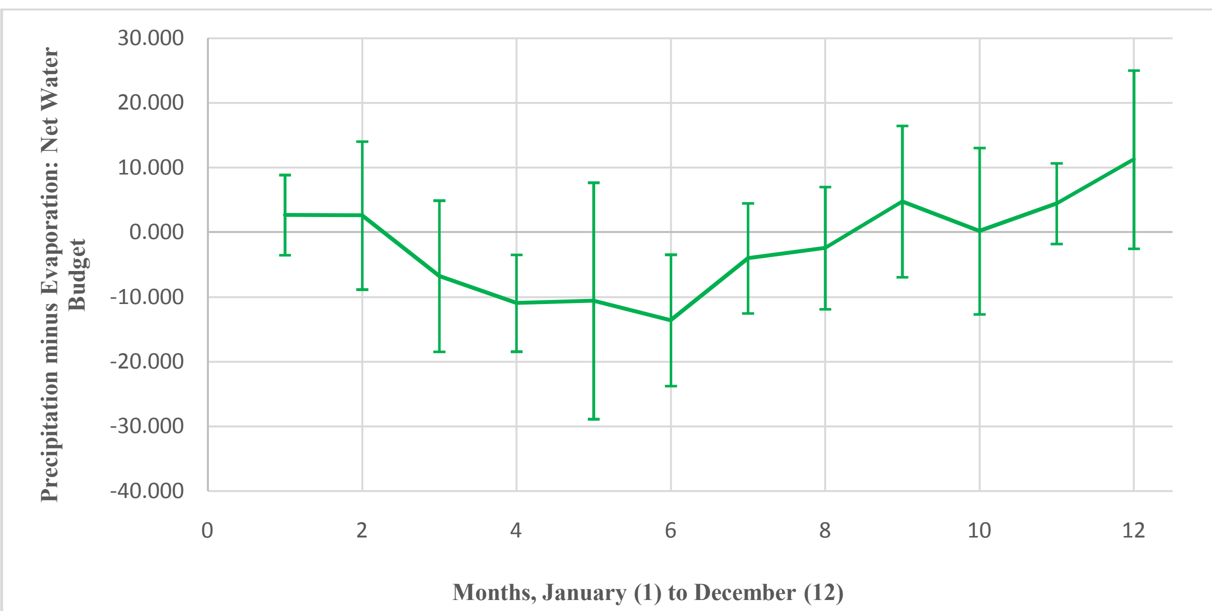

Figure 9. Mean monthly water budgets during 2013 to 2015. In this average annual cycle, the lowest water budget occurs in June.

4.2.3 Auxiliary datasets

The following datasets are used in this study to automatically perform quality assurance/ quality control (QA/QC); i)USA urban areas shapefile (http://www.arcgis.com/home/item.html?id=069b5cafe3e34a2585e24ba63cd12b9e)(called Esri urban shapefile in this study) to remove urban areas; ii) 90 meter resolution Shuttle Radar Topography Mission (SRTM) Digital Elevation Model (DEM) data set (http://www.cgiar-csi.org/data/srtm-90m-digital-elevation-database-v4-1) to remove snow and clouds; iii) National Land Cover Database (NLCD2011 edition) (https://www.mrlc.gov/nlcd11_data.php) to remove urban and impervious areas (classes 22, 23, and 24); iv) The 15-second HydroSHEDS drainage basin dataset (Lehner, Verdin, and Jarvis, 2008) (www.hydrosheds.org) was used to be able to discrete each drainage basin for the statistical analysis of the results.

Chapter 5 - Methodology

This chapter provides detailed information about the process of mapping saltpans and salt playas during this study. Figure 10 is provided for a quick view of the methodology.

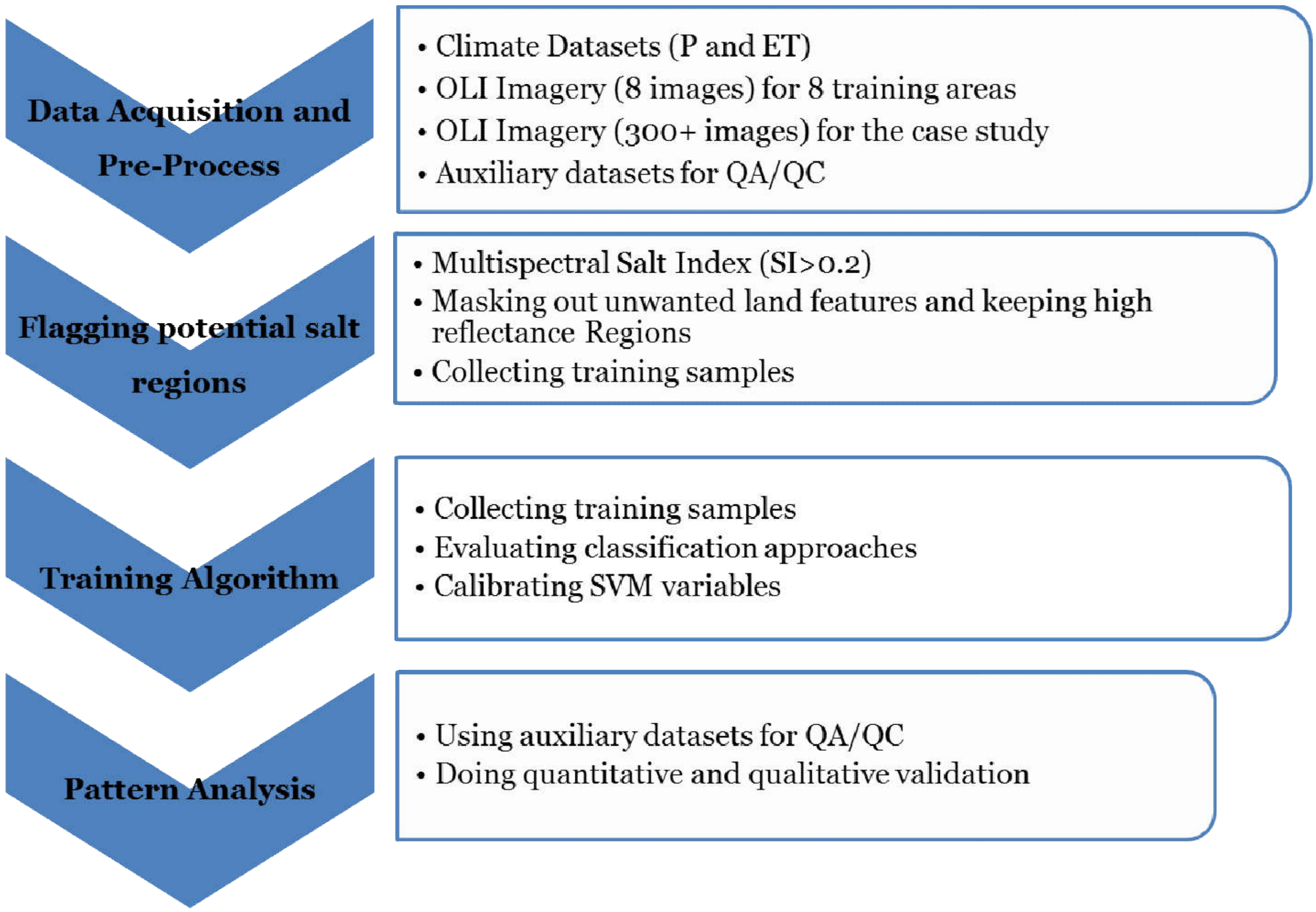

Figure 10. Methodology overview

5.1 Algorithmic development motivation

The most important reason to develop a single framework of mapping salt pans and salt playas is to provide highly accurate maps efficiently. In previous studies some of the indices suggested to map salt affected areas did not include a single technique applicable to multiple locations. Providing a simple mapping framework is currently needed to map salt pans (with different chemicals) on multiple locations.

5.2 Defining a multispectral index for potential salt regions

Supervised classification, requires quantitative information from the land cover classes of interest based on sampling information of classes (training data set) (Rees, 2006) which emphasizes the need of having prior knowledge about classes. Next, signature analysis will be possible by using comprehensive training sites' statistical information to characterize the reflectance of each class. This allows us to design a single index useful to flag potential salt pixels including different kinds of salts across the continental surfaces of the earth.

Due to different salt chemicals in different locations, indices used in the previous studies were not accurate in highlighting salt pixels in several locations. Therefore, identifying high reflectance regions where salt pans may occur was done to easily collect training samples. To do so, first it was necessary to create a spectral signature of different land features based on their mean value of surface reflectance in bands 2 to 7. These features were used to characterize salt compared to other land features such as soil, water, and vegetation (Figure 11). The reason for using bands 2-7 was that bands 1, 9, and Q do not contain useful information for the focus of this study.

Based on spectral behavior of different types of salt an index works more successfully in highlighting salt pans in different locations of the earth, compared to the suggested indices in previous studies. The designed Index in this study was the mean value of bands 2 to 4, which highlights all salt chemicals:

$$SI = (band2 + band3 + band4)/3 \quad (5)$$

Where: *band2* is the blue (B) region of electromagnetic spectrum, *band3* is the green (G) region of electromagnetic spectrum, and *band4* is the red (R) region of electromagnetic spectrum.

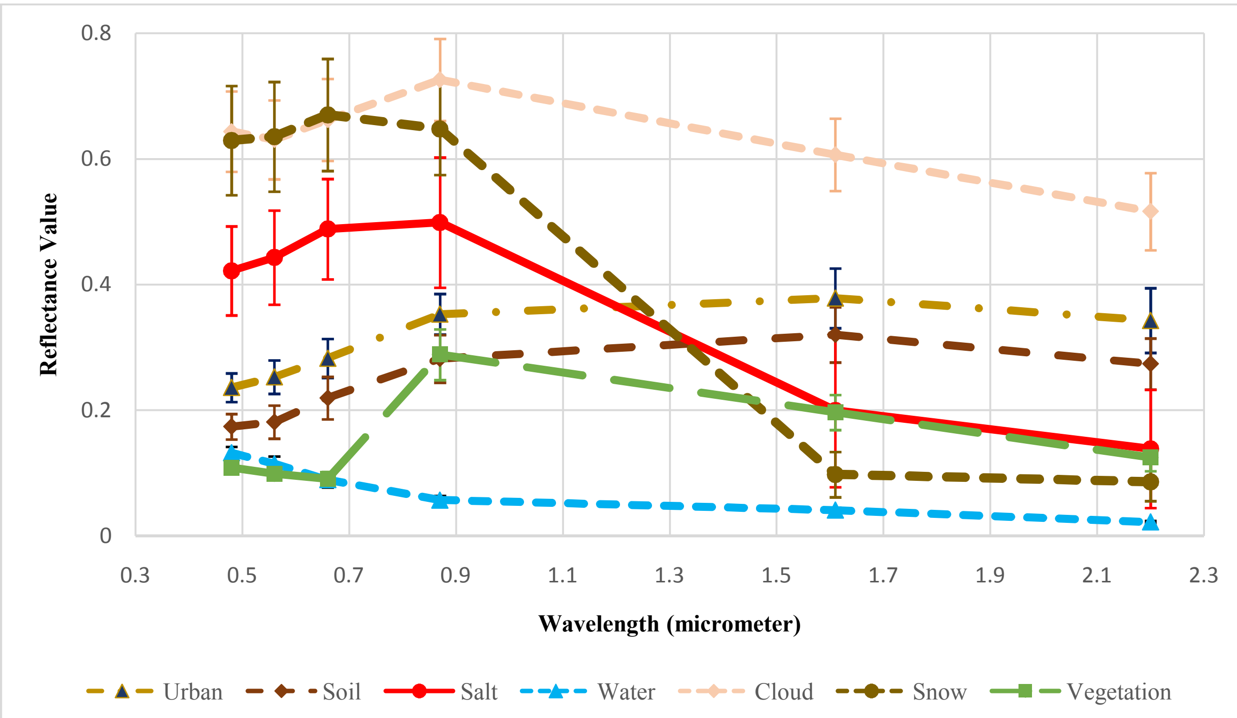

Figure 11. Mean values of spectral reflectance of different land features across all training areas.Values in the x-axis represent band 2 to band 7 for Landsat-8 OLI images.

The next step would be masking unwanted features such as water and vegetation in order to narrow down and flag potential salt pixels. An important parameter in this part was to determine a single threshold value creating histograms, by using pixel values of features in a single region of interest (ROI), for each training area (Figure 12).

According to the density graph created for each TA (Figure 12)based on SI values for each location and frequency of reflectance for different land features, the most appropriate threshold value for separating salt from other features is 0.2, which can mask out undesired features across all training areas. In other words, the values greater than or equal to 0.2 existing on the SI image (Figure 13 panel b) contain unwanted land features such as vegetation, water, and some kinds of soil which should be eliminated in order to flag potential salt pixels and delete non-salt features (Figure 13 panel c).

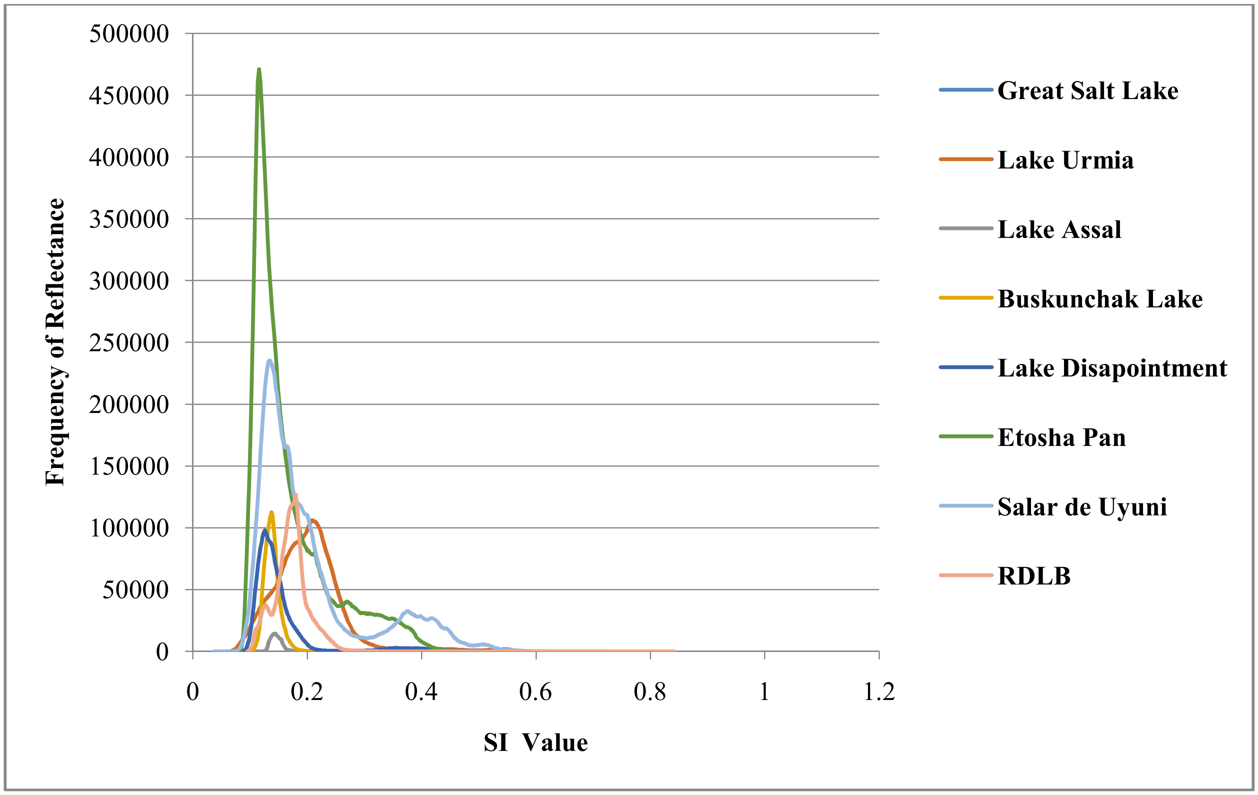

Figure 12. Distribution of SI values for each training area. Pixels with lower reflectance tend to cluster with SI values lower than 0.2. In the other word, SI values higher than 0.2 have higher reflectance and are more likely to belong to salt land features and can be masked out.

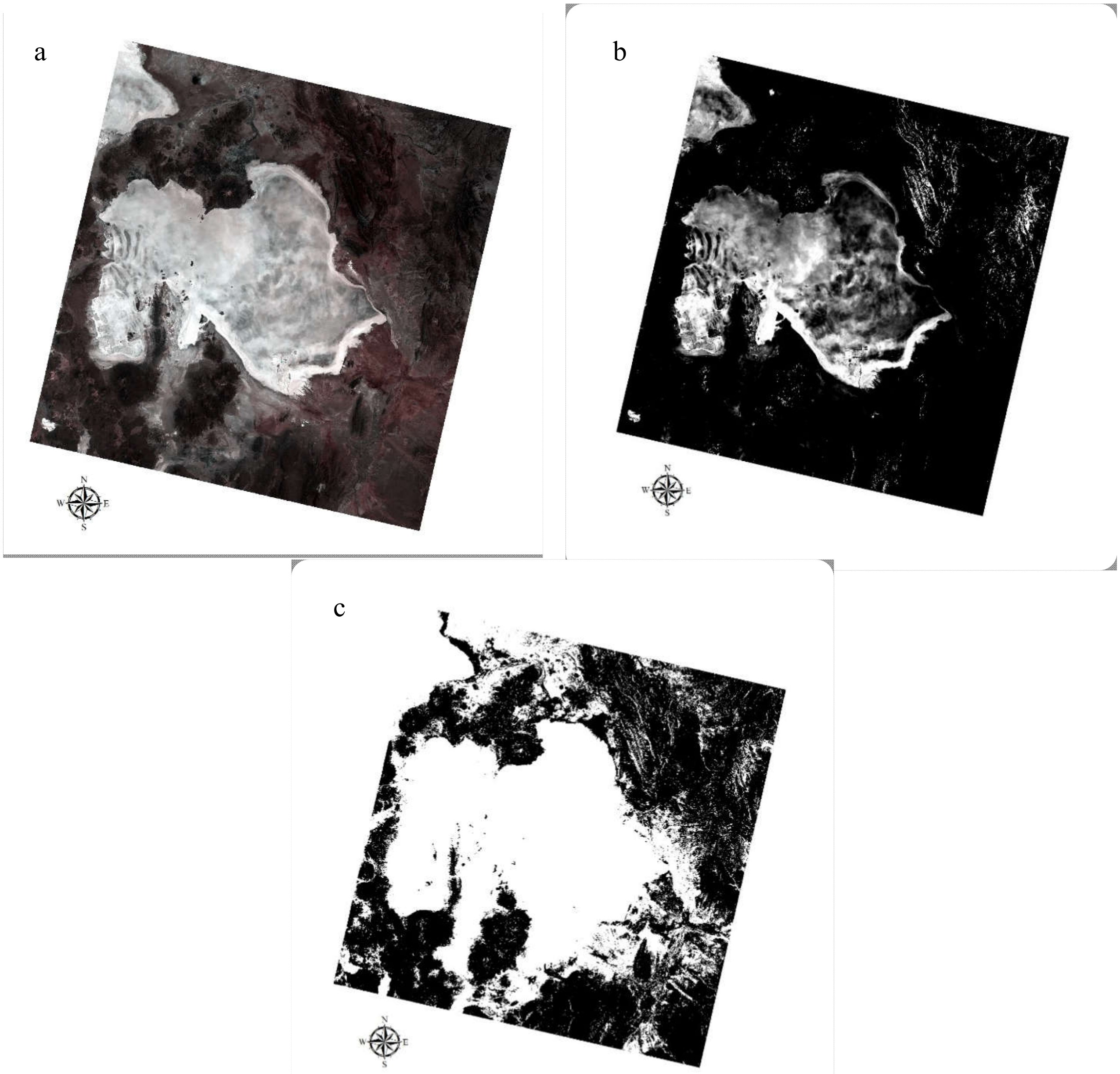

Figure 13. Landsat-8 OLIscene (TOAR) above Salar de Uyuni Salt Pan (Panel a), SI image (Panel b) applied on TOAR imagery, Masked image (Panel c) showing flagged potential salt pixels derived from panel c.

5.3 Evaluating different classifiers

There are several classification methods which are tested during this research to map salt pans across the continental surfaces of the Earth.

Different parametric methods of classification for all training areas were examined, but each of them has accuracy issues in extracting salt-affected regions. Function of parametric classifier works using probability of statistical distribution of each class (Yugal and Sahoo, 2012). Classifications are done on Landsat-8 OLI top of atmosphere reflectance (TOAR) imagery (Figure 13, panel a).

5.4 Building a comprehensive spectral library

Due to the similar spectral behavior of some types of salt to those of soil there are difficulties in masking non-salt features. Furthermore, according to several experiments during this study, it can be concluded that salt is prone to be confused in terms of spectral behavior with other features such as snow, clouds and some kinds of soil. Therefore, to separate salt from the aforementioned features, building spectral libraries for both soil and "non-salt" can be useful and it will accelerate the process. To build spectral library (training data) sampling both features ("salt" and "non-salt" pixels) within non-masked areas was done. According to the trials of this study it can be concluded that having more sampled pixels of salt in the same continent increases the accuracy of the results.

Another strong reason for building SPL, according to Howari et al. (2002) and the results of this study, is to cover different types of salt which have different spectral behaviors due to their chemical composition (Figure 16).

By comparing spectral signatures of different types of salt (Figure 14) located in eight training areas to those of Howari et al. (2002) (Figure 1) it can be judged that Urmia Lake is mostly covered by halite, and Etosha Pan is covered by gypsum. Lake Assal's dominant chemical is gypsum. Rosamond Dry Lake is covered by about 50 percent of gypsum, at least. It can be inferred based on the aforementioned results that Lake Disappointment is likely to be a source of halite, and according to Bastrakov et al. 2013 it is also a source of potash KO2 (Bastrakov et al., 2013).

According to Kucera, 1984 Baskunchak Lake provides halite. According to its spectral reflectance compared to Figure 1, however, it should not contain only halite. The topsoil composition of Great Salt Lake includes mirabilite, halite, sulfides, carbonates, gypsum, and clays (Jones, 2008). It is not easy to fit Salar de Uyuni's spectral signature to a spectral signature represented in Figure 1 due to the variety of chemicals existed in this area. According to Ericksen, 2012 Salar de Uyuni contains widespread lithium-rich brines which are basically saturated with halite (with highly sulfated, but scantly carbonated) (Ericksen, 2012). Potassium and magnesium values are relatively high (Ericksen, 2012).

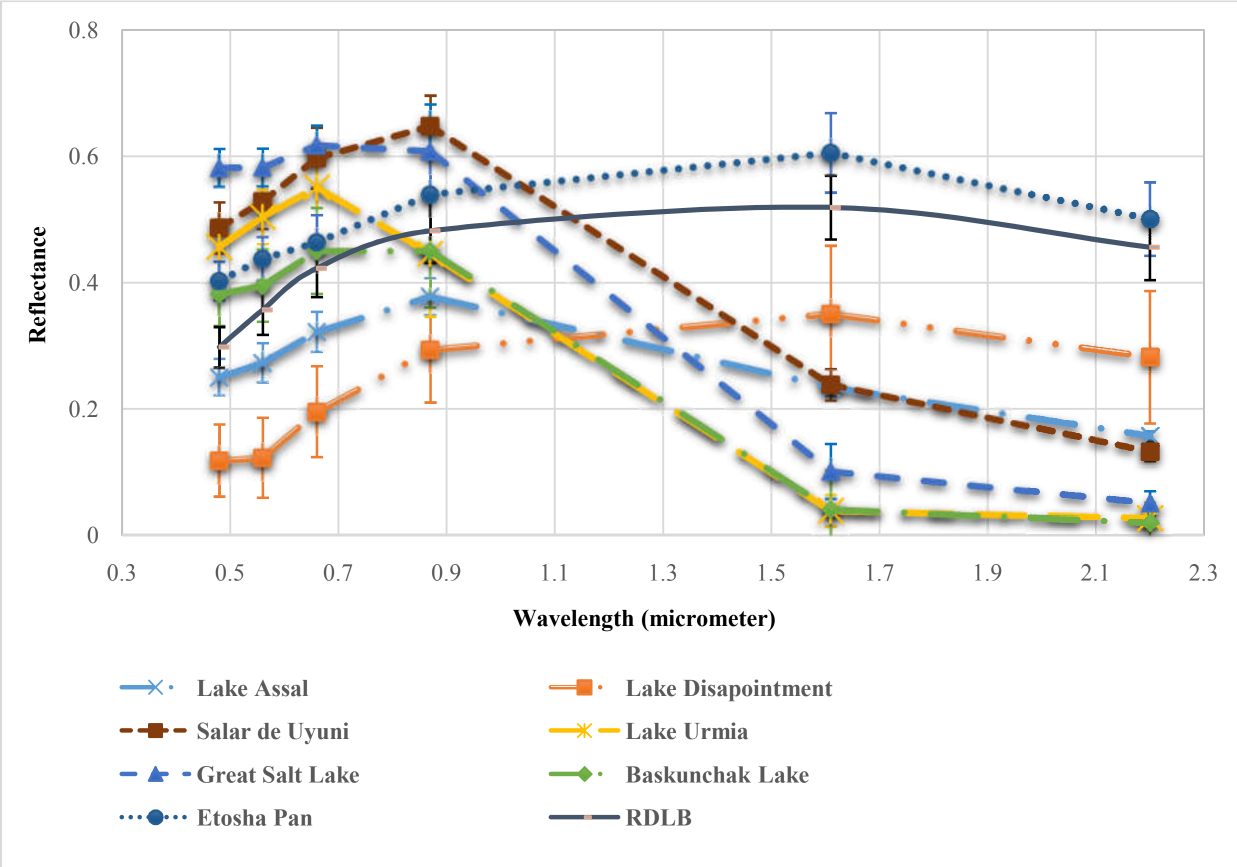

Figure 14. Mean values of spectral reflectance of different salt chemicals across all training areas.

Generally saline soil has higher spectral reflectance in visible and NIR regions compared to non-saline soil (Wu et al., 2014). Therefore, the more salt exists in the soil, the more spectral reflectance will result (Metternicht and Zinck, 2003; Rao et al., 1995). Furthermore, moisture in the salt-affected soil decreases spectral reflectance of the surface in the middle-NIR, and near-NIR shows unreliability of vegetation indices due to the misinterpretation of salinity (Wu.; et al., 2014).

In this study the function of the framework at different regions was examined using eight training areas. The developed algorithm was selected based on the accuracy of the resultant maps upon which all TA training was based.

Based on the results of classifiers (Figures 18- 20) and figure 12 (spectral reflectance of different land features) it was concluded that some kinds of salt are not easily distinguishable from other land features such as soil using the aforementioned approaches due to the similar spectral behaviors of salt and soil, and also due to the varying spectral behaviors of different salt chemicals (Figure 16).

The band values of salt and non-salt features were obtained within the unmasked regions (white pixels) of the mask imagery (Figure 15, white pixels) for all training areas. Stratified sampling was done to select training data (4000 pixel values for each class, salt and non-salt, for all sample locations to create spectral libraries for both salt and non-salt features (Figure 15). The reason for limiting training data is because; i) SVM does not necessarily require a big data-set (overfitting) to have the best function, and ii) using fewer training samples decreases the computation time for such a huge area and number of Landsat-8 images. To test the function of the spectral library, first about 20 pixels were used to create a spectral library for each land feature (salt and non-salt). Then more sampled pixels used for this purpose were tested. Figure 17 shows the result of SVM classifier using 4000 pixels of training samples across the training areas.

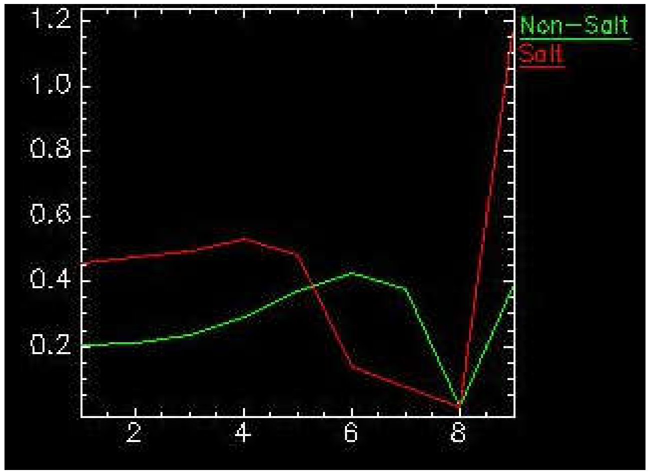

Figure 15. Generated spectral library (training samples) for salt and non-salt features using 4000 pixels for each class. Reflectance values of each band of Landsat-8 imagery within masked imageries of all training areas are used for this purpose. Red line represents the average spectral behavior for salt and green represents spectral behavior of non-salt. This graph is a screen shot generated from the software ENVI.

With that said the developed index (mean of RGB bands) and mask are helpful to highlight salt pixels across the TAs. The information of bands 2 to 7 are recorded in the training samples and accordingly (bands 2-7 values) the salt-affected surfaces in the case study can be mapped.

We assume that created training samples are applicable to other multispectral images such as TM and SPOT images.

5.5 Training SVM

The goal of SVM is to find the best linear function that separates classes (Melgani and Bruzzone, 2004). The best function of SVM is maximizing the margin between classes and minimizing the chance of having noise and errors in the result (Melgani and Bruzzone, 2004). SVM has been found as a highly accurate classifier rather than other classification techniques such as Maximum Likelihood and the Multilayer Perceptron Neural Network (Melgani and Bruzzone, 2004). Furthermore, SVM provides highly accurate results with little required training data (Hermes et al. 1999; Melgani and Bruzzone, 2004). In order to use SVM along with the created spectral library (training data) SVM parameters need to be optimized. “LIBSVM” is used to find the optimal values for SVM parameters (e.g., kernel values). The scaled training data used for spectral libraries produced better results compared to non-scaled training data in separating salt from non-salt. Due to the accurate and reliable performance of the radial basis function it is commonly used as kernel function (Chao and Horng 2015). In this case the value of kernel function equals two (Chang and Lin 2011). Other parameters such as Optimal Penalty and Gamma values in Kernel function were set according to LIBSVM based on the created training data (refer to Appendix D). Optimal Scaled Kernel Values were derived from LIBSVM using 4000 Pixels obtained from eight training areas for each class (salt and non-salt). The derived optimal Gamma parameter is 0.5 and the derived optimal Penalty parameter is 8.

5.6 Quality assurance/ quality control

After achieving accurate results on a specific TA, the framework was tested on the other training areas and it provided reliable results. There is some confusion in distinguishing salt from other land features (tables 2 and 3) in the results which should be tackled in this study. The performance of the developed framework will be demonstrated in the next chapter (Results). Next, the framework was applied on the case study and provided a highly accurate salt pans map.

In this research posterior quality assurance/ quality control (QA/QC) was done on the raw results of the developed framework automatically using auxiliary datasets (refer to Chapter 5 for detailed information of datasets).

Quantitative and qualitative validations were done on the resultant maps to inspect the accuracy and reliability of the framework using auxiliary datasets. In this study qualitative QA/QC was done on some regions which at first glance did not look to be salt-affected. The

United States Department of Agriculture(USDA) Natural Resource Conservation Service was utilized to do qualitative analysis validation in this study (obtaining surface texture information) (https://websoilsurvey.sc.egov.usda.gov/app/WebSoilSurvey.aspx). Confusion matrix and Kappa statistics were used in the quantitative validation stage to prove the reliability of the results. Both quantitative and qualitative validations demonstrated high accuracy of the developed framework.

To do noise removal from the results of the developed framework within the case study area, auxiliary datasets utilized and all mutual areas between resultant map and auxiliary datasets were deleted in ArcGIS. Esri urban shapefile was used to eliminate urban areas from the results. In order to use the 90-meter resolution SRTM DEM data-set to remove snow, a slope-map was created in ArcGIS. Classifying the ground slopes is useful to determine the slope analysis of the area (Anderson, 2000). The created slope-map was reclassified to five classes based on the following categories of land slope which is considered in many areas as follows; i) 0 – 3 percent is flat; ii) 3 – 10 percent is moderately sloping; iii)10 – 15 percent is hillside; iv) 15 – 30 percent is steep hillside; v) over 30 percent is very steep (Anderson, 2000). Since the existence of snow in June is more likely to occur in high elevations (e.g., mountains and high slopes), the last category was kept to snow removal. The subsequent slope file (obtained from SRTM DEM files) was useful to illustrate the snow-covered areas and manual snow removal was done based on the illustrations, to not miss valuable data of salt pan areas from the results. NLCD (2011 edition) within the border of the case study was reclassified to remove infra-structures, parking lots, and impervious area from the results (Table1). As the last step, manual QA/QC was needed to remove omission errors.

Table 1. Specific Classes used in this study to recognize impervious surfaces, obtained from NLCD 2011 classification scheme (modified from the Anderson Land Cover Classification Scheme)(https://www.mrlc.gov/nlcd11_data.php).

Class\Value	Classification Description
22	"**Developed, Low Intensity-** areas with a mixture of constructed materials and vegetation. Impervious surfaces account for 20% to 49% percent of total cover. These areas most commonly include single-family housing units."
23	"**Developed, Medium Intensity** -areas with a mixture of constructed materials and vegetation. Impervious surfaces account for 50% to 79% of the total cover. These areas most commonly include single-family housing units."
24	"**Developed High Intensity**-highly developed areas where people reside or work in high numbers. Examples include apartment complexes, row houses and commercial/industrial. Impervious surfaces account for 80% to 100% of the total cover."
31	**"Barren Land (Rock/Sand/Clay)** - areas of bedrock, desert pavement, scarps, talus, slides, volcanic material, glacial debris, sand dunes, strip mines, gravel pits and other accumulations of earthen material. Generally, vegetation accounts for less than 15% of total cover."

Chapter 6 - Results

6.1 Results of evaluating different classifiers in training areas

Parallelepiped was the first evaluated approach as one of the simplest and fastest supervised classification methods. However, this approach is not capable of differentiating pixels located in overlapping parallelepipeds or outside a parallelepiped (Souri et al., 2012). The results represent poor performance in delineating salt regions. Parallelepiped (Figure 16 panel a) left many pixels unclassified (white parts in Figure 16 panel a). Minimum distance to the mean was the next approach to be tested. In this approach a sample is classified into the class whose estimated distribution is the most similar estimated distribution (in terms of distance in the space of distribution function) of the sample to be classified (Wacker and Landgrebe, 1972). Results of the minimum distance classifier shows a high level of confusion between salt and non-salt features such as water and soil (Figure 16 panel b). The Maximum Likelihood approach, a supervised classification method, shows inaccurate results as well (Figure 16 panel c). This approach is time-consuming due to the need of sampling training data on each imagery.

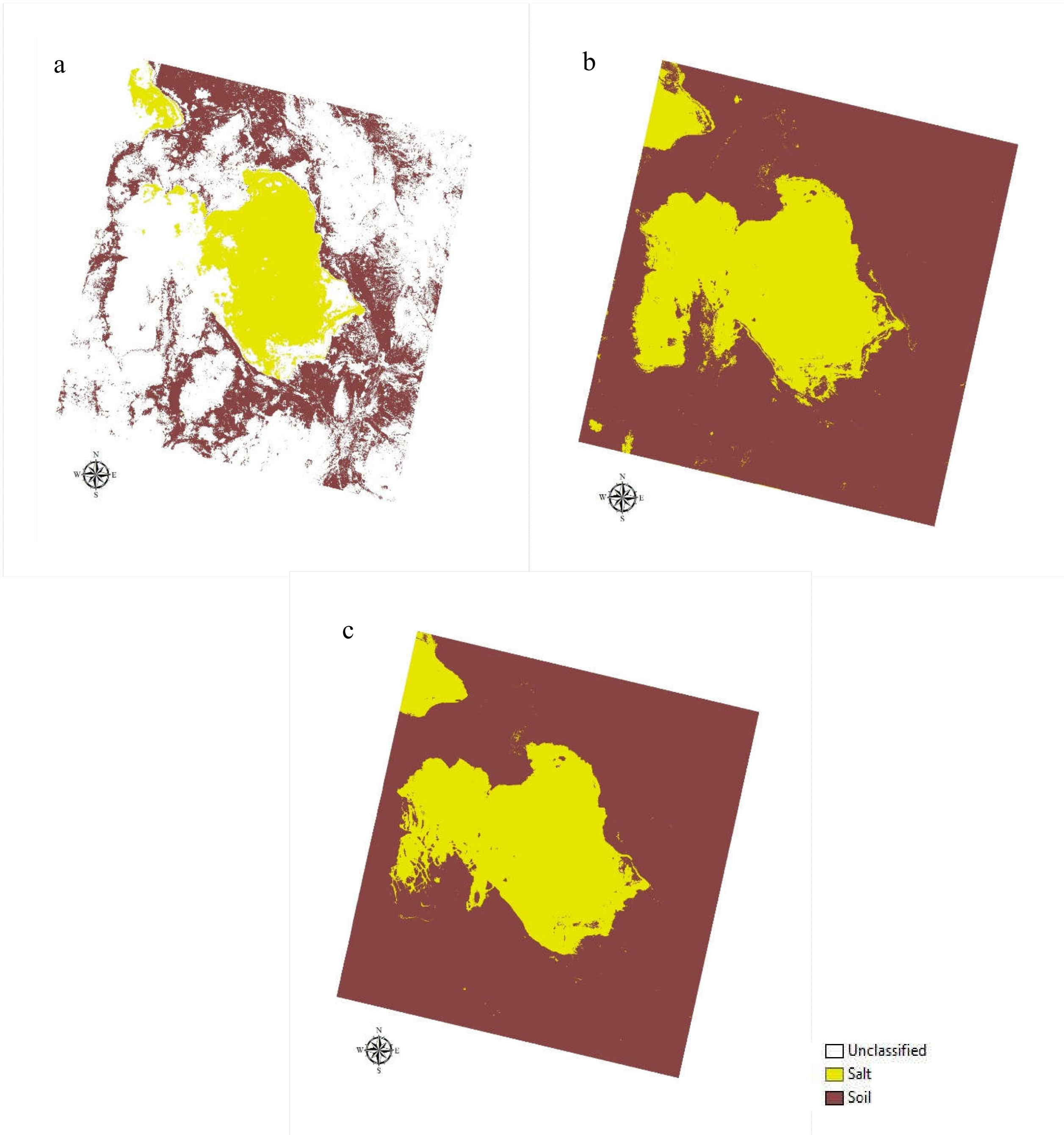

Figure 16. Results of different classification algorithms on Landsat-8 OLI above Salar de Uyuni salt pan (figure 13 panel a); parallelepiped performance (panel a), minimum distance to the mean performance (panel b), maximum Likelihood performance (panel c).

Accuracy assessments were not done on the results of the aforementioned classification approaches, due to their poor performance in delineating salt pan areas located in training areas.

6.2Raw results of framework application

Performance of the developed framework was highly accurate across all training areas. Figure 17 displays obtained results of the developed framework to map salt pans across the training areas, before doing QA/QC. The results represent the framework's strong ability in delineating salt pans.

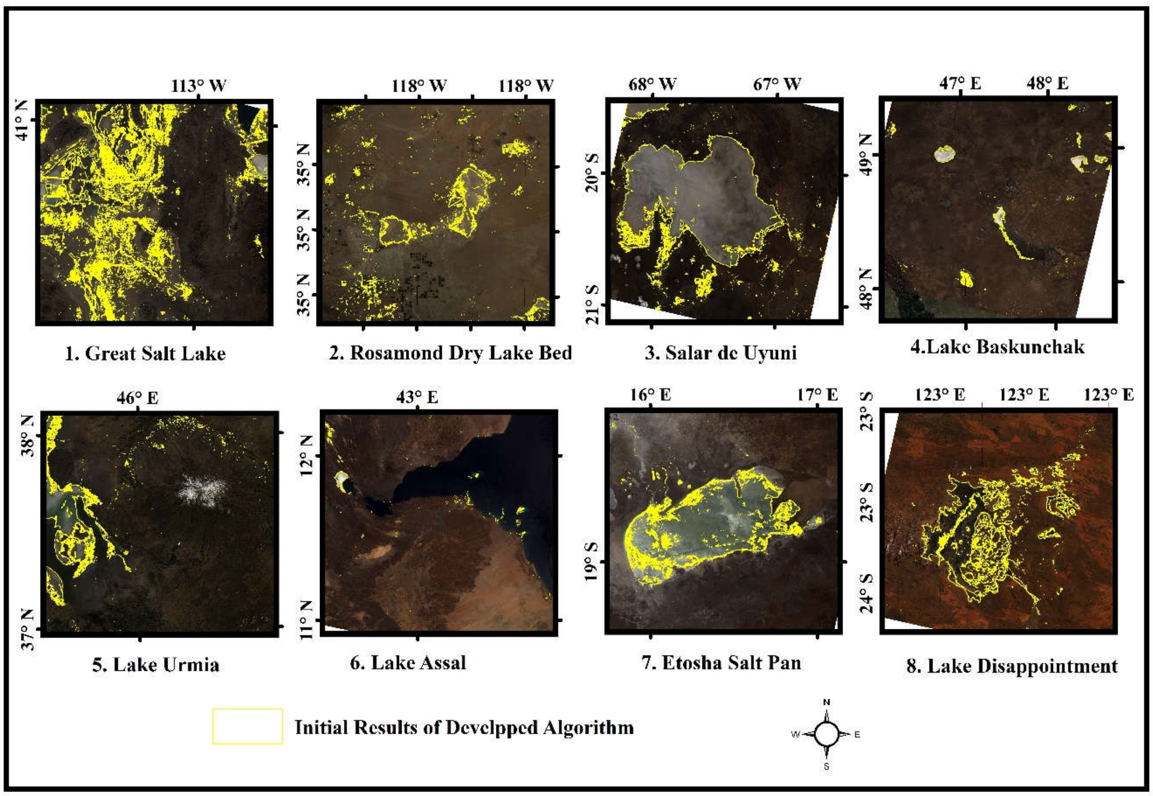

Figure 17. Initial results of the developed framework in each training area. Background image source: Landsat-8 Imagery Natural Color Display (Appendix C).

The results before applying QA/QC (initial results), and after applying QA/QC (final results)are shown in figures 18 and 19. The entire case study area involves 450 endorheic basins

(698,999.8 km^2 in total) in which a total area of 7700 km^2 is mapped as salt pans. In other words about 1.1015 percent of the entire study area is covered with salt pans (the detailed calculated areas are shown in table 1).

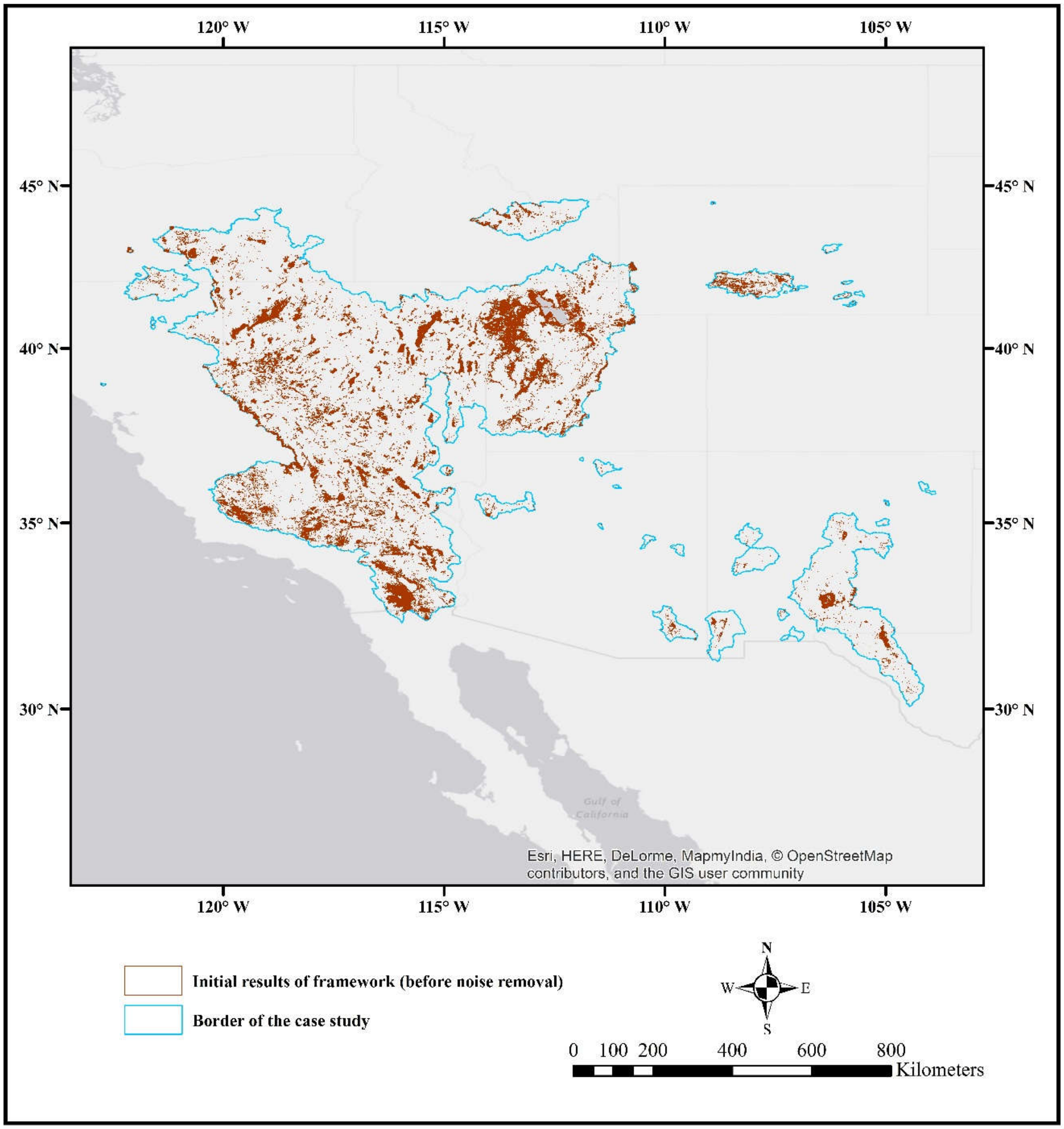

Figure 18. Initial results of the developed framework before QA/QC. This map shows confusion in separating salt from urban, snow (e.g., left margin of the border), and clouds. Background image source: World Light Gray Canvas Basemap: Esri.

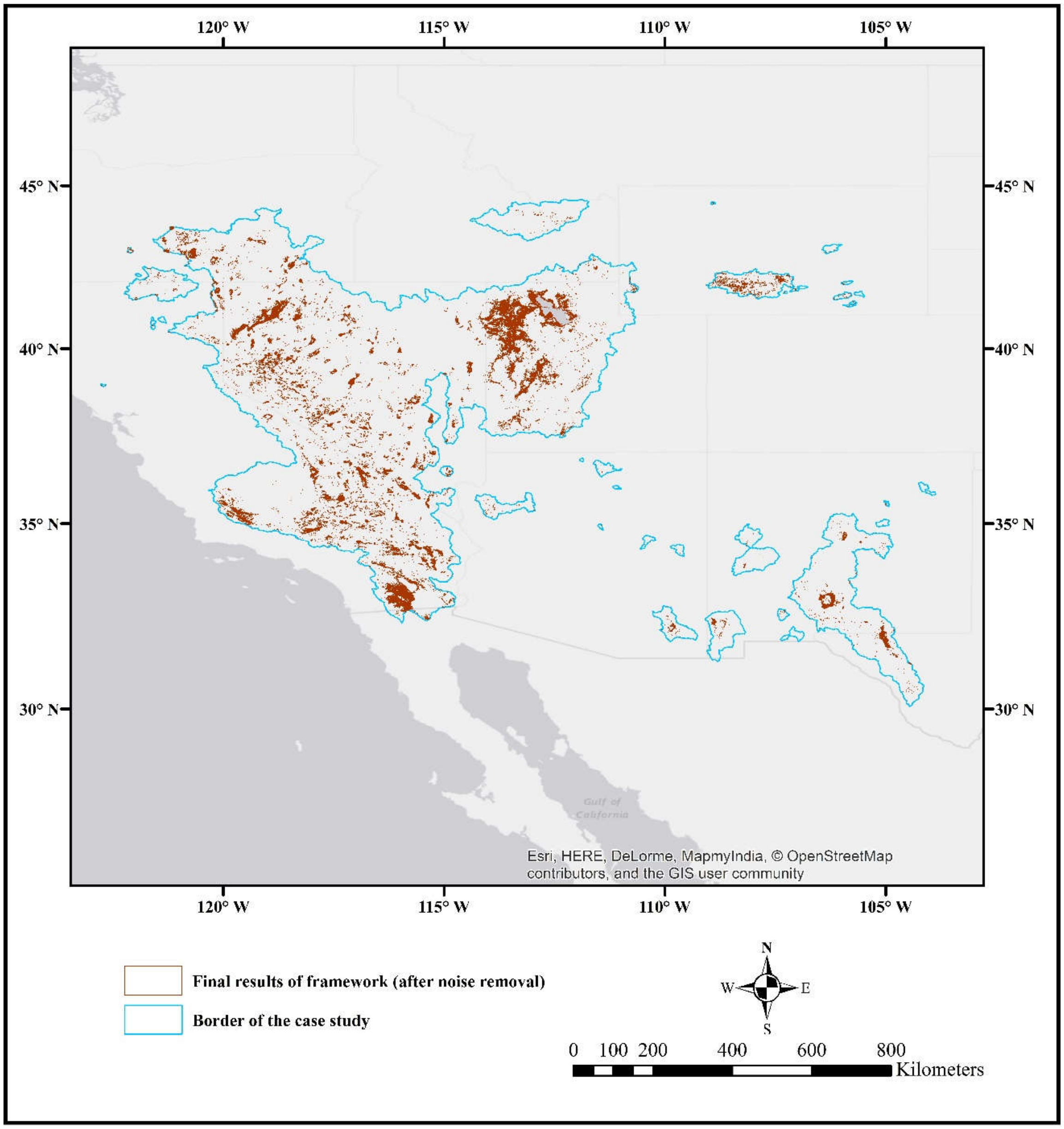

Figure 19. Final results of the developed framework (salt pans dataset) within the case study area after doing QA/QC.1.10 percent of the entire case study area is covered by salt. Background image source: World Light Gray Canvas Basemap: Esri.

6.3Result validation in the case study

According to the quantitative and qualitative results, the developed framework provides valid maps of salt pans/ playas across the continental surfaces of the Earth.

6.3.1 Quantitative validation (confusion matrix)

A standard practice for accuracy assessment is using reference data with higher resolution than the map classification (Braget, 2017). However, the reference data used for accuracy assessment are the same Landsat-8 images used in this study to examine the accuracy of the algorithm function. An overall accuracy of 99.95% is obtained for the developed algorithm. Because of the high overall accuracy, which represents the probability of classifying a randomly selected point correctly (Braget, 2017), it can be concluded that the high probability of a randomly selected point shows that SVM provides acceptable performance in classifying salt pans in the study area. User's accuracy represents the probability of correctly classifying a referenced pixel, and procedure accuracy represents the probability of a pixel on the map representing the same category on the ground (Braget, 2017). In order to do QA/QC, an area of 643,887,468.65 m^2 (about 715,430 pixels) for salt, and 4,166,956,215.56 m^2 (about 4,629,950 pixels) for non-salt were randomly generated across the case study. Before QA/QC, obtained accuracy of the developed framework was 97.97% (Table 2). According to the results of QA/QC, 100% of salt pixels have been classified correctly and 2.92% of non-salt pixels have been classified incorrectly (2,690 pixels classified as salt). Obtained accuracy of the framework is 99.95% (Table 3). According to the results (both before and after QA/QC) it is concluded that the developed framework performs with high accuracy and reliability.

Table 2. SVM confusion matrix before QA/QC

Class	Class types obtained from Landsat-8		Totals	User's Accuracy
	Salt (pixel)	Non-salt (pixel)		
Salt (pixel)	715430	135124	850554	84
Non-salt (pixel)	0	4494826	4494827	100
Totals	715430	4629950	5345381	
Procedure Accuracy	100	97		**Overall 0.97**

Table 3. SVM confusion matrix after QA/QC

Class	Class types obtained from Landsat-8		Totals	User's Accuracy
	Salt (pixel)	Non-salt (pixel)		
Salt (pixel)	715430	2693	718123	99.62
Non-salt (pixel)	0	4627257	4627257	100
Totals	715430	4629950	5345380	
Procedure Accuracy	100	99.94		**Overall 0.99**

6.3.2 Kappa statistics

Kappa is an evaluation technique to ascertain the effectiveness and success of a model (Pontius, Cornell, and Hall, 2001), and therefore it is considered in this study. Kappa analysis can examine whether a generated land-cover map using remotely sensed data is accurate or not (Pontius et al., 2001). Kappa ranges from -1 to 1, representing a correlation between classification and reference data. A Kappa value of 1 represents perfect agreement, and 0 represents chance agreement (Viera and Garrett, 2005). The Kappa coefficient provides a measure of difference between the observed agreement between classifier and the reference data used to execute the classification against the probability of agreement between the reference and random classifier (Adam et al., 2014).

The Kappa score obtained for the developed framework before QA/QC is 0.899, and after QA/QC the developed framework's Kappa score obtained was 1, which verifies high reliability and correlation of the developed algorithm between the classification results and reference data.

6.3.3 Qualitative validation

There was an area within the case study, the Salton Lake region, which seemed to be overestimated by the developed algorithm at first glance. Therefore, investigations needed to confirm the existence of salt in surface textures of the area. USDA Natural Resource Conservation Service was a reliable source to do qualitative QA in this study) was used as a reliable resource to obtain surface texture of desired areas. The suspicious region was the western part of Salton Lake (Figure 20), located in Imperial County, California. According to the USDA, the region was found as a saline area containing 0-2 percent saline texture. The playa of the region contains clay and river-wash (consisting of coarse sand, silty clay and loam). According to Ponce (2005), the lake has a large drainage area (Figure 21) which can be affected by saline water of the lake and it can be concluded that saline water can reach the farthest reaches of the lake. In case of evaporation there can be salt evaporites left on the surface.

In order to examine the performance of the algorithm in differentiating salt from other land features, surface texture information of some randomly selected locations was obtained.

The area around Rosamond Dry Lake bed (Figure 22), located in Kern County, California, was the first examined region in term of surface texture. According to USDA, the region's surface texture is saline-alkai, containing tray loam, and sandy loam.

Churchill County is a county (Figure 23) in the western U.S. state of Nevada, explored for salt deposits. According to USDA, this area is strongly saline.

Torrance County located in the state of New Mexico (Figure 24), was the last area examined in term of surface texture. According to USDA, this region has a high concentration of saline soil, and playas containing silty clay loam and fine sandy loam.

To sum up, and according to the information of locations, and explorations, it can be concluded that the developed framework is a reliable automated framework to map salt-affected areas and salt pans. The developed framework identifies thin accumulations of salt across the surface.

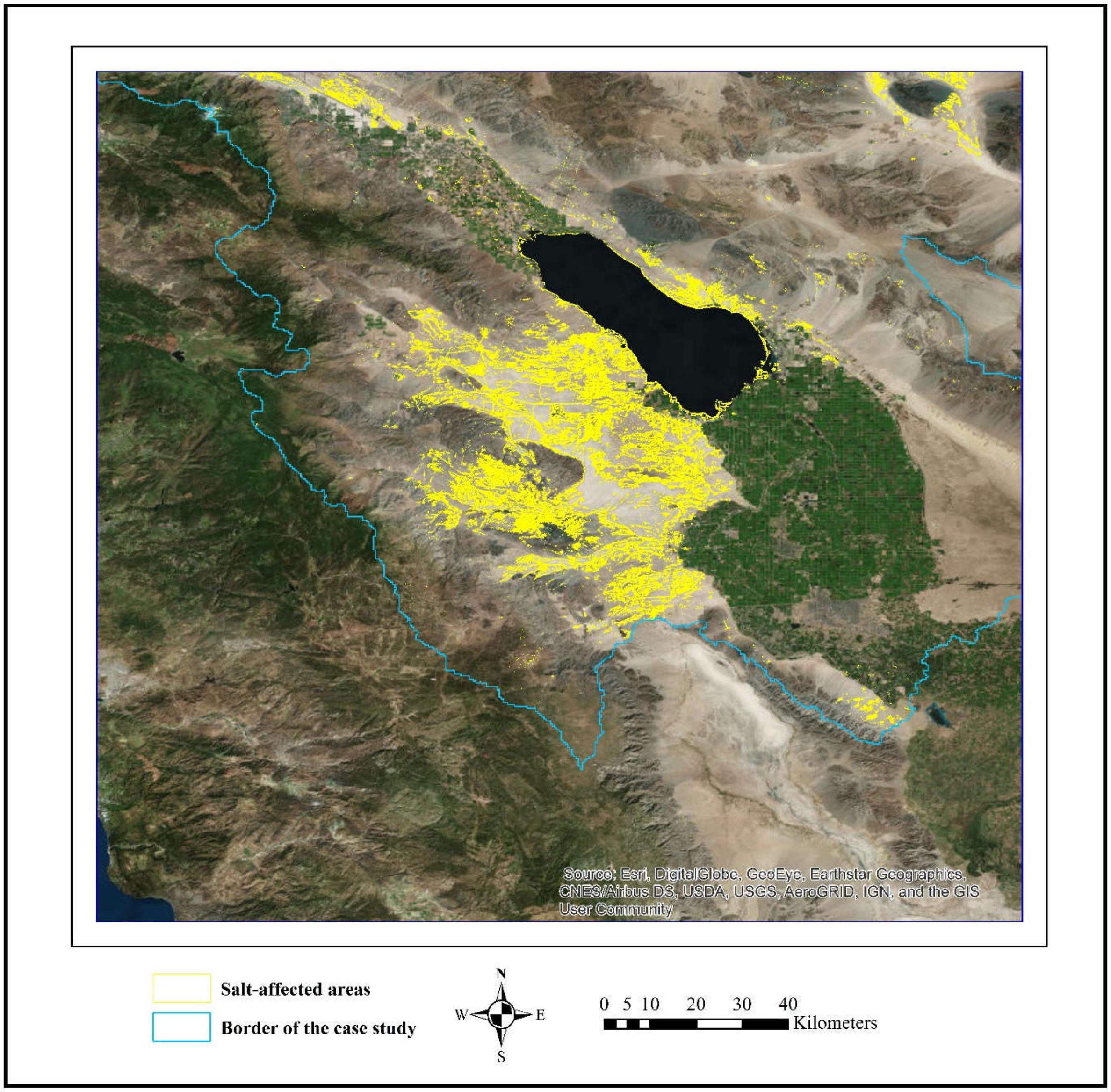

Figure 20. Salton Sea area. Background image source: Esri digital globe, GeoEye, Earthstar Geographic, CNES/Airbus DS, USDA, USGS, AeroGRID, IGN, and the GIS User Community.

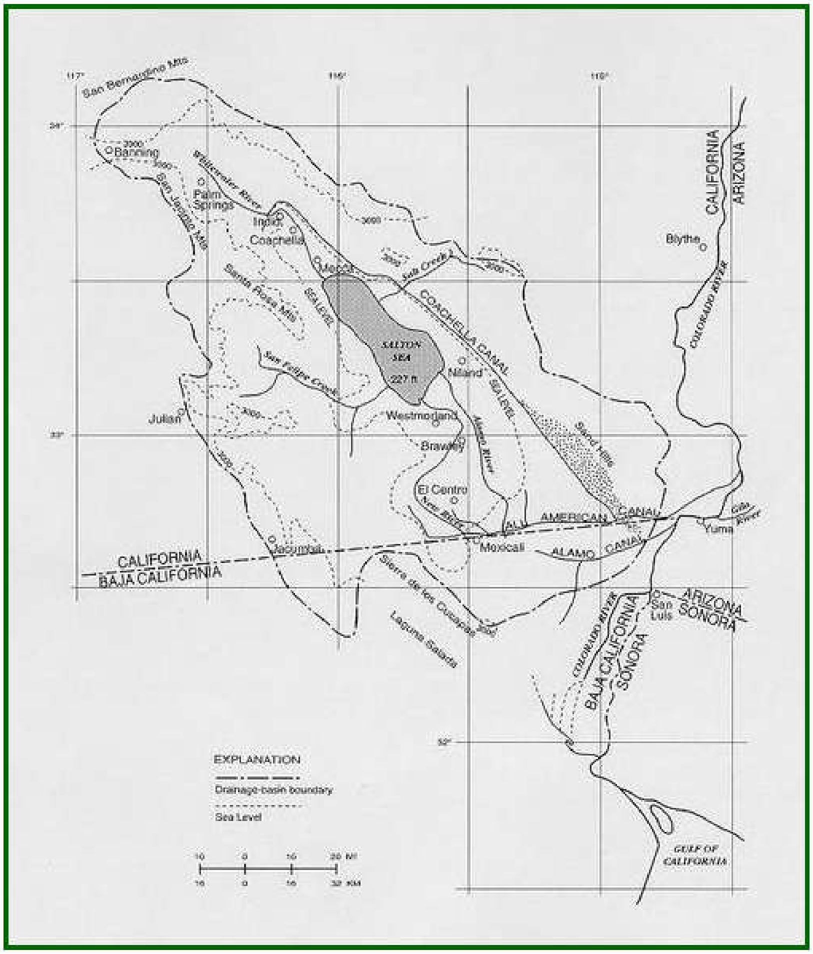

Figure 21. Salton Sea drainage area (reprinted from Ponce, 2005)

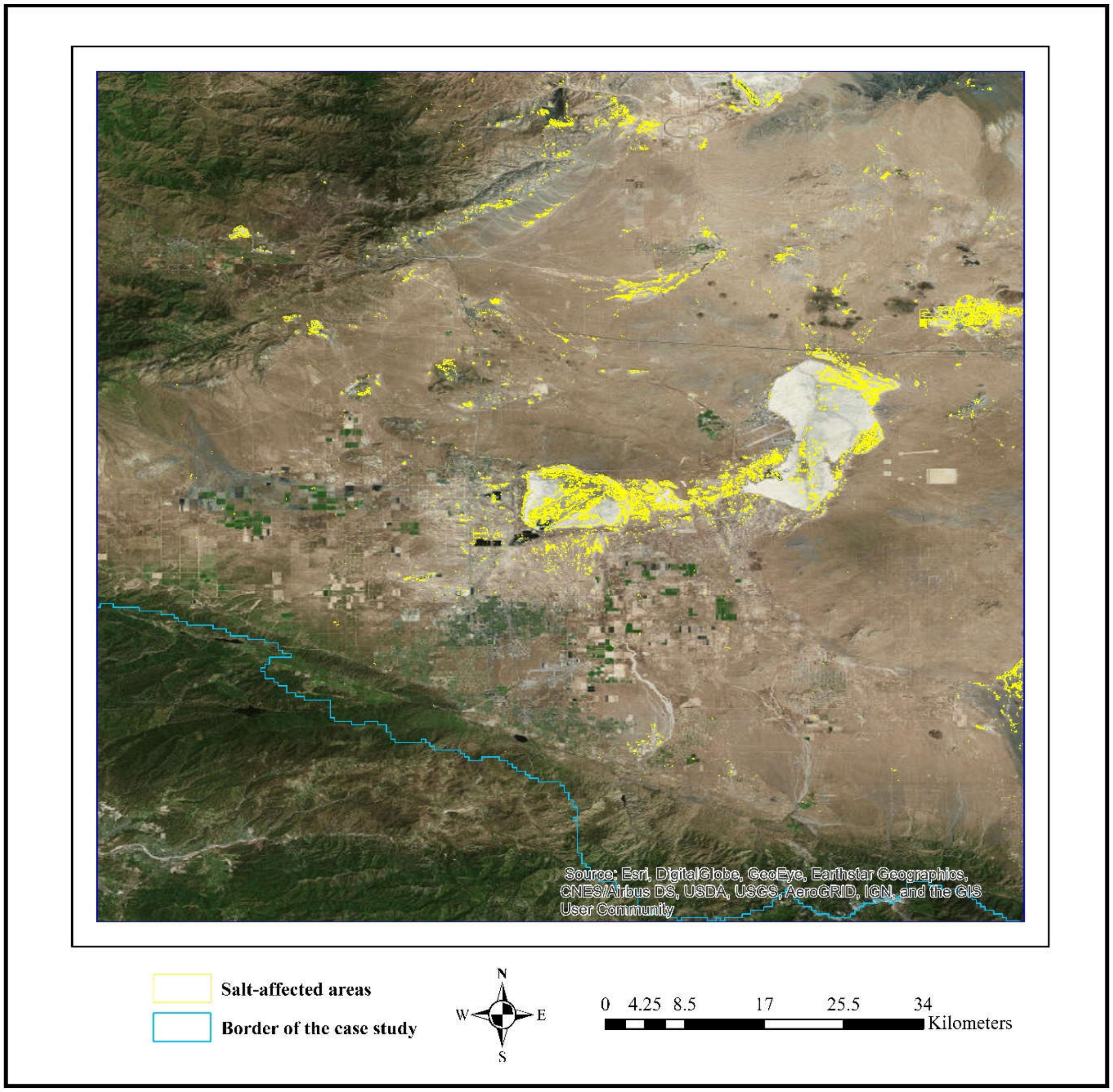

Figure 22. Rosamond Dry Lake bed region. Background image source: Esri digital globe, GeoEye, Earthstar Geographic, CNES/Airbus DS, USDA, USGS, AeroGRID, IGN, and the GIS User Community.

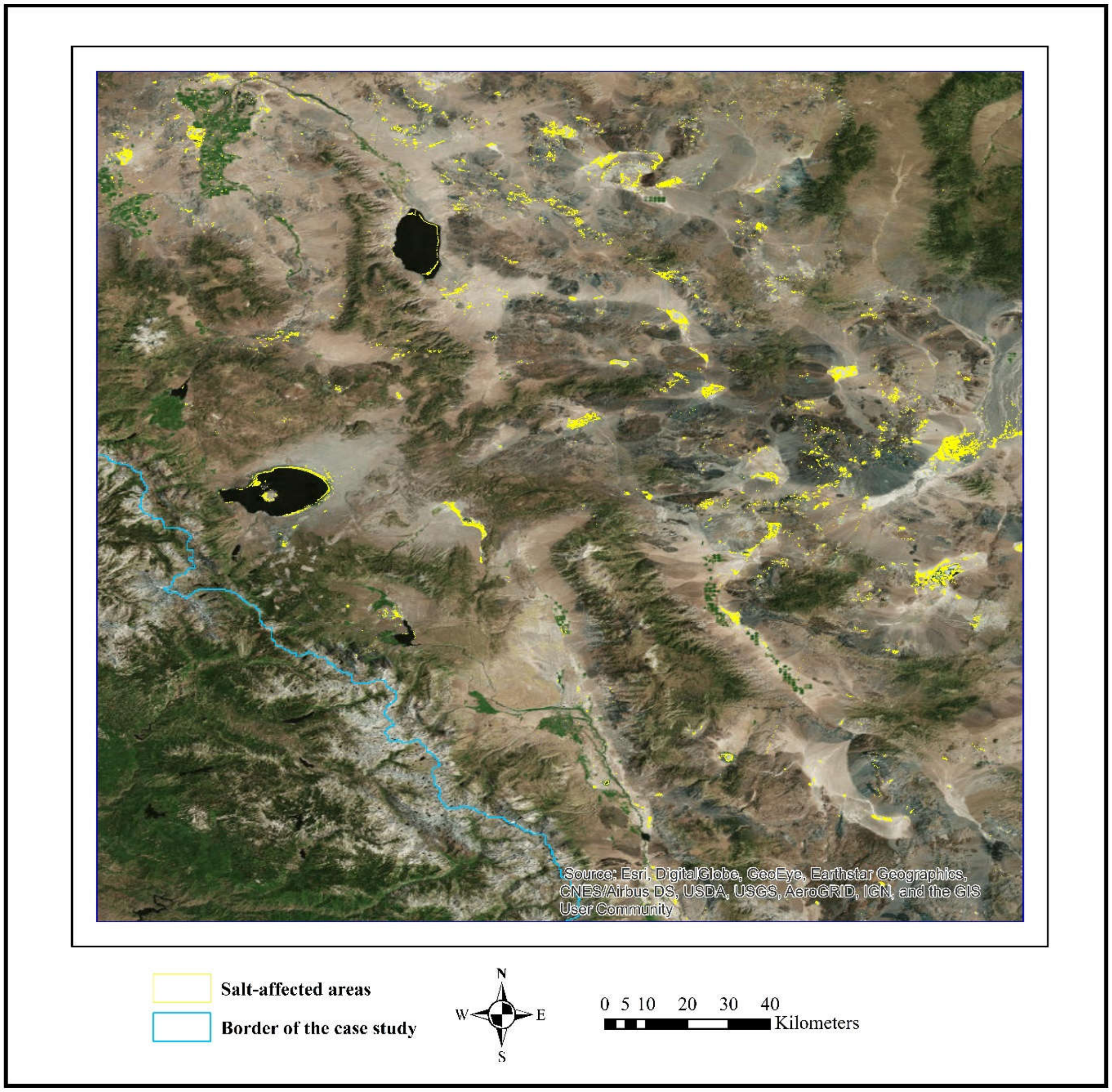

Figure 23. Churchill County region. Background image source: Esri digital globe, GeoEye, Earthstar Geographic, CNES/Airbus DS, USDA, USGS, AeroGRID, IGN, and the GIS User Community.

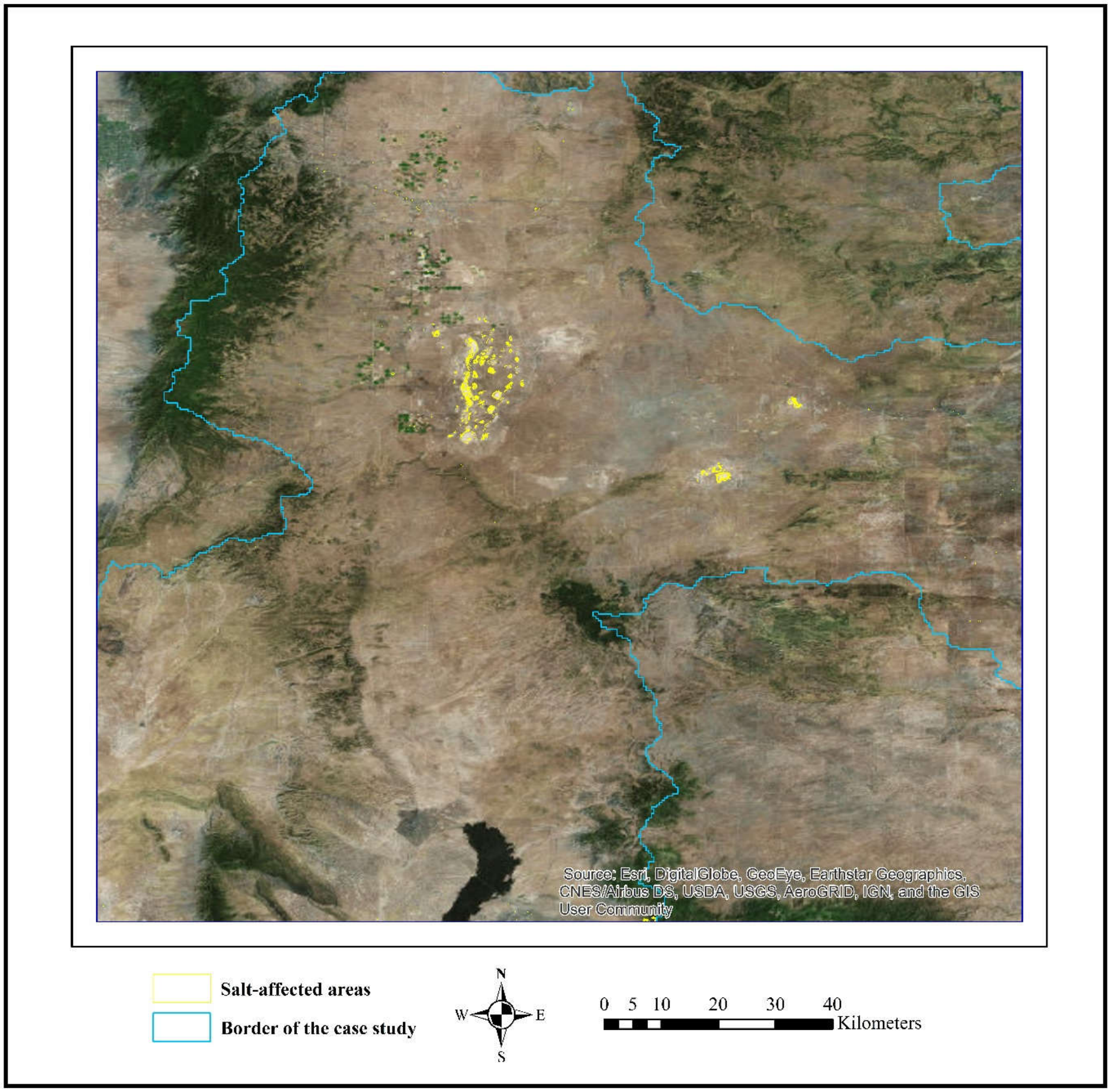

Figure 24. Torrance County region. Background image source: Esri digital globe, GeoEye, Earthstar Geographic, CNES/Airbus DS, USDA, USGS, AeroGRID, IGN, and the GIS User Community.

6.4 Results of quality assurance/ quality control

Figure 25 shows the raw resultant map of the salt-affected areas before using auxiliary datasets to do posterior QA/QC which create confusion in detecting salt pixels among urban, snow, and impervious areas. Figures 26 and 27 show the application and result of using auxiliary datasets on the salt pan maps. Once posterior QA/QC was done the results show the value of the aforementioned datasets to accurately eliminate confusion in framework performance.

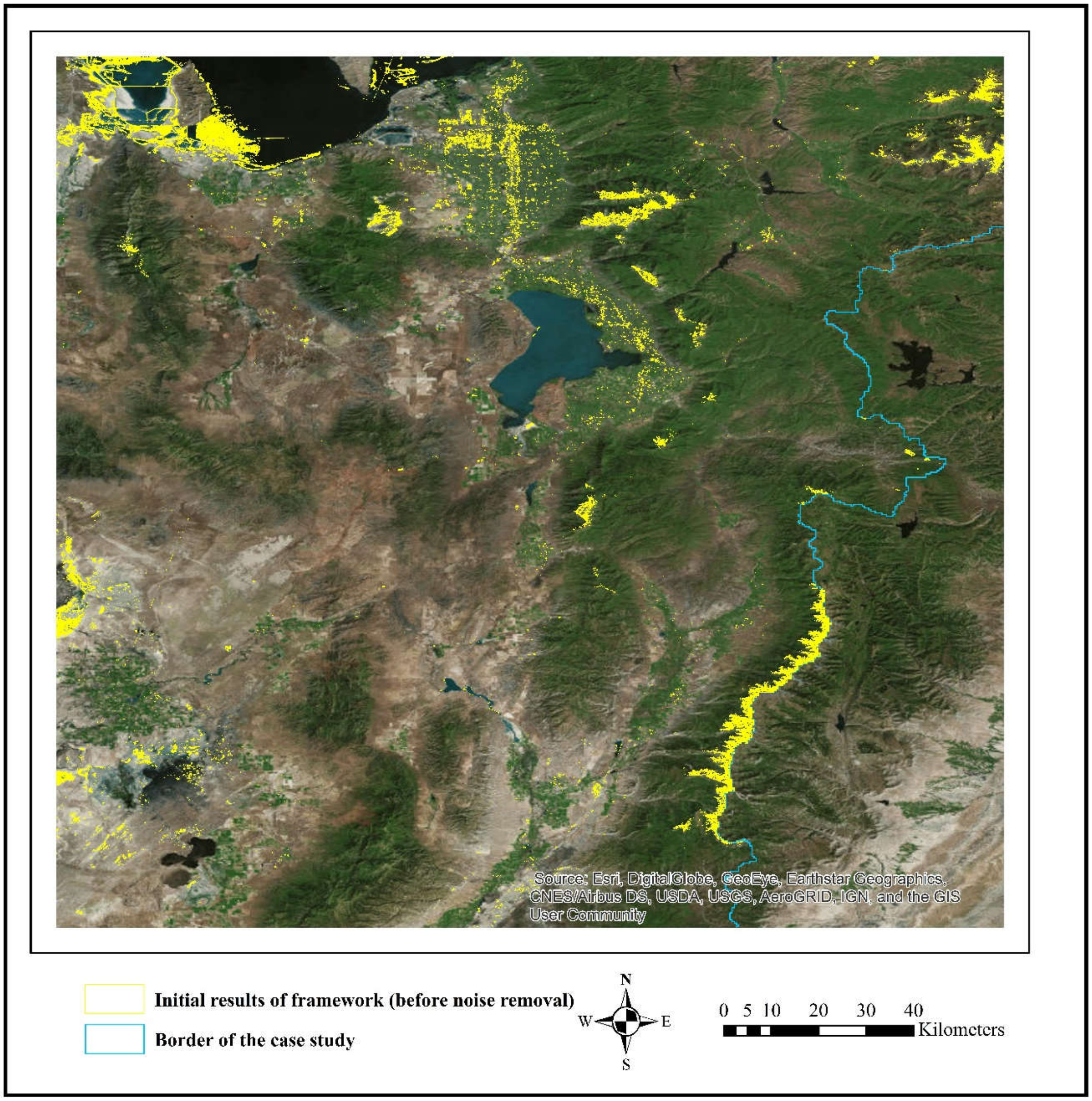

Figure 25. The initial results of the developed framework before doing QA/QC. Background image source: Esri digital globe, GeoEye, Earthstar Geographic, CNES/Airbus DS, USDA, USGS, AeroGRID, IGN, and the GIS User Community.

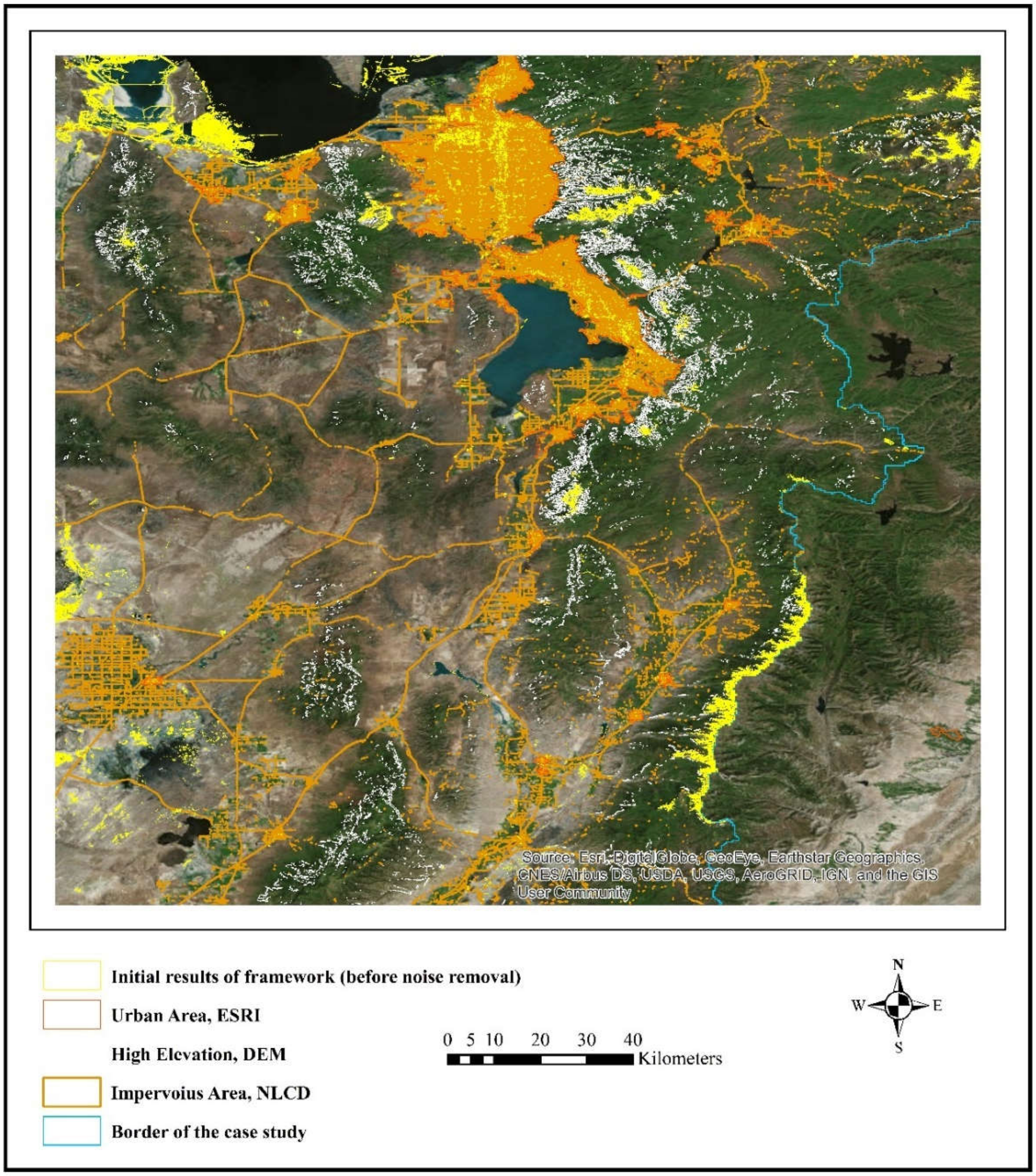

Figure 26. Initial result of the developed framework to map salt affected areas. This map shows auxiliary datasets overlaying the initial results in order to do noise removal. (1) urban shapefile achieved from Esri, (2) 90 m resolution SRTM DEM illustrates steep hill areas to remove snow from the results, (3) impervious area achieved from National Land Cover Database (NLCD) (2011 edition). Background image source: Esri digital globe, GeoEye, Earthstar Geographic, CNES/Airbus DS, USDA, USGS, AeroGRID, IGN, and the GIS User Community.

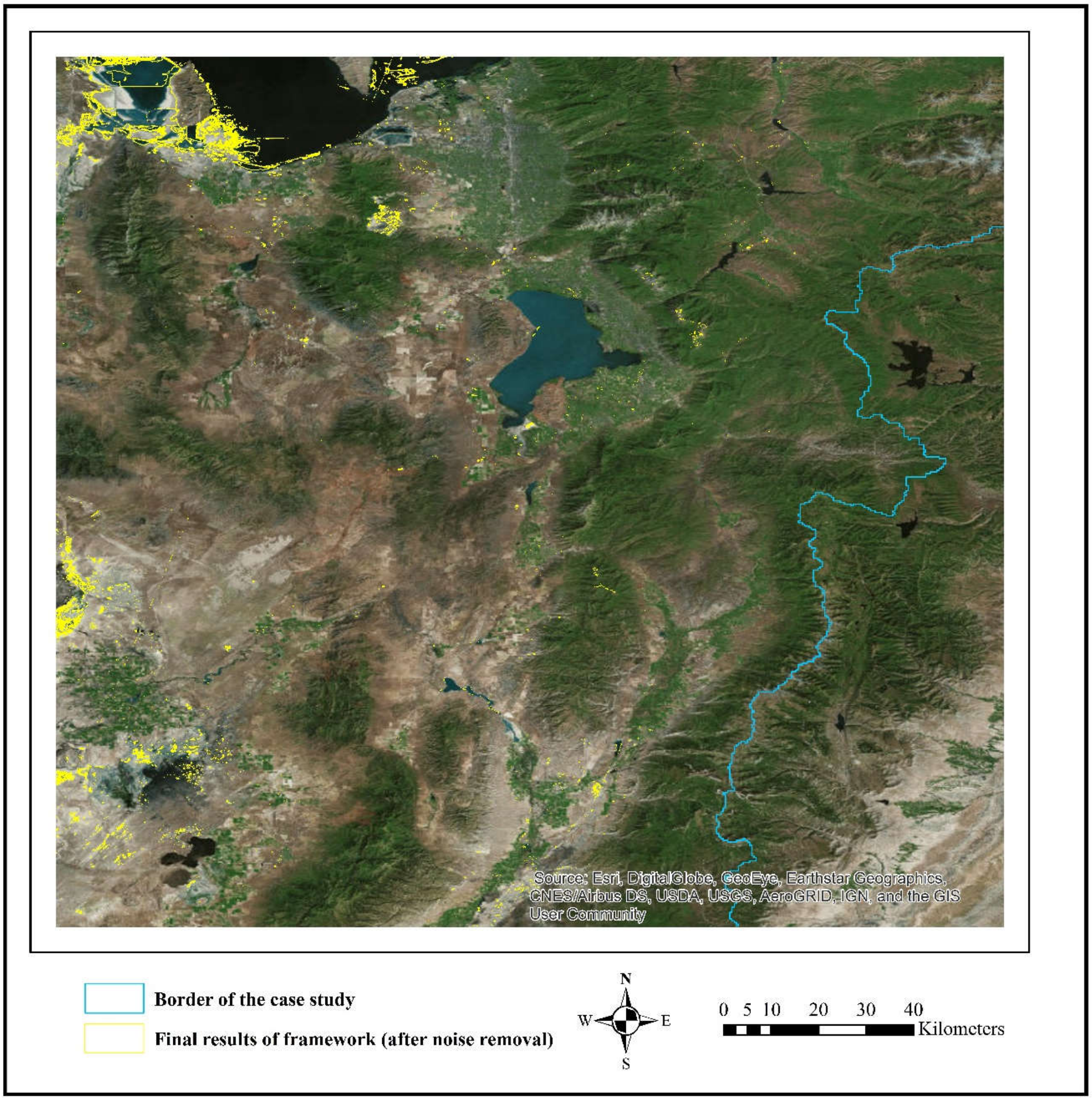

Figure 27. Final results of the developed framework after doing QA/QC using auxiliary datasets. Background image source: Esri digital globe, GeoEye, Earthstar Geographic, CNES/Airbus DS, USDA, USGS, AeroGRID, IGN, and the GIS User Community.

During this study, salt pans were found classified as barren lands in NLCD. In order to qualify the function of the developed framework and compare the results with NLCD, a few locations were explored. Results represent the ability of the developed framework to separate salt pans from barren lands (Figure 28) successfully, which is currently lacking in NLCD.

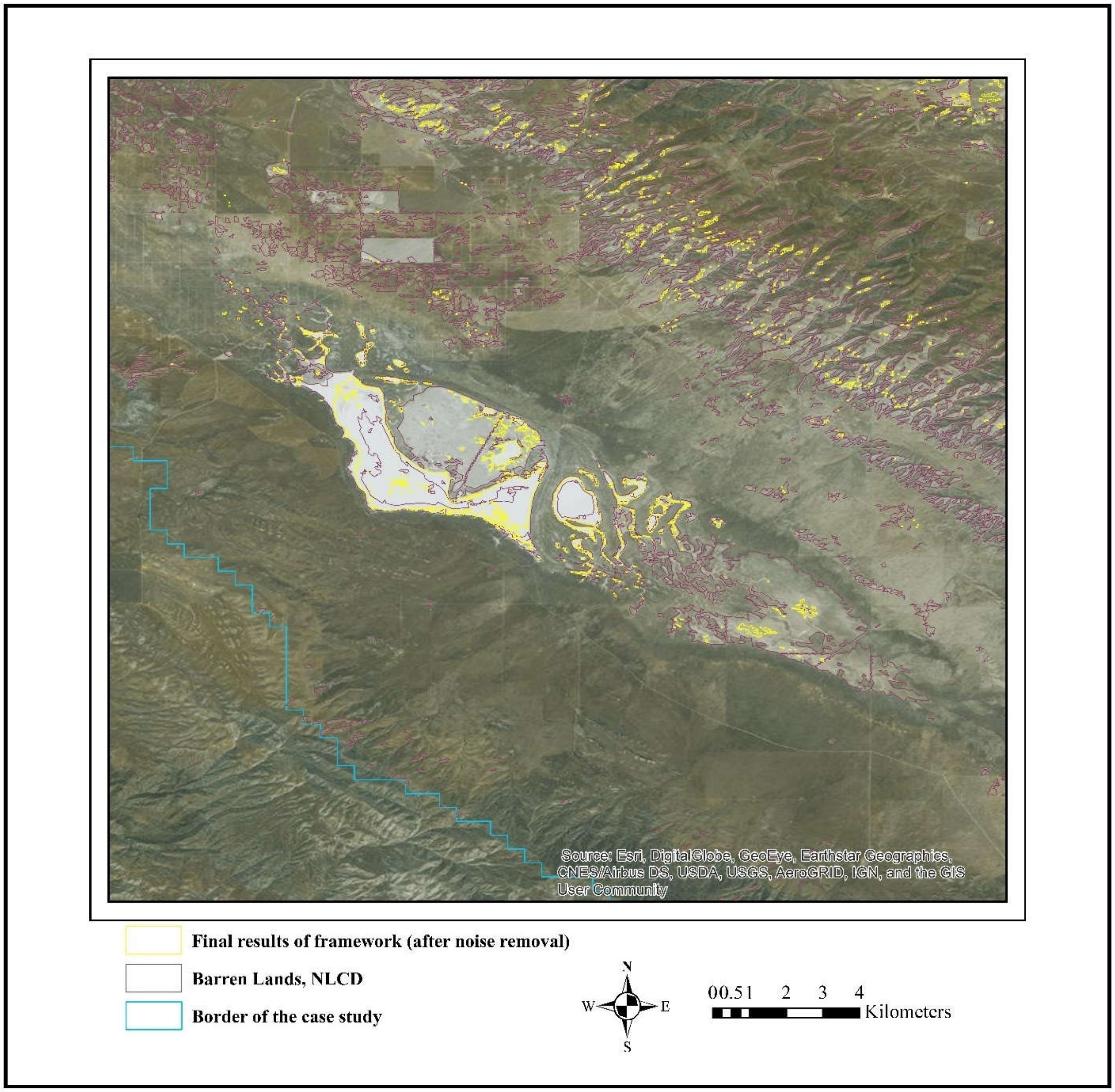

Figure 28. Confusion between barren lands and salt pans in the NLCD.

In order to find the correlation between salt pan coverage within an area of endorheic basins, variables of the resulting statistics were examined (refer to Appendix E, table.6 for more details of generated by the salt pan map). Figure 29 represents the correlation between the distribution of the salt pan area and the endorheic basin area on a logarithmic scale graph (R^2= 0.52). Generally the area of salt pans and salt-affected areas within the endorheic basins increase as the area of endorheic basin increases. Figure 30 visualizes the distribution of salt pans across the case study within individual endorheic basins.

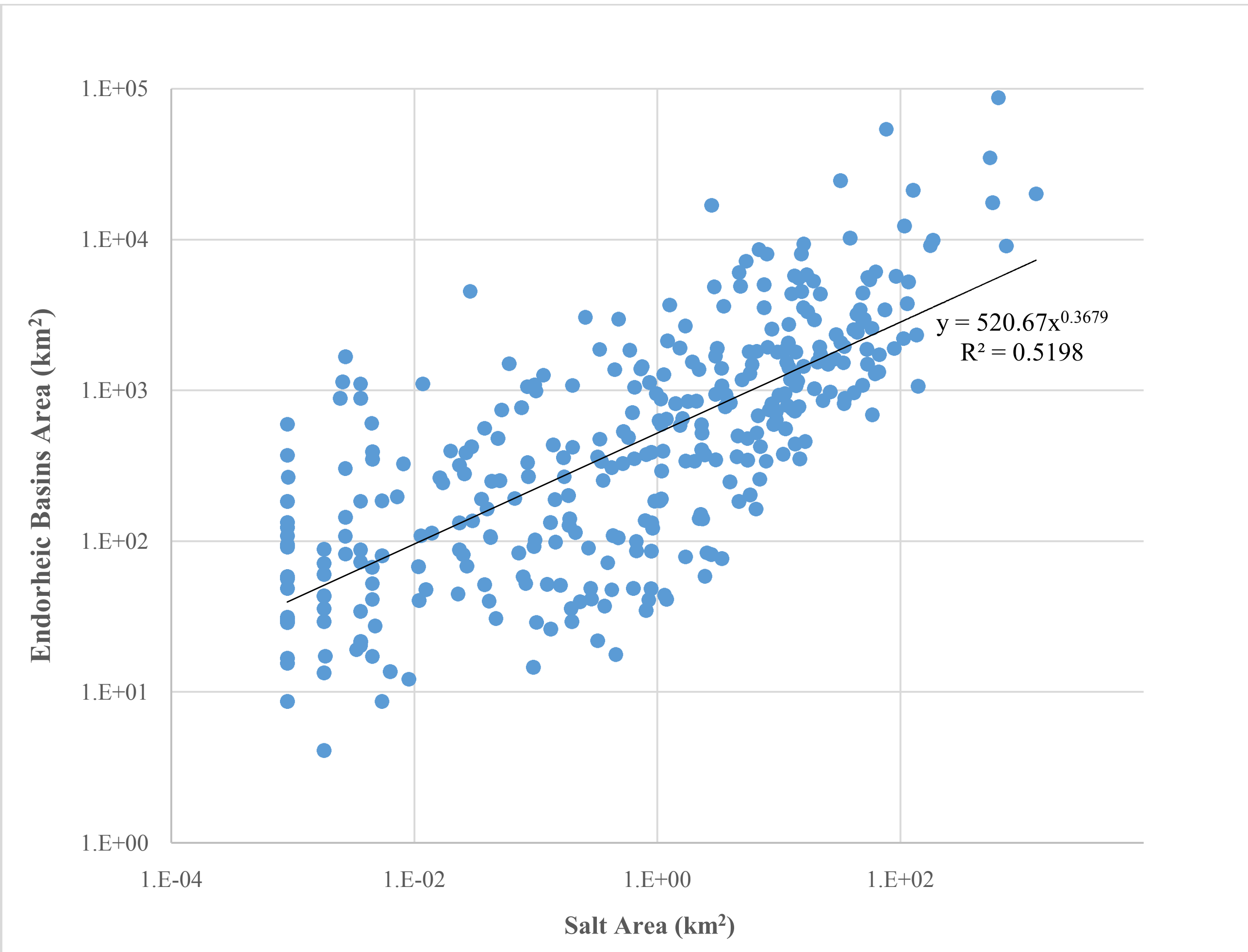

Figure 29. Relationship between endorheic basin areas and their salt pan areas. Endorheic basin areas versus salt pan areas, showing positive correlation between, variable in logarithmic scale.

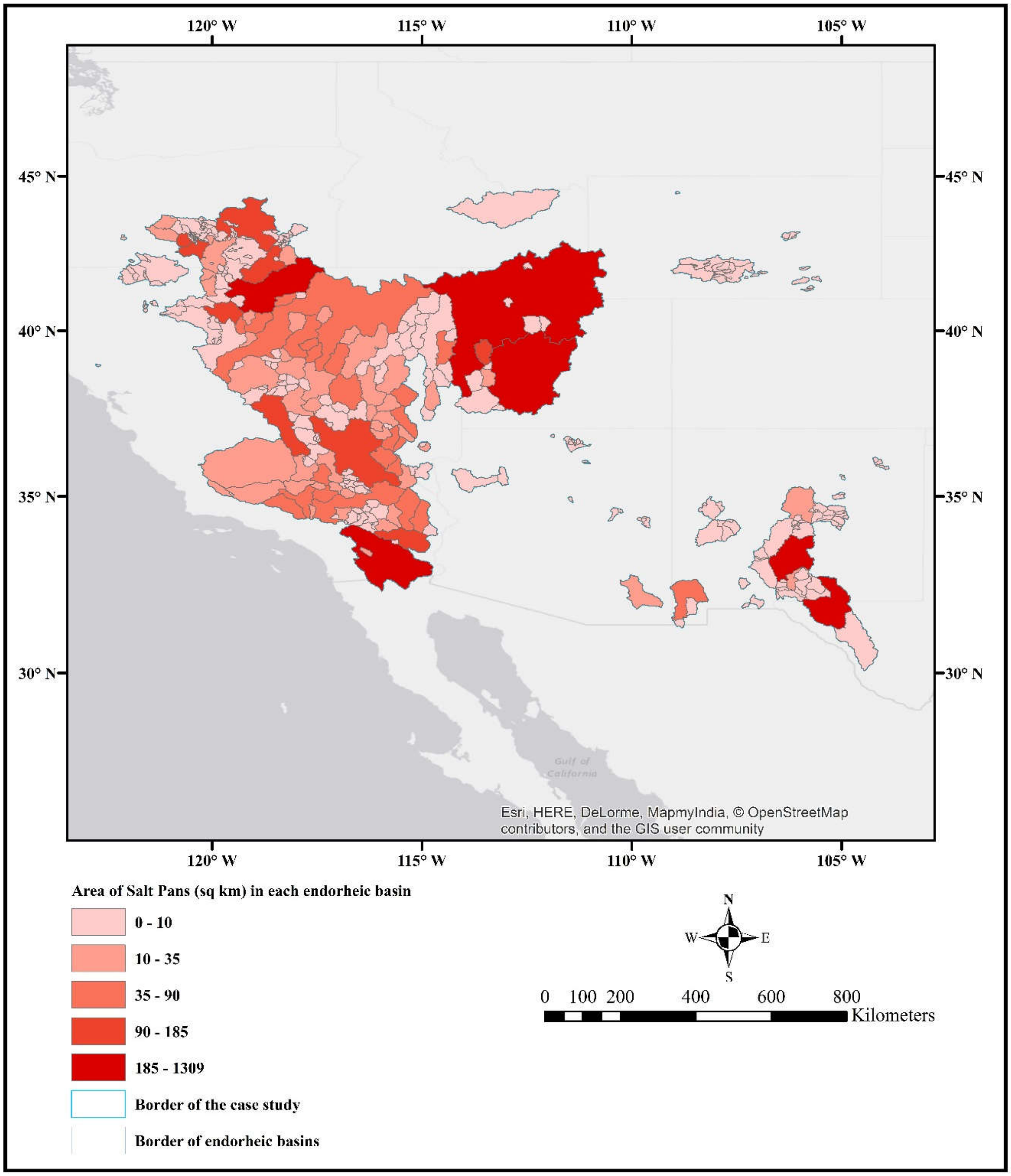

Figure 30. The total salt pan area in each endorheic basin across studied Western North America. This map, shows the distribution of salt pans across the case study in each individual endorheic basin. The darkest red represents largest area (km^2) of salt pans across the basin, and the lightest color represents the smallest salt pan area (km^2) existing in the basin. Background image source: World Light Gray Canvas Basemap: Esri.

Figure 31 represents the constant relationship between salt pan coverage and each endorheic basin located in the case study. R-square (0.0846) represents the week relationship between variables. It can be observe that as the endorheic basin area increases the salt pan coverage increases accordingly.

Figure 32visualizes the percentage of salt pan coverage across the case study within each endorheic basin. According to this plot, the percentage of distribution of salt pans across each individual endorheic basin does not vary widely.

There might be some other factors affecting salt pan areas in each basin such as temperature or net water budget of each basin. Population was not considered in this study, either.

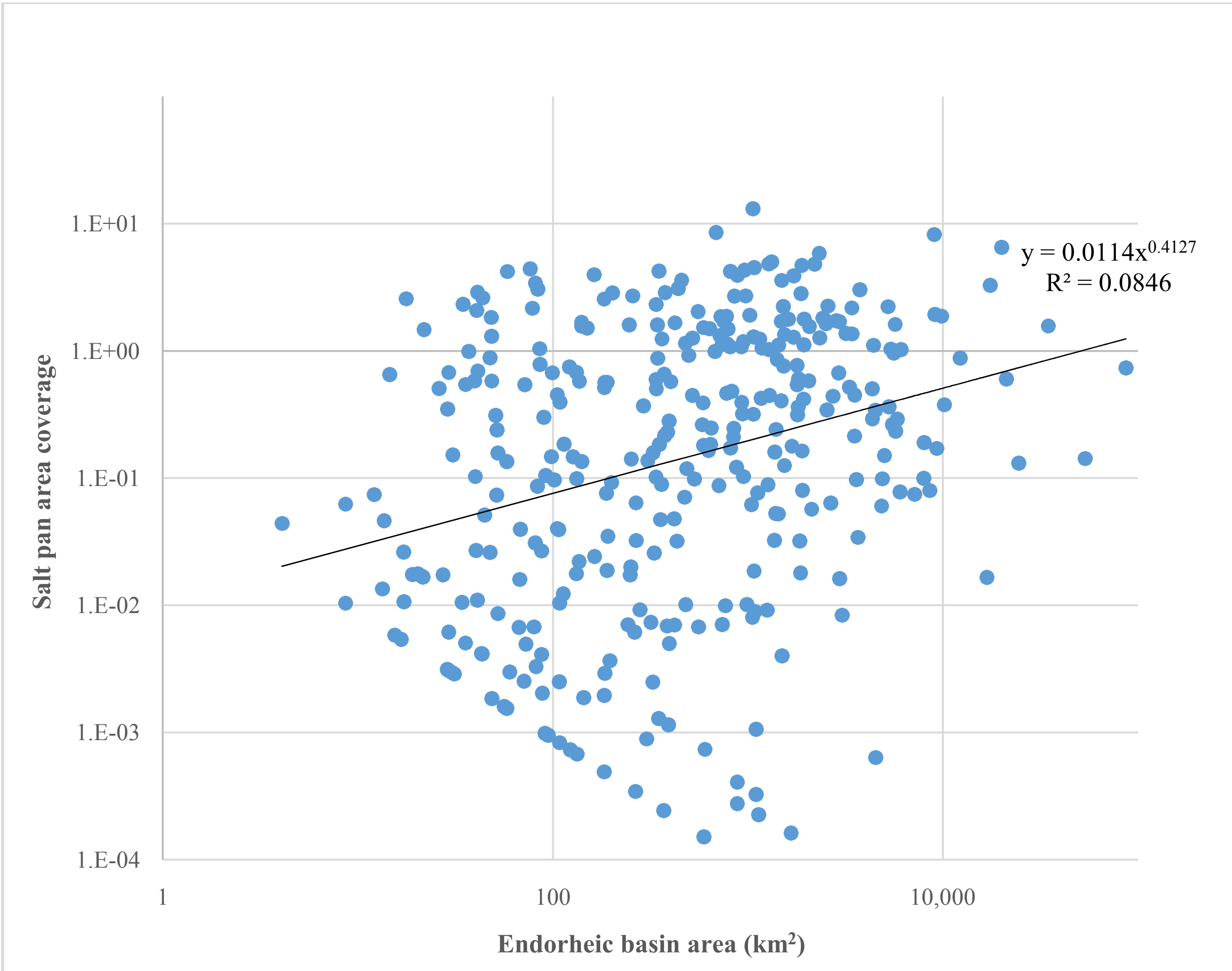

Figure 31. The salt pan area coverage as percentage of endorheic basins areas(logarithmic scale).This graph shows constant relationship between variables (percentage of salt coverage and endorheic basins areas).

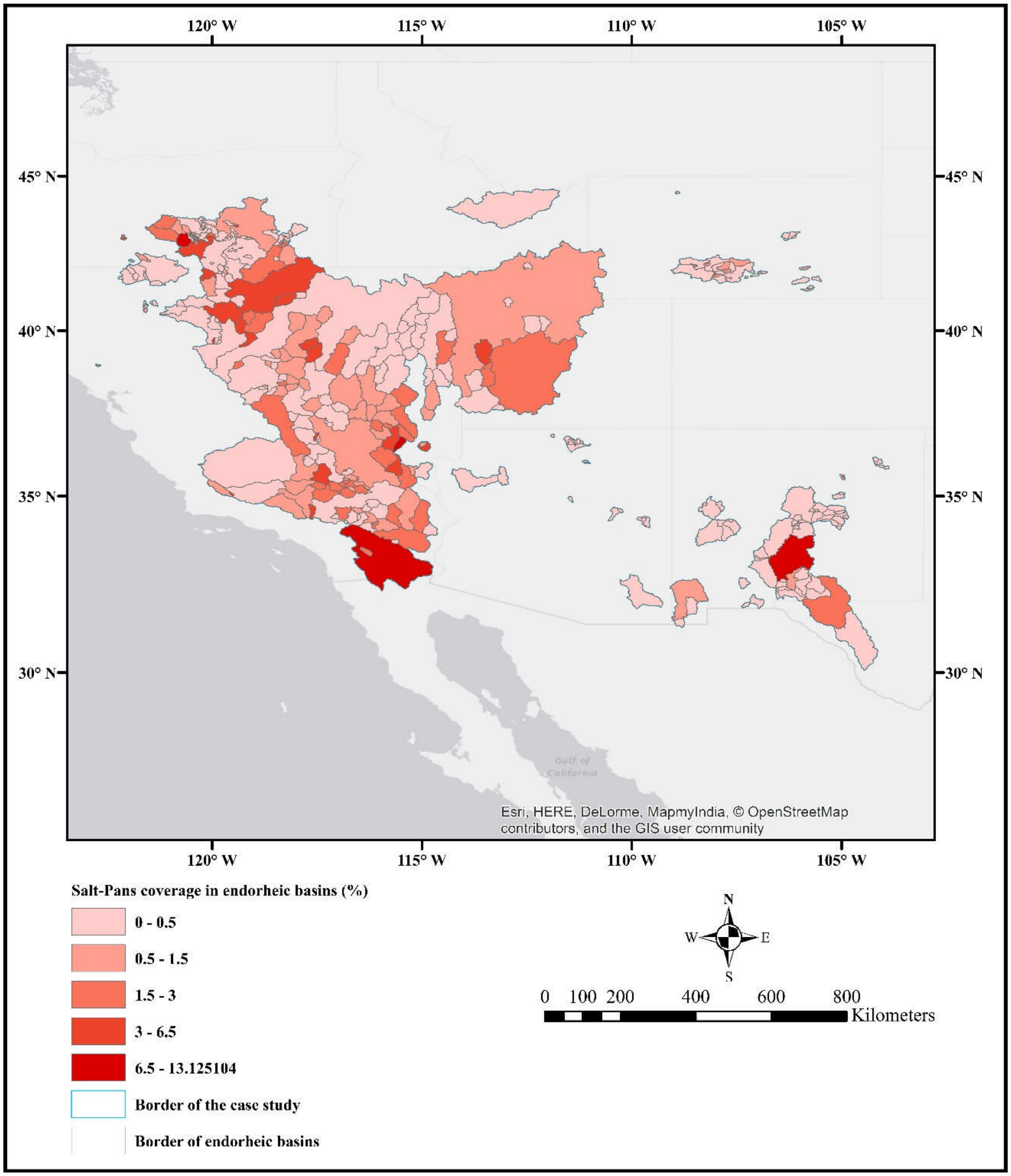

Figure 32. The percentage of salt pan coverage across the case study in each endorheic basin. Darkest red represents largest the percentage of salt pan coverage in each individual endorheic basin area, and the lightest color represents the lowest percentage of salt pan coverage in each individual endorheic basin area. Background image source: World Light Gray Canvas Basemap: Esri.

Chapter 7 - Discussion

Some studies have been done so far in order to find a way to extract salt-affected areas, but there is still no useful model for mapping different salt pans distributed in different locations of the earth with high accuracy.

All indices suggested in existing studies were examined in this study for training areas and none worked as accurately as the SI developed in this study.

7.1 Challenges confronted

The SI$((band2 + band3 + band4)/3)$ suggested through this research had some confusing results at first. Cloud, snow, and some parts of urban areas were classified as salt. Urban areas can be removed using existing urban shape-files, and snow can be removed using digital elevation model (DEM) files. The Landsat-8 QA band has cloud mask information, but its band quality is not good enough to determine the accuracy of the proposed model. However, since most of the Landsat-8 images do not contain heavy clouds, manually excluding clouds from resultant maps was a feasible solution to the problem. Figures32-34 show the initial results of the developed algorithm with confusion in differentiating salt and other land features in the training areas, and effects of posterior QA/QC using auxiliary datasets.

A fundamental aspect of this study is making a comprehensive training data set for salt and non-salt features in order to develop a useful algorithm that would be applicable for any region. For this reason, containing all salt chemicals in the training data was crucial. A challenging process of this study was to find different salt chemicals to make a comprehensive training samples. Fortunately, after some trials the training data produced satisfactory results in this study.

Chapter 8 - Summary, Conclusions, and Future Work

8.1 Summary and conclusion

Driven from aforementioned objectives, a developed framework was qualified in this study as the most accurate procedure among other classification approaches. This section summarizes the findings of this study and provides suggestions and directions for further research for salt pan studies.

Soil salinization is a significant environmental hazard caused either by natural processes or human activities (Al-Khaier, 2003). Monitoring salt pans is important especially for agricultural management in arid or semi-arid regions because salt pans can negatively affect human life, wildlife, and ecology. Identifying salt-affected areas is important to justify agricultural management, particularly in arid and semi-arid regions.

This study examined different classification algorithms using eight " training areas " which have different types of salt and produced a single appropriate salt index useful for different locations. Moreover, the most accurate framework of mapping salt pans or salt playas across the earth was developed.

The general procedure of this framework is listed below;

- Acquire and preprocess Landsat-8 imagery for different location of the earth (training areas)
- Evaluate different classification approaches
- Define a multi-spectral index applicable to all training areas
- Mask unwanted land features in order to flag potential salt pixels
- Generate a spectral library using different salt chemicals located in different locations of the earth (training areas) in order to better distinguish salt from other land features

- Calibrate the comprehensive training samples and SVM parameters using LIBSVM to obtain optimal SVM parameters and testing training samples on all training areas. This is done in order to make sure that the generated training sample covers all salt chemicals.

- Validate performance of the developed framework was done based on visual interpretation results compared to appearance of input Landsat-8 images, and generating error matrix (Table 2).

- Interpreting statistics.

The function of this algorithm is reliable according to the high values of 0.9583 and 0.9006 for overall accuracy and Kappa statistics, respectively.

According to the current literature, critically reviewing different techniques of classification and their advantages and disadvantages, calibration, validation and variable analysis the following conclusions have been achieved:

i) A single index suitable to extract salt pixels located in all training areas can be defined$SI = ((band2 + band3 + band4)/3)$; ii) Bands 2, 3, and 4 representing blue, green and red are useful bands to define SI and are useful for multiple locations; iii) The proper threshold value to mask out non-salt land features is defined as 0.2; iv) Building a spectral library is a useful tool for distinguishing more accurately between salt and other land features; v) The appropriate number of sampled pixels used for building a spectral library affects the resulting maps, but over fitting is not necessarily required for SVM; vi) The spectral library generated in this study is a comprehensive spectral library useful to detect all salt chemicals across the entire continental surface; vii) DEM data-sets are useful to detect and extract snow and clouds which have similar spectral reflectance with salt; viii) Although there are useful sources of data for noise removal (e.g., NLCD and DEM), manual editing is inevitable in the process of quality control; ix) The developed mapping framework is highly reliable due to the extreme accuracy of performance of the framework, either quantitatively or qualitatively; x) A positive correlation between salt pan areas with the endorheic basins in which salt pans are located was found, xi) The distribution of salt pans existing in endorheic basins cannot be predicted because the percentage of salt pan coverage across the case study is constant; xii) NLCD can be improved in separating barren lands and impervious areas from salt pans using this framework.

8.2 Future work

Several types of satellite images can be applied for future studies to examine the function of the developed algorithm. The same number of images used for each scene would be a beneficial to facilitate and accelerate the calculation of the maximal and minimal extension of salt pans in IDL. In this study the number of used Landsat-8 imagery for each scene varies across the entire case study. Therefore, obtaining maximal and minimal extension of salt pans was not achieved. Field observation would be a good way to support the results, especially to validate lightly salt-affected areas. In order to find a variable which affects salt pan areas and serves as a model to predict salt pan distribution, a climate dataset for each individual endorheic basin may be important variables useful for future studies. The application of Landsat-8 thermal band to separate snow and cloud from salt needs to be examined. Principal component analysis would be a better and more useful way to eliminate undesired land features from the results.

Bibliography

Adam, E., Mutanga, O., Odindi, J., & Abdel-Rahman, E. M. (2014). Land-use/cover Classification in a Heterogeneous Coastal Landscape Using RapidEye Imagery: Evaluating the Performance of Random Forest and Support Vector Machines Classifiers. International Journal of Remote Sensing, 3440-3458.

Alavi Panah, S. K. (2000). The Use of Remote Sensing and GIS to Detect Salt Crust in the Iranian Deserts International Archive of Photogrammetry and Remote Sensing, 39-45.

Albed, A., & Kumar, L. (2013). Soil salinity mapping and monitoring in arid and semi-arid regions using remote sensing technology: A review. Advanced remote sensing, 373-385.

Al-Khaier, F. (2003). Soil Salinity Detection Using Satellite Remote Sensing. (Master's), International Institute for GEO-information science and Earth observation.

Ambast, S. K. (1997). Monitoring And Evaluation of Irrigation System Performance in Saline Irrigated Command Using Satellite Remote Sensing and GIS (471). Retrieved from DLO Winand Staring Center, Netherland

Anderson, L. T. (2000). Planning the Built Environment: APA Planners Press.

Asfaw, E., Suryabhagavan, K. V., & Argaw, M. (2016). Soil Salinity Modeling and Mapping Using Remote Sensing and GIS: The Case of Wonji Sugar Cane Irrigation Farm. Journal of the Saudi Society of Agricultural Sciences.

Bastrakov, E. N., Clarke, J. D. A., Caritat, P., English, P. M., Howard, F. J. F., Jaireth, S., Wilford, J. R. (2013). A Review of Australian Salt Lakes and Assessment of their Potential for Strategic Resources (T. P. Mernagh Ed.).

Blair, F. J., David, L. N., Ronald, J. S., & Charles, G. O. (2008). Geochemical Evolution of Great Salt Lake, Utah, USA. Aquat Geochem.

Braget, M. P. (2017). A Novel Approach to Mapping Flooding Extent in the Chobe River Basin from 2014 to 2016 Using A Training Library. (Master), Kansas State University.

Carpenter, D., Groat, C. G., Matz, D., Motts, W. S., & Walker, R. F. (May 1969). Geology and Hydrology of Selected Playas in Western United States. Retrieved from Chang, C. C., & Lin, C. J. (2011).

Chang, C. C., & Lin, C. J. (2011). LIBSVM: a Library for Support Vector Machines. ACM Transactions on Intelligent Systems and Technology.

Chao, C. F., & Horng, M. H. (2015). The Construction of Support Vector Machine Classifier Using the Firefly Algorithm. Computational Intelligence and Neuroscience.

Dehni, A., & Lounis, M. (2012). Remote Sensing Techniques for Salt Affected Soil Mapping: Application to the Oran Region of Algeria, Procedia Engineering, 33, 188-198.

Dictionary, O. E. "art, n.1": Oxford University Press.

Dwivedi, R. S. (1969). Monitoring of Salt Affected Soils of The Indo-Gangetic Alluvial Plains Using Principal Component Analysis. International Journal of Remote Sensing, 17, 1907-1914.

Dwivedi, R. S., Ramana, K. V., Thammappa, S. S., & SinghA, A. N. (2001). The utility o fIRS-1C LISS-III and Pan-Merged Data for Mapping Salt-Affected Soils. Photogrammetric Engineering & Remote sensing, 1167-1175.

Dwivedi, R. S., Sreenivas, K., & Ramana, K. V. (1999). Inventory of Salt-Affected Soils and Waterlogged Areas: A Remote Sensing Approach. International Journal of Remote Sensing, 20, 1589-1599.

Ericksen, G. E., Vine, J. D., & Raul, B. A. (2012). Chemical Composition and Distribution of Lithium-Rich Brines in Salar de Uyuni and Nearby Salars in Southwestern Bolivia. Retrieved from https://pubs.er.usgs.gov/publication/70012613

Farifteh, J., Meer, F., Meijde, M., & Atzberger, C. (2008). Spectral characteristics of salt-affected soils: A laboratory experiment. Geoderma, 196-206.

Farifteh, J., Van der Meer, F., Atzberger, C., & Carranza, E. J. M. (2007). Quantitative Analysis of Salt-Affected Soil Reflectance Spectra: A Comparison of Two Adaptive Methods (PLSR and ANN). Remote Sensing of Environment, 110, 59-78.

Floyd, F. S. (2007). Remote Sensing: Principles and Interpretation, Third Edition. Long Grove, Illinois: Waveland Press.

Hermes, L., Frieauff, D., Puzicha, J., & Buhmann, J. M. (1999). Support Vector Machines for Land Usage Classification in Landsat TM Imagery. IGARSS, 348-350.

Howari, F. M., Goodell, P. C., & Miyamoto, S. (2002). Spectral Properties of Salt Crusts Formed on Saline Soils. Journal of Environment Quality, 1456-1461.

Iqba, S., & Mastorakis, N. (2015). Soil Salinity Mapping and Monitoring Using Remote Sensing GIS. Paper presented at the Dubai Agriculture science biotechnology, food and animal sciences (ABIFA 15).

Kucera, M. (1984). Industrial Minerals and Rocks (D. Doc. RNDr. Jan Petranek Ed.).

Lehner, B., Verdin, K., & Jarvis, A. (2006). HydroSHEDS Technical Documentation, version 1.0. World Wildlife Fund US, 1-27.

Lowenstein, T. K., & Hardie, L. A. (1985). Criteria for the Recognition of Salt Evaporites. Sedimentology, 32, 627-644.

Melgani, F., & Bruzzone, L. (2004). Classification of Hyperspectral Remote Sensing Images With Support Vector Machines. IEEE Transactions on Geoscience and Remote Sensing, 42.

Menenti, M., Lorkeers, A., & Vissers, M. (1986). An Application of Thematic Mapper Data in Tunisia. ITC Journal, 35-42.

Metternicht, G. I., & Zinck, J. A. (1996). Modelling Salinity and Alkalinity Classes for Mapping Salt Affected Topsoils in the Semi-Arid Valleys of Cochabamba (Bolivia). ITC Journal, 125-135.

Metternicht, G. I., & Zinck, J. A. (2003). Remote Sensing of Soil Salinity: Potentials and Constraints. Remote Sensing of Environment, 1-20.

Mougenot, B., Pouget, M., & Epema, G. (1993). Remote Sensing of Salt-Affected Soils. Remote Sensing, 241-259.

Mulders, M. A., & Epema, G. F. (1986). The thematic mapper: A new tool for soil mapping in arid areas. . ITC Journal, 24-29.

Ponce, V. M. (2005). Agricultural Drain in the Imperial valley, California, the Source of the Salton Sea.

Pontius, R. G. J., Cornell, J. D., & Hall, C. A. S. (2001). Modeling the spatial pattern of land-use change with GEOMOD2: Application and Validation for Costa Rica. Agriculture, Ecosystems and Environment, 1-13.

Rao, B., Sankar, T., Dwivedi, R., Thammappa, S., Venkataratnam, L., Sharma, R., & Das, S. (1995). Spectral Behavior of Salt-Affected Soils. Int. J. Remote Sens, 2125-2136.

Rao, B. R. M., Dwivdi, R. S., Venkataratnam L, L., Ravishankar, T., Thammappa, S. S., Bhargawa, G. P., & Singh, A. N. (1991). Mapping the magnitude of Sodicity in Part on Indo-Gangetic Plains of Uttar Pradesh, Northern India Using Landsat data. International Journal of Remote Sensing, 12.

Rees, W. G. (2006). Remote Sensing of Snow and Ice: CRC Press.

Research, T. N. C. f. A. (07 Jul 2017). The Climate Data Guide: Precipitation Reconstruction Land (PREC/L): 1948-present. Retrieved from https://climatedataguide.ucar.edu/climate-data/precipitation-reconstruction-land-precl-1948-present

Rodell, M., Houser, P. R., Jambor, U., Gottschalck, J., Mitchell, K., Meng, C. J., Toll, D. (2004). The global land data assimilation system. Bulletin of the American Meteorological Society, 85(3), 381.

Rokni, K., Ahmad, A., Selamat, A., Selamat, A., & Hazini, S. (2014). Water Feature Extraction and Change Detection Using Multitemporal Landsat Imagery. Remote Sensing, 4173-4189. S.K., A. (1997). Monitoring and evaluation of irrigation system performance in saline irrigated command using satellite remote sensing and GIS. Retrieved from Netherlands

Scheffers, A. M., & Kelletat, D. H. (2016). Lakes of the World with Google Earth Understanding our Environment.

Shrestha, D. P., & Farshad, A. (2009). Mapping Salinity Hazard: An Integrated Application of Remote Sensing and Modeling-Based Techniques.

Simin, C., Rongqun, Z., Liming, L., & De, Z. (2010). A Method of Salt-Affected Soil Information Extraction Based on A Support Vector Machine With Texture Features. Mathematical and Computer Modelling, 1319-1325.

Sing, R. P., & Sirohi, A. (1994). Spectral Reflectance Properties of Different Types of Soil Surface. ISPRS Journal of Photogrammetry and Remote Sensing, 49, 37-40.

Souri, A. H., Saradjian, M., Shahrisvand, M., & Parang, S. (2012). Improving parallelepiped Classification by Using Elliptical Shape and Combining Minimum Distance Multispectral Imagery

Sridhar, P. N., Surendar, A., & RamanaI, V. (2008). Auto extraction technique-based digital classification of saltpans and aquaculture plots using satellite data. International journal of Remote Sensing, 29, 313-323.

Verburg, P. H., Kok, K., Pontius, R. G., & Veldkamp, A. (2006). Modeling land-use and land-cover change. Land-use and land-cover change, local processes and global impacts, 117-136.

Vidal, A., Maure, P., Durand, H., & Strosser, P. (1996). Remote Sensing Applied To Irrigation System Management: Example of Pakistan. Paper presented at the EURASY Colloquium on Satellite Observation for Sustainable Development in the Mediterranean Area ESA-ESRIN, Frascati, ITA.

Viera, A. J., & Garrett, J. M. (2005). Understanding Interobserver Agreement:

The Kappa Statistic. Family Medicine, 37, 360-363.

Wacker, A. G., & Landgrebe, D. A. (1972). Minimum Distance Classification in Remote Sensing. LARS Technical Reports. Paper 25. http://docs.lib.purdue.edu/larstech/25

Wang, J. (2008). A Multi-Thread Spatial Autocorrelation (Mu TSA) model, A Case Study of Urban Growth for Denver, Colorado State University of New York.

Wu, W., Mhaimeed, A. S., Al-Shafie, W. M., Ziadat, F., Dhehibi, B., Nangia, V., & Pauw, E. D. (2014). Mapping Soil Salinity Changes Using Remote Sensing in Central Iraq. Geoderma Regional, 21-31.

Yugal, K., & Sahoo, G. (2012). Analysis of Parametric & Non Parametric Classifiers for Classification Technique using WEKA. Retrieved from http://www.mecs-press.org/

Appendix A - Landsat-8 OLI spectral band properties

Bands	**Wavelength (micrometers)**	**Resolution (meters)**
Band 1 - Ultra Blue (coastal/aerosol)	0.43 - 0.45	30
Band 2 - Blue	0.45 - 0.51	30
Band 3 - Green	0.53 - 0.59	30
Band 4 - Red	0.64 - 0.67	30
Band 5 - Near Infrared (NIR)	0.85 - 0.88	30
Band 6 - Shortwave Infrared (SWIR) 1	1.57 - 1.65	30
Band 7 - Shortwave Infrared (SWIR) 2	2.11 - 2.29	30
Band 8 - Panchromatic	0.50 - 0.68	15
Band 9 - Cirrus	1.36 - 1.38	30
Band 10 - Thermal Infrared (TIRS) 1	10.60 - 11.19	100 * (30)
Band 11 - Thermal Infrared (TIRS) 2	11.50 - 12.51	100 * (30)

Landsat-8 data contain nine spectral bands with 30 meter spatial resolution for bands 1 to 7, and 9. Coastal and aerosol information can be obtained from the ultra-blue band (band 1), and cirrus cloud information can be obtained from band 9. Band 8 in panchromatic with 15 meters spatial resolution. Bands 10 and 11 provide surface temperature with 100 meter spatial resolution (https://landsat.usgs.gov/what-are-band-designations-landsat-satellites) ("What are the band designations for the Landsat satellites?,")

Appendix B - Landsat Thematic Mapper spectral band properties

Bands	**Wavelength (micrometers)**	**Resolution (meters)**
Band 1 - Blue	0.45-0.52	30
Band 2 - Green	0.52-0.60	30
Band 3 - Red	0.63-0.69	30
Band 4 - Near Infrared (NIR)	0.76-0.90	30
Band 5 - Shortwave Infrared (SWIR) 1	1.55-1.75	30
Band 6 - Thermal	10.40-12.50	120* (30)
Band 7 - Shortwave Infrared (SWIR) 2	2.08-2.35	30

* TM Band 6 was acquired at 120-meter resolution, but products are resampled to 30-meter pixels.

Appendix C - List of Landsat-8 OLI scenes used for this study

Properties of Landsat-8 OLI imageries, path and row, cloud cover (CC) cloud cover full (CCF), Sun Eleavation which is useful for converting data from DN value to Top of Atmospheric Reflectance, are listed below for the study area and case study.

Table 4. Properties of Landsat Images for All Training Areas

Landsat Scene ID	Sensor	Acquisition Date	Path	Row	CC	CCF	Day/Night	Sun Elevation	Nadir / Off Nadir
LC81680342014114LGN00	OLI_TIRS	4/24/2014	168	34	0	1.65	DAY	59.63543515	NADIR
LC82330742014009LGN00	OLI_TIRS	1/9/2014	233	74	0	0.68	DAY	60.68599685	NADIR
LC81790732016245LGN00	OLI_TIRS	9/1/2016	179	73	0	0.28	DAY	50.32327675	NADIR
LC81660522016138LGN00	OLI_TIRS	5/17/2016	166	52	0	0.11	DAY	65.20469373	NADIR
LC81700272013125LGN01	OLI_TIRS	5/5/2013	170	27	0	0.04	DAY	56.1620817	NADIR
LC81700262014304LGN00	OLI_TIRS	10/31/2014	170	26	0	0.72	DAY	26.11217915	NADIR
LC81090762015184LGN00	OLI_TIRS	7/3/2015	109	76	0	2.71	DAY	34.59839953	NADIR
LC81790732015130LGN00	OLI_TIRS	5/10/2015	179	73	0	7.49	DAY	43.77172147	NADIR

Table 5. Properties of Landsat Images for Case Study

Landsat Scene ID	Sensor	Acquisition Date	Path	Row	CC	CCF	Day/Night	Sun Elevation	Nadir / Off Nadir
LC80420322013172LGN00	OLI_TIRS	6/21/2013	42	32	0	1.78	DAY	66.342691	NADIR
LC80400322016295LGN00	OLI_TIRS	10/21/2016	40	32	0	1.57	DAY	36.54247079	NADIR
LC80420332014159LGN00	OLI_TIRS	6/8/2014	42	33	0	1.47	DAY	66.66935121	NADIR
LC80400312015164LGN00	OLI_TIRS	6/13/2015	40	31	0	1.35	DAY	65.20744292	NADIR
LC80400312015164LGN00	OLI_TIRS	6/13/2015	40	31	0	1.35	DAY	65.20744292	NADIR
LC80380322014275LGN00	OLI_TIRS	10/2/2014	38	32	0	1.31	DAY	43.35902025	NADIR
LC80420322013156LGN00	OLI_TIRS	6/5/2013	42	32	0	1.31	DAY	66.19100132	NADIR
LC80420342014175LGN00	OLI_TIRS	6/24/2014	42	34	0	1.25	DAY	67.07910799	NADIR
LC80420342013172LGN00	OLI_TIRS	6/21/2013	42	34	0	1.23	DAY	67.5749199	NADIR
LC80370322013153LGN00	OLI_TIRS	6/2/2013	37	32	0	1.22	DAY	65.98988456	NADIR
LC80400332013158LGN00	OLI_TIRS	6/7/2013	40	33	0	1.21	DAY	66.99492667	NADIR
LC80360322013178LGN01	OLI_TIRS	6/27/2013	36	32	0	1.05	DAY	66.04432618	NADIR
LC80380322015262LGN00	OLI_TIRS	9/19/2015	38	32	0	1.04	DAY	47.64848707	NADIR
LC80450302013161LGN00	OLI_TIRS	6/10/2013	45	30	0	1.01	DAY	64.83680008	NADIR
LC80410342013181LGN00	OLI_TIRS	6/30/2013	41	34	0	1	DAY	67.0498809	NADIR
LC80420322016245LGN00	OLI_TIRS	9/1/2016	42	32	0	0.99	DAY	53.09021075	NADIR
LC80360342014181LGN00	OLI_TIRS	6/30/2014	36	34	0	0.97	DAY	66.7001874	NADIR
LC80380302013160LGN00	OLI_TIRS	6/9/2013	38	30	0	0.95	DAY	64.79784228	NADIR

Table 5. Cont'd

LC80380312013160LGN00	OLI_TIRS	6/9/2013	38	31	0	0.95	DAY	65.61144317	NADIR
LC80310392015165LGN00	OLI_TIRS	6/14/2015	31	39	0	0.94	DAY	68.89901011	NADIR
LC80320312014153LGN00	OLI_TIRS	6/2/2014	32	31	0	0.94	DAY	64.86961457	NADIR
LC80320332014153LGN00	OLI_TIRS	6/2/2014	32	33	0	0.94	DAY	66.34925941	NADIR
LC80370322013281LGN00	OLI_TIRS	10/8/2013	37	32	0	0.94	DAY	41.33238848	NADIR
LC80410352013181LGN00	OLI_TIRS	6/30/2013	41	35	0	0.93	DAY	67.55108687	NADIR
LC80410362014168LGN00	OLI_TIRS	6/17/2014	41	36	0	0.93	DAY	68.22879923	NADIR
LC80370332013153LGN00	OLI_TIRS	6/2/2013	37	33	0	0.91	DAY	66.72074816	NADIR
LC80370352015159LGN00	OLI_TIRS	6/8/2015	37	35	0	0.89	DAY	67.63733611	NADIR
LC80340342014167LGN00	OLI_TIRS	6/16/2014	34	34	0	0.87	DAY	67.33880752	NADIR
LC80440302015176LGN00	OLI_TIRS	6/25/2015	44	30	0	0.87	DAY	64.2318599	NADIR
LC80400332013318LGN00	OLI_TIRS	11/14/2013	40	33	0	0.86	DAY	30.9496973	NADIR
LC80410352015171LGN00	OLI_TIRS	6/20/2015	41	35	0	0.86	DAY	67.57817043	NADIR
LC80420292013156LGN00	OLI_TIRS	6/5/2013	42	29	0	0.86	DAY	63.70329506	NADIR
LC80380332014179LGN00	OLI_TIRS	6/28/2014	38	33	0	0.85	DAY	66.28884042	NADIR
LC80410362015171LGN00	OLI_TIRS	6/20/2015	41	36	0	0.85	DAY	67.9907825	NADIR
LC80430342015153LGN00	OLI_TIRS	6/2/2015	43	34	0	0.84	DAY	66.80113197	NADIR
LC80310312013175LGN00	OLI_TIRS	6/24/2013	31	31	0	0.81	DAY	65.50504081	NADIR
LC80370342015159LGN00	OLI_TIRS	6/8/2015	37	34	0	0.8	DAY	67.09497601	NADIR
LC80400362013158LGN00	OLI_TIRS	6/7/2013	40	36	0	0.78	DAY	68.67182057	NADIR
LC80450302013225LGN00	OLI_TIRS	8/13/2013	45	30	0	0.76	DAY	56.74215135	NADIR
LC80370392014172LGN00	OLI_TIRS	6/21/2014	37	39	0	0.74	DAY	68.77568281	NADIR
LC80370342014156LGN01	OLI_TIRS	6/5/2014	37	34	0	0.73	DAY	67.16192614	NADIR
LC80390372015173LGN00	OLI_TIRS	6/22/2015	39	37	0	0.73	DAY	68.2359909	NADIR
LC80320342013166LGN00	OLI_TIRS	6/15/2013	32	34	0	0.72	DAY	67.72118291	NADIR
LC80440302013154LGN00	OLI_TIRS	6/3/2013	44	30	0	0.72	DAY	64.43950138	NADIR
LC80350332015177LGN00	OLI_TIRS	6/26/2015	35	33	0	0.7	DAY	66.25888658	NADIR
LC80360322014101LGN00	OLI_TIRS	4/11/2014	36	32	0	0.7	DAY	53.58726621	NADIR
LC80420312013156LGN00	OLI_TIRS	6/5/2013	42	31	0	0.7	DAY	65.41568638	NADIR
LC80440362013170LGN00	OLI_TIRS	6/19/2013	44	36	0	0.69	DAY	68.57716431	NADIR
LC80350312013155LGN00	OLI_TIRS	6/4/2013	35	31	0	0.67	DAY	65.34824251	NADIR
LC80350382014174LGN00	OLI_TIRS	6/23/2014	35	38	0	0.67	DAY	68.54755911	NADIR
LC80330292014160LGN00	OLI_TIRS	6/9/2014	33	29	0	0.66	DAY	63.65386074	NADIR
LC80320322014153LGN00	OLI_TIRS	6/2/2014	32	32	0	0.65	DAY	65.63949014	NADIR
LC80350302013171LGN00	OLI_TIRS	6/20/2013	35	30	0	0.65	DAY	64.87781057	NADIR
LC80400352013174LGN00	OLI_TIRS	6/23/2013	40	35	0	0.65	DAY	67.9896571	NADIR
LC80370392015175LGN00	OLI_TIRS	6/24/2015	37	39	0	0.64	DAY	68.51561683	NADIR
LC80440302014157LGN00	OLI_TIRS	6/6/2014	44	30	0	0.63	DAY	64.34625547	NADIR
LC80330312013157LGN00	OLI_TIRS	6/6/2013	33	31	0	0.61	DAY	65.47188929	NADIR
LC80350352014174LGN00	OLI_TIRS	6/23/2014	35	35	0	0.61	DAY	67.60942377	NADIR

Table 5. Cont'd

LC80370362013153LGN00	OLI_TIRS	6/2/2013	37	36	0	0.61	DAY	68.49627276	NADIR
LC80410322014152LGN00	OLI_TIRS	6/1/2014	41	32	0	0.58	DAY	65.56268132	NADIR
LC80410362014152LGN00	OLI_TIRS	6/1/2014	41	36	0	0.57	DAY	68.01124296	NADIR
LC80370312013153LGN00	OLI_TIRS	6/2/2013	37	31	0	0.56	DAY	65.19886618	NADIR
LC80420332013172LGN00	OLI_TIRS	6/21/2013	42	33	0	0.56	DAY	66.99417884	NADIR
LC80420332013172LGN00	OLI_TIRS	6/21/2013	42	33	0	0.56	DAY	66.99417884	NADIR
LC80420332013172LGN00	OLI_TIRS	6/21/2013	42	33	0	0.56	DAY	66.99417884	NADIR
LC80420332013172LGN00	OLI_TIRS	6/21/2013	42	33	0	0.56	DAY	66.99417884	NADIR
LC80400292015164LGN00	OLI_TIRS	6/13/2015	40	29	0	0.54	DAY	63.59029376	NADIR
LC80370332013169LGN01	OLI_TIRS	6/18/2013	37	33	0	0.52	DAY	67.08213196	NADIR
LC80370392014156LGN01	OLI_TIRS	6/5/2014	37	39	0	0.52	DAY	69.09020645	NADIR
LC80410332014152LGN00	OLI_TIRS	6/1/2014	41	33	0	0.52	DAY	66.27815203	NADIR
LC80320372015172LGN00	OLI_TIRS	6/21/2015	32	37	0	0.51	DAY	68.2798976	NADIR
LC80390372015157LGN00	OLI_TIRS	6/6/2015	39	37	0	0.51	DAY	68.44361761	NADIR
LC80410382015171LGN00	OLI_TIRS	6/20/2015	41	38	0	0.51	DAY	68.55596782	NADIR
LC80420332013156LGN00	OLI_TIRS	6/5/2013	42	33	0	0.51	DAY	66.90496224	NADIR
LC80420332013156LGN00	OLI_TIRS	6/5/2013	42	33	0	0.51	DAY	66.90496224	NADIR
LC80420332013156LGN00	OLI_TIRS	6/5/2013	42	33	0	0.51	DAY	66.90496224	NADIR
LC80420332013156LGN00	OLI_TIRS	6/5/2013	42	33	0	0.51	DAY	66.90496224	NADIR
LC80450302015231LGN00	OLI_TIRS	8/19/2015	45	30	0	0.51	DAY	54.91016161	NADIR
LC80420312015162LGN00	OLI_TIRS	6/11/2015	42	31	0	0.5	DAY	65.16405417	NADIR
LC80430342013163LGN00	OLI_TIRS	6/12/2013	43	34	0	0.5	DAY	67.72772621	NADIR
LC80330382013173LGN00	OLI_TIRS	6/22/2013	33	38	0	0.49	DAY	69.03441707	NADIR
LC80370312014156LGN01	OLI_TIRS	6/5/2014	37	31	0	0.49	DAY	65.08994199	NADIR
LC80390302015173LGN00	OLI_TIRS	6/22/2015	39	30	0	0.49	DAY	64.3569236	NADIR
LC80440342013170LGN00	OLI_TIRS	6/19/2013	44	34	0	0.48	DAY	67.6427054	NADIR
LC80320372014153LGN00	OLI_TIRS	6/2/2014	32	37	0	0.46	DAY	68.47532769	NADIR
LC80360372014165LGN00	OLI_TIRS	6/14/2014	36	37	0	0.45	DAY	68.62051025	NADIR
LC80420352014159LGN00	OLI_TIRS	6/8/2014	42	35	0	0.45	DAY	67.81143962	NADIR
LC80440332013154LGN00	OLI_TIRS	6/3/2013	44	33	0	0.44	DAY	66.7902265	NADIR
LC80380292015214LGN00	OLI_TIRS	8/2/2015	38	29	0	0.43	DAY	58.12145257	NADIR
LC80410322013181LGN00	OLI_TIRS	6/30/2013	41	32	0	0.43	DAY	65.82821568	NADIR
LC80350382015177LGN00	OLI_TIRS	6/26/2015	35	38	0	0.42	DAY	68.26613481	NADIR
LC80420312014159LGN00	OLI_TIRS	6/8/2014	42	31	0	0.42	DAY	65.25278031	NADIR
LC80370322016194LGN00	OLI_TIRS	7/12/2016	37	32	0	0.41	DAY	64.12273767	NADIR
LC80390362015157LGN00	OLI_TIRS	6/6/2015	39	36	0	0.41	DAY	68.05079732	NADIR
LC80400362014161LGN00	OLI_TIRS	6/10/2014	40	36	0	0.41	DAY	68.29097846	NADIR
LC80380352014163LGN00	OLI_TIRS	6/12/2014	38	35	0	0.4	DAY	67.86395286	NADIR
LC80450302013193LGN00	OLI_TIRS	7/12/2013	45	30	0	0.4	DAY	63.05354936	NADIR
LC80320292015172LGN00	OLI_TIRS	6/21/2015	32	29	0	0.39	DAY	63.57400191	NADIR

Table 5. Cont'd

LC80410302013181LGN00	OLI_TIRS	6/30/2013	41	30	0	0.39	DAY	64.35056194	NADIR
LC80430302013179LGN00	OLI_TIRS	6/28/2013	43	30	0	0.39	DAY	64.49781852	NADIR
LC80320382015172LGN00	OLI_TIRS	6/21/2015	32	38	0	0.38	DAY	68.51611972	NADIR
LC80330312014176LGN00	OLI_TIRS	6/25/2014	33	31	0	0.38	DAY	65.15831998	NADIR
LC80330322013157LGN00	OLI_TIRS	6/6/2013	33	32	0	0.38	DAY	66.2424615	NADIR
LC80400302015164LGN00	OLI_TIRS	6/13/2015	40	30	0	0.38	DAY	64.42526016	NADIR
LC80430292013179LGN00	OLI_TIRS	6/28/2013	43	29	0	0.37	DAY	63.67523872	NADIR
LC80370322015207LGN00	OLI_TIRS	7/26/2015	37	32	0	0.36	DAY	62.03677251	NADIR
LC80430332013179LGN00	OLI_TIRS	6/28/2013	43	33	0	0.36	DAY	66.62050932	NADIR
LC80320382014153LGN00	OLI_TIRS	6/2/2014	32	38	0	0.35	DAY	68.80176002	NADIR
LC80320392013166LGN00	OLI_TIRS	6/15/2013	32	39	0	0.35	DAY	69.45988026	NADIR
LC80330342014160LGN00	OLI_TIRS	6/9/2014	33	34	0	0.35	DAY	67.30295443	NADIR
LC80310342015181LGN00	OLI_TIRS	6/30/2015	31	34	0	0.34	DAY	66.562174	NADIR
LC80360322015088LGN00	OLI_TIRS	3/29/2015	36	32	0	0.34	DAY	48.59141282	NADIR
LC80360382014165LGN00	OLI_TIRS	6/14/2014	36	38	0	0.34	DAY	68.86799192	NADIR
LC80390372013167LGN00	OLI_TIRS	6/16/2013	39	37	0	0.34	DAY	69.01002612	NADIR
LC80410312013181LGN00	OLI_TIRS	6/30/2013	41	31	0	0.33	DAY	65.11871275	NADIR
LC80390372014170LGN00	OLI_TIRS	6/19/2014	39	37	0	0.32	DAY	68.49197225	NADIR
LC80340372015170LGN00	OLI_TIRS	6/19/2015	34	37	0	0.31	DAY	68.35482605	NADIR
LC80360372015152LGN00	OLI_TIRS	6/1/2015	36	37	0	0.31	DAY	68.25902411	NADIR
LC80450302013113LGN01	OLI_TIRS	4/23/2013	45	30	0	0.31	DAY	55.91135398	NADIR
LC80320382013166LGN00	OLI_TIRS	6/15/2013	32	38	0	0.3	DAY	69.29447261	NADIR
LC80370362014172LGN00	OLI_TIRS	6/21/2014	37	36	0	0.29	DAY	68.09792677	NADIR
LC80330382015163LGN00	OLI_TIRS	6/12/2015	33	38	0	0.28	DAY	68.76344378	NADIR
LC80350352013155LGN00	OLI_TIRS	6/4/2013	35	35	0	0.28	DAY	68.08146225	NADIR
LC80360372015168LGN00	OLI_TIRS	6/17/2015	36	37	0	0.28	DAY	68.41513474	NADIR
LC80370372014172LGN00	OLI_TIRS	6/21/2014	37	37	0	0.28	DAY	68.41438511	NADIR
LC80370372013153LGN00	OLI_TIRS	6/2/2013	37	37	0	0.28	DAY	68.92913424	NADIR
LC80450342014164LGN00	OLI_TIRS	6/13/2014	45	34	0	0.28	DAY	67.35594666	NADIR
LC80350332013171LGN00	OLI_TIRS	6/20/2013	35	33	0	0.27	DAY	67.02924862	NADIR
LC80390352013167LGN00	OLI_TIRS	6/16/2013	39	35	0	0.27	DAY	68.22645785	NADIR
LC80430342015169LGN00	OLI_TIRS	6/18/2015	43	34	0	0.27	DAY	67.13795417	NADIR
LC80450342014180LGN00	OLI_TIRS	6/29/2014	45	34	0	0.27	DAY	66.7713967	NADIR
LC80340352015170LGN00	OLI_TIRS	6/19/2015	34	35	0	0.26	DAY	67.61010543	NADIR
LC80390352015173LGN00	OLI_TIRS	6/22/2015	39	35	0	0.26	DAY	67.50329925	NADIR
LC80390352014170LGN00	OLI_TIRS	6/19/2014	39	35	0	0.26	DAY	67.76485661	NADIR
LC80320332013166LGN00	OLI_TIRS	6/15/2013	32	33	0	0.25	DAY	67.12370861	NADIR
LC80350352014158LGN00	OLI_TIRS	6/7/2014	35	35	0	0.25	DAY	67.78382389	NADIR
LC80420302014159LGN00	OLI_TIRS	6/8/2014	42	30	0	0.25	DAY	64.45584756	NADIR
LC80330302015179LGN00	OLI_TIRS	6/28/2015	33	30	0	0.24	DAY	64.06196457	NADIR

Table 5. Cont'd

LC80370372014156LGN01	OLI_TIRS	6/5/2014	37	37	0	0.24	DAY	68.57852713	NADIR
LC80370372013169LGN01	OLI_TIRS	6/18/2013	37	37	0	0.24	DAY	68.95183427	NADIR
LC80330392015163LGN00	OLI_TIRS	6/12/2015	33	39	0	0.23	DAY	68.93782251	NADIR
LC80340392013164LGN00	OLI_TIRS	6/13/2013	34	39	0	0.23	DAY	69.51183578	NADIR
LC80390352014154LGN00	OLI_TIRS	6/3/2014	39	35	0	0.23	DAY	67.62275947	NADIR
LC80420292015162LGN00	OLI_TIRS	6/11/2015	42	29	0	0.23	DAY	63.53278954	NADIR
LC80420352014175LGN00	OLI_TIRS	6/24/2014	42	35	0	0.23	DAY	67.55856077	NADIR
LC80360322015104LGN00	OLI_TIRS	4/14/2015	36	32	0	0.22	DAY	54.48008218	NADIR
LC80370322016178LGN00	OLI_TIRS	6/26/2016	37	32	0	0.22	DAY	65.655892	NADIR
LC80430332015169LGN00	OLI_TIRS	6/18/2015	43	33	0	0.22	DAY	66.56426793	NADIR
LC80440332014157LGN00	OLI_TIRS	6/6/2014	44	33	0	0.22	DAY	66.58813851	NADIR
LC80450332014180LGN00	OLI_TIRS	6/29/2014	45	33	0	0.22	DAY	66.21700817	NADIR
LC80450332014164LGN00	OLI_TIRS	6/13/2014	45	33	0	0.22	DAY	66.77170175	NADIR
LC80320392015172LGN00	OLI_TIRS	6/21/2015	32	39	0	0.21	DAY	68.66012742	NADIR
LC80360322015168LGN00	OLI_TIRS	6/17/2015	36	32	0	0.21	DAY	65.93382211	NADIR
LC80360322015168LGN00	OLI_TIRS	6/17/2015	36	32	0	0.21	DAY	65.93382211	NADIR
LC80360322015168LGN00	OLI_TIRS	6/17/2015	36	32	0	0.21	DAY	65.93382211	NADIR
LC80360322015168LGN00	OLI_TIRS	6/17/2015	36	32	0	0.21	DAY	65.93382211	NADIR
LC80410312014152LGN00	OLI_TIRS	6/1/2014	41	31	0	0.21	DAY	64.78761013	NADIR
LC80320362013166LGN00	OLI_TIRS	6/15/2013	32	36	0	0.2	DAY	68.68177817	NADIR
LC80360292013178LGN01	OLI_TIRS	6/27/2013	36	29	0	0.2	DAY	63.74270216	NADIR
LC80360372014181LGN00	OLI_TIRS	6/30/2014	36	37	0	0.2	DAY	67.89962632	NADIR
LC80360382015152LGN00	OLI_TIRS	6/1/2015	36	38	0	0.2	DAY	68.60419548	NADIR
LC80440292014157LGN00	OLI_TIRS	6/6/2014	44	29	0	0.2	DAY	63.48922602	NADIR
LC80450302014100LGN00	OLI_TIRS	4/10/2014	45	30	0	0.2	DAY	51.16693815	NADIR
LC80360322014181LGN00	OLI_TIRS	6/30/2014	36	32	0	0.19	DAY	65.52087829	NADIR
LC80360322014181LGN00	OLI_TIRS	6/30/2014	36	32	0	0.19	DAY	65.52087829	NADIR
LC80360312013178LGN01	OLI_TIRS	6/27/2013	36	31	0	0.19	DAY	65.33456405	NADIR
LC80360322014181LGN00	OLI_TIRS	6/30/2014	36	32	0	0.19	DAY	65.52087829	NADIR
LC80360342013178LGN01	OLI_TIRS	6/27/2013	36	34	0	0.19	DAY	67.26407637	NADIR
LC80360322014181LGN00	OLI_TIRS	6/30/2014	36	32	0	0.19	DAY	65.52087829	NADIR
LC80360382014181LGN00	OLI_TIRS	6/30/2014	36	38	0	0.18	DAY	68.12999668	NADIR
LC80360382013162LGN00	OLI_TIRS	6/11/2013	36	38	0	0.18	DAY	69.36582259	NADIR
LC80380342013160LGN00	OLI_TIRS	6/9/2013	38	34	0	0.18	DAY	67.68547084	NADIR
LC80420302013156LGN00	OLI_TIRS	6/5/2013	42	30	0	0.18	DAY	64.58465855	NADIR
LC80420352013172LGN00	OLI_TIRS	6/21/2013	42	35	0	0.18	DAY	68.07888859	NADIR
LC80450302015183LGN00	OLI_TIRS	7/2/2015	45	30	0	0.18	DAY	63.75721943	NADIR
LC80370382014156LGN01	OLI_TIRS	6/5/2014	37	38	0	0.17	DAY	68.88044744	NADIR
LC80360302014181LGN00	OLI_TIRS	6/30/2014	36	30	0	0.16	DAY	64.08460799	NADIR
LC80450302013209LGN00	OLI_TIRS	7/28/2013	45	30	0	0.16	DAY	60.37369087	NADIR

Table 5. Cont'd

LC80380342013176LGN00	OLI_TIRS	6/25/2013	38	34	0	0.15	DAY	67.38478447	NADIR
LC80440332014173LGN00	OLI_TIRS	6/22/2014	44	33	0	0.15	DAY	66.61388004	NADIR
LC80310382015165LGN00	OLI_TIRS	6/14/2015	31	38	0	0.14	DAY	68.7343348	NADIR
LC80360382013178LGN01	OLI_TIRS	6/27/2013	36	38	0	0.14	DAY	68.75665957	NADIR
LC80420302015162LGN00	OLI_TIRS	6/11/2015	42	30	0	0.14	DAY	64.3746436	NADIR
LC80440312013154LGN00	OLI_TIRS	6/3/2013	44	31	0	0.14	DAY	65.27971616	NADIR
LC80340362015170LGN00	OLI_TIRS	6/19/2015	34	36	0	0.13	DAY	68.02505819	NADIR
LC80350322013171LGN00	OLI_TIRS	6/20/2013	35	32	0	0.13	DAY	66.37538815	NADIR
LC80370382013169LGN01	OLI_TIRS	6/18/2013	37	38	0	0.13	DAY	69.20212469	NADIR
LC80400342013174LGN00	OLI_TIRS	6/23/2013	40	34	0	0.13	DAY	67.48879229	NADIR
LC80440322014157LGN00	OLI_TIRS	6/6/2014	44	32	0	0.13	DAY	65.90127318	NADIR
LC80440332015176LGN00	OLI_TIRS	6/25/2015	44	33	0	0.13	DAY	66.31197817	NADIR
LC80310382013159LGN00	OLI_TIRS	6/8/2013	31	38	0	0.12	DAY	69.3768864	NADIR
LC80330362014160LGN00	OLI_TIRS	6/9/2014	33	36	0	0.12	DAY	68.28021874	NADIR
LC80360302013178LGN01	OLI_TIRS	6/27/2013	36	30	0	0.12	DAY	64.56570745	NADIR
LC80330382014160LGN00	OLI_TIRS	6/9/2014	33	38	0	0.11	DAY	68.91794133	NADIR
LC80360362014181LGN00	OLI_TIRS	6/30/2014	36	36	0	0.11	DAY	67.58194782	NADIR
LC80360372013178LGN01	OLI_TIRS	6/27/2013	36	37	0	0.11	DAY	68.51377115	NADIR
LC80450302015055LGN00	OLI_TIRS	2/24/2015	45	30	0	0.1	DAY	33.74841538	NADIR
LC80450302014196LGN00	OLI_TIRS	7/15/2014	45	30	0	0.1	DAY	62.39797185	NADIR
LC80310392014162LGN00	OLI_TIRS	6/11/2014	31	39	0	0.09	DAY	69.07963968	NADIR
LC80330382013157LGN00	OLI_TIRS	6/6/2013	33	38	0	0.09	DAY	69.36179366	NADIR
LC80440312014157LGN00	OLI_TIRS	6/6/2014	44	31	0	0.09	DAY	65.15197787	NADIR
LC80310372015165LGN00	OLI_TIRS	6/14/2015	31	37	0	0.08	DAY	68.4768449	NADIR
LC80350312013171LGN00	OLI_TIRS	6/20/2013	35	31	0	0.08	DAY	65.6563722	NADIR
LC80350392013171LGN00	OLI_TIRS	6/20/2013	35	39	0	0.08	DAY	69.27561629	NADIR
LC80350392013155LGN00	OLI_TIRS	6/4/2013	35	39	0	0.08	DAY	69.56172145	NADIR
LC80360332014181LGN00	OLI_TIRS	6/30/2014	36	33	0	0.08	DAY	66.14523355	NADIR
LC80370382014172LGN00	OLI_TIRS	6/21/2014	37	38	0	0.08	DAY	68.64130404	NADIR
LC80390362013167LGN00	OLI_TIRS	6/16/2013	39	36	0	0.08	DAY	68.66181988	NADIR
LC80440322013154LGN00	OLI_TIRS	6/3/2013	44	32	0	0.08	DAY	66.06531916	NADIR
LC80340382013164LGN00	OLI_TIRS	6/13/2013	34	38	0	0.07	DAY	69.33769079	NADIR
LC80350382013155LGN00	OLI_TIRS	6/4/2013	35	38	0	0.07	DAY	69.32771135	NADIR
LC80350392014158LGN00	OLI_TIRS	6/7/2014	35	39	0	0.07	DAY	69.10296959	NADIR
LC80380362013176LGN00	OLI_TIRS	6/25/2013	38	36	0	0.07	DAY	68.30215406	NADIR
LC80390362015173LGN00	OLI_TIRS	6/22/2015	39	36	0	0.07	DAY	67.9121974	NADIR
LC80450312015167LGN00	OLI_TIRS	6/16/2015	45	31	0	0.07	DAY	65.22818739	NADIR
LC80310362015181LGN00	OLI_TIRS	6/30/2015	31	36	0	0.06	DAY	67.45874302	NADIR
LC80310362013159LGN00	OLI_TIRS	6/8/2013	31	36	0	0.06	DAY	68.68949818	NADIR
LC80340312015170LGN00	OLI_TIRS	6/19/2015	34	31	0	0.06	DAY	65.19662249	NADIR

Table 5. Cont'd

LC80350342013171LGN00	OLI_TIRS	6/20/2013	35	34	0	0.06	DAY	67.61190615	NADIR
LC80360332015168LGN00	OLI_TIRS	6/17/2015	36	33	0	0.06	DAY	66.58063977	NADIR
LC80370382013153LGN00	OLI_TIRS	6/2/2013	37	38	0	0.06	DAY	69.27340258	NADIR
LC80380342014179LGN00	OLI_TIRS	6/28/2014	38	34	0	0.06	DAY	66.84263314	NADIR
LC80380362014179LGN00	OLI_TIRS	6/28/2014	38	36	0	0.06	DAY	67.72031146	NADIR
LC80380362013160LGN00	OLI_TIRS	6/9/2013	38	36	0	0.06	DAY	68.703538	NADIR
LC80390362014170LGN00	OLI_TIRS	6/19/2014	39	36	0	0.06	DAY	68.17148475	NADIR
LC80310372013159LGN00	OLI_TIRS	6/8/2013	31	37	0	0.05	DAY	69.07851817	NADIR
LC80310392013159LGN00	OLI_TIRS	6/8/2013	31	39	0	0.05	DAY	69.58048216	NADIR
LC80350382014158LGN00	OLI_TIRS	6/7/2014	35	38	0	0.05	DAY	68.90821631	NADIR
LC80380362014163LGN00	OLI_TIRS	6/12/2014	38	36	0	0.05	DAY	68.29637994	NADIR
LC80380372015166LGN00	OLI_TIRS	6/15/2015	38	37	0	0.05	DAY	68.46015664	NADIR
LC80380372013176LGN00	OLI_TIRS	6/25/2013	38	37	0	0.05	DAY	68.6338919	NADIR
LC80450322015167LGN00	OLI_TIRS	6/16/2015	45	32	0	0.05	DAY	65.94176522	NADIR
LC80330352014160LGN00	OLI_TIRS	6/9/2014	33	35	0	0.04	DAY	67.8315015	NADIR
LC80340352015154LGN00	OLI_TIRS	6/3/2015	34	35	0	0.04	DAY	67.43625464	NADIR
LC80350382013171LGN00	OLI_TIRS	6/20/2013	35	38	0	0.04	DAY	69.12454908	NADIR
LC80380292016217LGN00	OLI_TIRS	8/4/2016	38	29	0	0.04	DAY	57.54835359	NADIR
LC80380372014179LGN00	OLI_TIRS	6/28/2014	38	37	0	0.04	DAY	68.03497786	NADIR
LC80380372014163LGN00	OLI_TIRS	6/12/2014	38	37	0	0.04	DAY	68.64324909	NADIR
LC80380372013160LGN00	OLI_TIRS	6/9/2013	38	37	0	0.04	DAY	69.08609121	NADIR
LC80390342014170LGN00	OLI_TIRS	6/19/2014	39	34	0	0.04	DAY	67.2770116	NADIR
LC80450312014180LGN00	OLI_TIRS	6/29/2014	45	31	0	0.04	DAY	64.90457571	NADIR
LC80320332014169LGN00	OLI_TIRS	6/18/2014	32	33	0	0.03	DAY	66.73604493	NADIR
LC80330392013157LGN00	OLI_TIRS	6/6/2013	33	39	0	0.03	DAY	69.57990854	NADIR
LC80340352014167LGN00	OLI_TIRS	6/16/2014	34	35	0	0.03	DAY	67.83587335	NADIR
LC80340362015154LGN00	OLI_TIRS	6/3/2015	34	36	0	0.03	DAY	67.9334555	NADIR
LC80340382015170LGN00	OLI_TIRS	6/19/2015	34	38	0	0.03	DAY	68.59498218	NADIR
LC80360342015168LGN00	OLI_TIRS	6/17/2015	36	34	0	0.03	DAY	67.15737252	NADIR
LC80360362014165LGN00	OLI_TIRS	6/14/2014	36	36	0	0.03	DAY	68.28297308	NADIR
LC80360392013178LGN01	OLI_TIRS	6/27/2013	36	39	0	0.03	DAY	68.9066686	NADIR
LC80390342015173LGN00	OLI_TIRS	6/22/2015	39	34	0	0.03	DAY	67.0138335	NADIR
LC80390342014154LGN00	OLI_TIRS	6/3/2014	39	34	0	0.03	DAY	67.05702223	NADIR
LC80440312015176LGN00	OLI_TIRS	6/25/2015	44	31	0	0.03	DAY	64.98595536	NADIR
LC80440352013170LGN00	OLI_TIRS	6/19/2013	44	35	0	0.03	DAY	68.15099925	NADIR
LC80310352015181LGN00	OLI_TIRS	6/30/2015	31	35	0	0.02	DAY	67.0497268	NADIR
LC80320342015172LGN00	OLI_TIRS	6/21/2015	32	34	0	0.02	DAY	67.05271221	NADIR
LC80320362014153LGN00	OLI_TIRS	6/2/2014	32	36	0	0.02	DAY	68.06192415	NADIR
LC80330392014160LGN00	OLI_TIRS	6/9/2014	33	39	0	0.02	DAY	69.09915333	NADIR
LC80340372015154LGN00	OLI_TIRS	6/3/2015	34	37	0	0.02	DAY	68.34850158	NADIR

Table 5. Cont'd

LC80340382015154LGN00	OLI_TIRS	6/3/2015	34	38	0	0.02	DAY	68.67676427	NADIR
LC80340392015154LGN00	OLI_TIRS	6/3/2015	34	39	0	0.02	DAY	68.91392278	NADIR
LC80350362014158LGN00	OLI_TIRS	6/7/2014	35	36	0	0.02	DAY	68.24450351	NADIR
LC80350362013171LGN00	OLI_TIRS	6/20/2013	35	36	0	0.02	DAY	68.54199683	NADIR
LC80360332013162LGN00	OLI_TIRS	6/11/2013	36	33	0	0.02	DAY	67.10411671	NADIR
LC80360362015168LGN00	OLI_TIRS	42172	36	36	0	0.02	DAY	68.07977989	NADIR
LC80360362013178LGN01	OLI_TIRS	6/27/2013	36	36	0	0.02	DAY	68.18133793	NADIR
LC80370322014268LGN00	OLI_TIRS	9/25/2014	37	32	0	0.02	DAY	45.74796848	NADIR
LC80370342013169LGN01	OLI_TIRS	6/18/2013	37	34	0	0.02	DAY	67.66994698	NADIR
LC80370362014156LGN01	OLI_TIRS	6/5/2014	37	36	0	0.02	DAY	68.18836059	NADIR
LC80370362013169LGN01	OLI_TIRS	6/18/2013	37	36	0	0.02	DAY	68.61000347	NADIR
LC80380292016233LGN00	OLI_TIRS	8/20/2016	38	29	0	0.02	DAY	53.46409034	NADIR
LC80390342013167LGN00	OLI_TIRS	6/16/2013	39	34	0	0.02	DAY	67.70891439	NADIR
LC80440322015176LGN00	OLI_TIRS	6/25/2015	44	32	0	0.02	DAY	65.6810414	NADIR
LC80450322014180LGN00	OLI_TIRS	6/29/2014	45	32	0	0.02	DAY	65.59297076	NADIR
LC80320322014169LGN00	OLI_TIRS	6/18/2014	32	32	0	0.01	DAY	66.09840255	NADIR
LC80330312015179LGN00	OLI_TIRS	6/28/2015	33	31	0	0.01	DAY	64.81407549	NADIR
LC80350352013171LGN00	OLI_TIRS	6/20/2013	35	35	0	0.01	DAY	68.11794238	NADIR
LC80350372014158LGN00	OLI_TIRS	6/7/2014	35	37	0	0.01	DAY	68.62084504	NADIR
LC80350372013171LGN00	OLI_TIRS	6/20/2013	35	37	0	0.01	DAY	68.87888685	NADIR
LC80360342013162LGN00	OLI_TIRS	6/11/2013	36	34	0	0.01	DAY	67.71862384	NADIR
LC80360352014165LGN00	OLI_TIRS	6/14/2014	36	35	0	0.01	DAY	67.85943594	NADIR
LC80360352013178LGN01	OLI_TIRS	6/27/2013	36	35	0	0.01	DAY	67.76317802	NADIR
LC80360392015152LGN00	OLI_TIRS	6/1/2015	36	39	0	0.01	DAY	68.85913288	NADIR
LC80360392014181LGN00	OLI_TIRS	6/30/2014	36	39	0	0.01	DAY	68.27029782	NADIR
LC80360392014165LGN00	OLI_TIRS	6/14/2014	36	39	0	0.01	DAY	69.02216558	NADIR
LC80370322015287LGN00	OLI_TIRS	10/14/2015	37	32	0	0.01	DAY	39.14073552	NADIR
LC80370322015255LGN00	OLI_TIRS	9/12/2015	37	32	0	0.01	DAY	49.92144777	NADIR
LC80370352014156LGN01	OLI_TIRS	6/5/2014	37	35	0	0.01	DAY	67.71442418	NADIR
LC80380352014179LGN00	OLI_TIRS	6/28/2014	38	35	0	0.01	DAY	67.32151511	NADIR
LC80380352013176LGN00	OLI_TIRS	6/25/2013	38	35	0	0.01	DAY	67.88420342	NADIR
LC80380352013160LGN00	OLI_TIRS	6/9/2013	38	35	0	0.01	DAY	68.23484025	NADIR
LC80440292015176LGN00	OLI_TIRS	6/25/2015	44	29	0	0.01	DAY	63.4238348	NADIR
LC80450302015263LGN00	OLI_TIRS	9/20/2015	45	30	0	0.01	DAY	44.99807484	NADIR
LC80450302015199LGN00	OLI_TIRS	7/18/2015	45	30	0	0.01	DAY	61.8006071	NADIR
LC80450302014276LGN00	OLI_TIRS	10/3/2014	45	30	0	0.01	DAY	40.59012946	NADIR
LC80450302014244LGN00	OLI_TIRS	9/1/2014	45	30	0	0.01	DAY	51.28399472	NADIR
LC80320352015172LGN00	OLI_TIRS	6/21/2015	32	35	0	0	DAY	67.54389157	NADIR
LC80320362015172LGN00	OLI_TIRS	6/21/2015	32	36	0	0	DAY	67.9545488	NADIR
LC80320392014153LGN00	OLI_TIRS	6/2/2014	32	39	0	0	DAY	69.03690161	NADIR

Table 5. Cont'd

LC80360352015168LGN00	OLI_TIRS	6/17/2015	36	35	0	0	DAY	67.65884834	NADIR
LC80370352013169LGN01	OLI_TIRS	6/18/2013	37	35	0	0	DAY	68.18112575	NADIR
LC80450352014180LGN00	OLI_TIRS	6/29/2014	45	35	0	0	DAY	67.25083914	NADIR
LC80400372014097LGN00	OLI_TIRS	4/7/2014	40	37	0	0.61	DAY	56.93034541	NADIR
LC80430302013179LGN00	OLI_TIRS	6/28/2013	43	30	0	0.39	DAY	64.49781852	NADIR
LC80430312014134LGN00	OLI_TIRS	5/14/2014	43	31	0	0.7	DAY	62.11914543	NADIR
LC80430312016236LGN00	OLI_TIRS	8/23/2016	43	31	0	0.82	DAY	54.6495722	NADIR
LC80430322013227LGN00	OLI_TIRS	8/15/2013	43	32	0	0.89	DAY	58.12909105	NADIR
LC80430322014134LGN00	OLI_TIRS	5/14/2014	43	32	0	0.95	DAY	62.99714866	NADIR
LC80420352013220LGN00	OLI_TIRS	8/8/2013	42	35	0	0.11	DAY	62.16708619	NADIR
LC80420352016229LGN00	OLI_TIRS	8/16/2016	42	35	0	0.12	DAY	60.02837742	NADIR
LC80420362013108LGN01	OLI_TIRS	4/18/2013	42	36	0	0.08	DAY	60.04498207	NADIR
LC80420362015226LGN00	OLI_TIRS	8/14/2015	42	36	0	0.15	DAY	61.31669832	NADIR
LC80390332014170LGN00	OLI_TIRS	6/19/2014	39	33	0	1.3	DAY	66.71290918	NADIR
LC80410292014248LGN00	OLI_TIRS	9/5/2014	41	29	0	0.01	DAY	48.9474822	NADIR
LC80410292016206LGN00	OLI_TIRS	7/24/2016	41	29	0	0.04	DAY	59.84104385	NADIR
LC80390312016272LGN00	OLI_TIRS	9/28/2016	39	31	0	3.28	DAY	43.20167392	NADIR
LC80390322016272LGN00	OLI_TIRS	9/28/2016	39	32	0	5.17	DAY	44.39040985	NADIR
LC80320352016159LGN00	OLI_TIRS	6/7/2016	32	35	0	0	DAY	67.7153389	NADIR
LC80320352015172LGN00	OLI_TIRS	6/21/2015	32	35	0	0	DAY	67.54389157	NADIR
LC80380302016233LGN00	OLI_TIRS	8/20/2016	38	30	0	0.02	DAY	54.48162928	NADIR
LC80380302016313LGN00	OLI_TIRS	11/8/2016	38	30	0	0.91	DAY	28.40000087	NADIR
LC80420342013172LGN00	OLI_TIRS	6/21/2013	42	34	0	1.23	DAY	67.5749199	NADIR
LC80390382014122LGN00	OLI_TIRS	5/2/2014	39	38	0	0.3	DAY	64.91635617	NADIR
LC80390382013279LGN00	OLI_TIRS	10/6/2013	39	38	0	0.34	DAY	49.10894368	NADIR
LC80320352016159LGN00	OLI_TIRS	6/7/2016	32	35	0	0	DAY	67.7153389	NADIR
LC80320352015172LGN00	OLI_TIRS	6/21/2015	32	35	0	0	DAY	67.54389157	NADIR
LC80370292016178LGN00	OLI_TIRS	6/26/2016	37	29	0	0.75	DAY	63.38925009	NADIR
LC80390292015253LGN00	OLI_TIRS	9/10/2015	39	29	0	0.01	DAY	47.21725947	NADIR
LC80390292016272LGN00	OLI_TIRS	9/28/2016	39	29	0	0.02	DAY	40.79290149	NADIR
LC80390292013215LGN00	OLI_TIRS	8/3/2013	39	29	0	0.09	DAY	58.19515636	NADIR

Appendix D - SVM optimal parameters

SVM optimal parameters obtained from LIBSVM are listed as following;

THRESH = 0.0, PYRAMID_LEVELS = 0, KERNEL_TYPE = 2, KERNEL_GAMMA = 0.5, PENALTY = 32

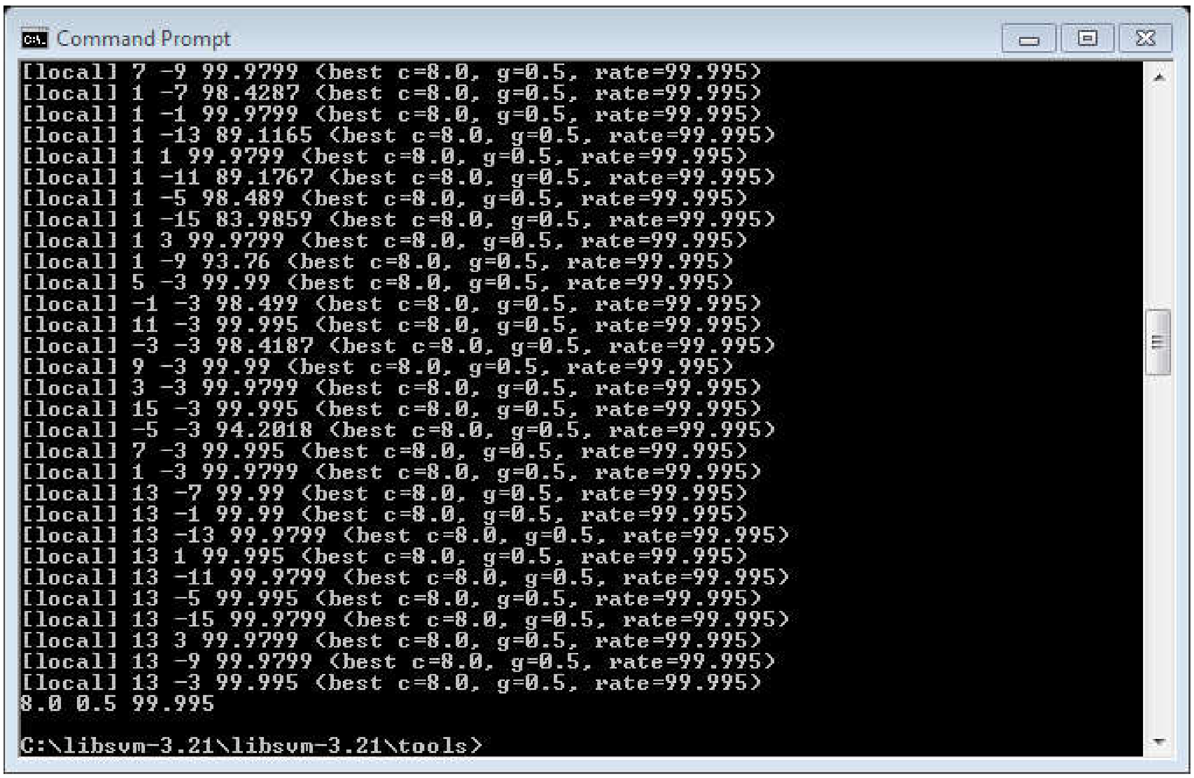

Figure 33. Optimal scaled kernel values derived from LIBSVM using 4000 Pixels obtained from 8 training areas for each class (Salt and Non-Salt), the last 'g' value represents optimal Gamma parameter, and the last 'c' value represents optimal Penalty parameter

Appendix E - Inventory of all endorheic basins and their salt pans areas

Table 6. Area of the each endorheic basin, and salt pans located in each basin. The coverage of each endorheic basin with salt pans (percentage and area), are displayed in the table.

Salt Area (km^2)	Salt Percentage (%)	Endorheic Basin Area (km^2)
0.00	0.00	91.15
0.00	0.00	48.62
0.00	0.00	594.66
0.00	0.00	29.33
0.00	0.00	94.68
0.00	0.00	132.99
0.00	0.00	369.98
0.00	0.01	16.69
0.00	0.00	30.46
0.00	0.00	28.74
0.00	0.01	8.65
0.00	0.00	183.25
0.00	0.00	122.97
0.00	0.00	56.28
0.00	0.00	31.26
0.00	0.01	15.45
0.00	0.00	108.20
0.00	0.00	58.07
0.00	0.00	265.17
0.00	0.01	35.62
0.00	0.00	60.12
0.00	0.01	13.36
0.00	0.01	29.21
0.00	0.04	4.08
0.00	0.00	43.04
0.00	0.00	43.36
0.00	0.00	71.15
0.00	0.00	88.33
0.00	0.01	17.25
0.00	0.00	882.68
0.00	0.00	1134.71

Table 6. Cont'd

0.00	0.00	107.76
0.00	0.00	302.90
0.00	0.00	1666.22
0.00	0.00	143.80
0.00	0.00	81.96
0.00	0.02	19.04
0.00	0.00	1101.78
0.00	0.00	183.48
0.00	0.00	87.43
0.00	0.01	34.18
0.00	0.02	21.10
0.00	0.02	20.30
0.00	0.00	72.70
0.00	0.00	882.30
0.00	0.02	21.57
0.00	0.00	602.95
0.00	0.01	67.00
0.00	0.03	17.18
0.00	0.01	41.03
0.00	0.01	52.30
0.00	0.00	391.51
0.00	0.00	349.11
0.00	0.02	27.33
0.01	0.06	8.65
0.01	0.00	184.95
0.01	0.01	79.92
0.01	0.05	13.63
0.01	0.00	196.32
0.01	0.00	325.30
0.01	0.07	12.13
0.01	0.02	67.58
0.01	0.03	40.34
0.01	0.01	108.40
0.01	0.00	1102.26
0.01	0.03	47.62
0.01	0.01	112.99
0.02	0.01	262.56
0.02	0.01	242.78

Table 6. Cont'd

0.02	0.01	395.42
0.02	0.05	44.62
0.02	0.01	318.05
0.02	0.02	132.03
0.02	0.03	87.45
0.03	0.03	81.25
0.03	0.01	279.62
0.03	0.01	385.73
0.03	0.04	68.20
0.03	0.00	4523.08
0.03	0.01	421.44
0.03	0.02	136.20
0.04	0.02	189.62
0.04	0.07	51.46
0.04	0.01	559.00
0.04	0.02	163.65
0.04	0.10	39.99
0.04	0.04	107.04
0.04	0.04	105.36
0.04	0.02	249.06
0.05	0.15	30.67
0.05	0.01	479.86
0.05	0.02	251.28
0.05	0.01	739.48
0.06	0.00	1498.56
0.07	0.03	191.42
0.07	0.09	83.46
0.08	0.01	766.76
0.08	0.14	57.97
0.08	0.16	52.26
0.08	0.01	1055.41
0.09	0.03	330.94
0.09	0.03	267.24
0.10	0.65	14.58
0.10	0.10	91.95
0.10	0.01	1086.57
0.10	0.10	101.59
0.10	0.01	988.29
0.10	0.35	28.88

Table 6. Cont'd

0.12	0.01	1257.68
0.12	0.24	51.66
0.13	0.10	132.52
0.13	0.51	26.09
0.14	0.03	433.36
0.14	0.08	188.17
0.15	0.15	98.30
0.16	0.31	50.96
0.17	0.05	356.86
0.17	0.06	267.14
0.18	0.09	200.09
0.19	0.15	126.97
0.19	0.13	140.54
0.19	0.54	35.72
0.20	0.68	29.23
0.20	0.02	1076.15
0.20	0.05	418.61
0.21	0.19	113.98
0.23	0.58	39.66
0.25	0.01	3045.93
0.27	0.30	89.94
0.28	0.58	48.59
0.29	0.69	41.24
0.32	1.47	21.83
0.32	0.09	360.86
0.33	0.02	1864.44
0.34	0.07	473.53
0.34	0.10	337.67
0.36	0.14	252.35
0.37	0.99	37.09
0.39	0.54	71.78
0.42	0.88	47.55
0.42	0.14	306.58
0.43	0.40	108.73
0.44	0.03	1370.13
0.45	2.57	17.67
0.48	0.45	105.25
0.48	0.02	2956.29
0.52	0.16	326.56

Table 6. Cont'd

0.52	0.10	531.90
0.58	0.12	486.01
0.59	0.03	1844.23
0.62	0.09	710.94
0.63	1.30	48.52
0.64	0.18	351.45
0.65	0.06	1044.77
0.67	0.67	99.42
0.67	0.78	85.95
0.73	0.05	1386.30
0.75	0.05	1432.30
0.79	0.58	136.83
0.80	2.32	34.63
0.81	0.22	374.57
0.85	2.08	40.72
0.86	0.08	1123.78
0.89	1.83	48.30
0.89	0.23	387.04
0.89	1.04	85.64
0.90	0.68	132.03
0.91	0.75	121.64
0.95	0.52	183.74
0.98	0.10	949.97
1.03	0.16	627.82
1.04	0.56	184.50
1.07	0.12	874.92
1.07	0.18	592.14
1.08	0.57	190.05
1.08	0.37	291.67
1.11	0.28	394.89
1.13	0.09	1268.91
1.14	2.62	43.73
1.18	0.18	644.10
1.19	2.89	41.07
1.21	0.06	2124.41
1.26	0.03	3675.00
1.41	0.17	815.27
1.53	0.08	1905.09
1.54	0.26	583.93

Table 6. Cont'd

1.61	0.25	650.06
1.70	0.06	2665.56
1.70	2.17	78.60
1.71	0.50	339.19
1.78	0.21	843.85
1.93	0.13	1540.52
2.02	0.60	338.17
2.09	0.25	846.54
2.20	0.16	1373.31
2.20	1.57	140.64
2.27	1.51	150.03
2.30	0.39	589.81
2.31	0.57	402.92
2.32	0.45	519.42
2.35	1.68	140.48
2.45	0.66	372.46
2.46	4.20	58.51
2.55	3.06	83.59
2.77	3.41	81.36
2.79	0.02	16824.43
2.93	0.06	4850.63
3.00	0.32	938.60
3.00	0.18	1684.63
3.02	0.87	345.24
3.10	0.16	1898.09
3.37	0.24	1396.53
3.38	4.42	76.46
3.39	0.32	1068.09
3.51	0.10	3604.16
3.62	0.46	778.37
3.66	0.39	930.13
3.94	1.60	246.59
3.98	0.48	826.72
4.50	1.24	362.82
4.59	0.92	497.67
4.68	2.56	183.17
4.70	0.08	6029.83
4.83	0.10	4894.88
4.97	0.42	1171.63

Table 6. Cont'd

5.35	0.07	7169.23
5.50	1.15	478.07
5.51	1.60	343.71
5.68	0.32	1800.41
5.77	0.45	1291.56
5.78	2.86	202.07
6.01	0.41	1483.65
6.47	3.97	162.92
6.56	0.36	1811.28
6.56	1.26	520.42
6.72	0.99	678.35
6.85	0.08	8566.76
6.96	2.71	256.83
7.03	1.66	422.61
7.54	0.21	3526.21
7.56	0.15	5014.88
7.83	2.32	338.08
7.96	0.10	7990.29
8.06	0.42	1928.51
8.34	1.13	739.38
8.73	1.08	810.54
8.74	0.34	2544.93
8.86	1.13	784.63
9.04	1.52	592.91
9.51	1.32	720.59
9.52	1.49	637.12
9.71	0.54	1791.85
9.97	1.08	926.74
10.83	2.88	376.70
10.96	0.60	1819.15
11.21	1.18	947.41
11.33	2.04	555.31
11.61	0.76	1527.59
11.75	1.49	790.86
11.95	0.58	2052.73
12.03	0.44	2730.69
12.10	0.86	1413.56
12.46	1.06	1180.75
12.73	0.29	4354.11

Table 6. Cont'd

12.89	1.71	751.71
13.17	1.03	1284.38
13.43	0.23	5733.10
13.52	1.86	726.38
13.61	3.09	439.75
13.80	0.77	1789.46
13.81	1.29	1070.13
14.24	1.24	1149.18
14.54	0.26	5518.75
14.57	1.87	777.54
14.83	4.24	350.07
15.28	0.19	8018.14
15.38	0.34	4512.13
15.88	0.45	3532.12
15.94	1.11	1437.76
15.95	0.17	9318.90
16.44	3.60	457.04
16.94	0.29	5836.07
17.20	0.52	3319.81
19.24	0.36	5294.27
19.54	1.91	1023.49
19.60	0.67	2923.82
20.75	1.35	1540.94
21.65	1.12	1937.56
21.87	0.50	4346.40
22.04	1.28	1717.34
23.00	2.70	853.07
25.31	1.70	1485.32
26.37	2.71	973.54
28.69	1.78	1614.08
29.53	1.27	2334.47
32.11	0.13	24502.14
32.27	1.56	2070.04
33.95	2.23	1519.35
34.33	4.21	814.76
34.54	1.78	1945.87
34.84	3.94	885.31
38.46	0.38	10190.52
41.19	1.64	2518.64

Table 6. Cont'd

41.42	4.31	961.40
43.51	1.75	2487.57
43.82	1.38	3186.56
44.01	1.81	2425.99
46.50	1.36	3419.57
48.77	4.52	1078.89
48.91	1.11	4413.84
49.06	1.72	2844.66
50.10	1.70	2949.98
52.94	2.83	1871.58
53.43	3.58	1490.65
53.80	0.96	5603.19
55.90	1.03	5410.24
58.05	2.25	2575.13
58.68	8.54	687.40
61.80	4.82	1281.22
62.55	1.03	6100.73
66.17	5.00	1323.00
66.83	3.89	1719.03
74.30	2.18	3411.50
76.44	0.14	53694.31
88.85	4.70	1891.10
91.95	1.62	5691.64
106.05	4.82	2199.92
107.65	0.88	12275.07
113.61	3.03	3754.74
116.43	2.23	5229.92
127.24	0.60	21178.99
135.65	5.84	2322.84
139.46	13.13	1062.52
176.34	1.94	9100.53
185.10	1.88	9864.37
546.02	1.57	34745.36
573.91	3.28	17516.60
640.03	0.74	87005.93
742.52	8.22	9034.07
1308.99	6.53	20041.54